

Spatial Stochastic Modelling of Ecosystems

Fabio Peruzzo



Submitted in accordance with the requirements for
the degree of Doctor of Philosophy

The University of Leeds
School of Mathematics

May 2019

The candidate confirms that the work submitted is his own and that appropriate credit has been given where reference has been made to the work of others.

This copy has been supplied on the understanding that it is copyright material and that no quotation from the thesis may be published without proper acknowledgement.

Acknowledgements

I thank NERC DTP for funding this research project.

I also thank my supervisors, Sandro Azaele and Mauro Mobilia, for the useful feedback, comments and suggestions received throughout these three and a half years.

Abstract

The modelling of spatial effects in ecological systems has often been overlooked for its intrinsic complexity, both from a computational and a mathematical point of view. But real ecological systems are spatially extended and there is proved empirical evidence that this strongly influences their dynamics.

At its core this thesis analyses a simple spatial extension of a birth death process with linear rates. In the regime of large fluctuations the model is amenable to analytical treatment, which, for example, leads to an explicit formula for the probability distribution of the number of individuals living in a given volume in any dimension. Comparison to simulated data shows excellent agreement where expected. Despite the lack of time reversibility at the individual level, at the community level the dynamics of the model satisfies time reversibility.

These results are applied to infer the spatial empirical distributions of tree species in two lowland tropical forest inventories. In fact, the model allows to link observations of some of the most important ecological descriptors into a unified framework, and the predictions are shown to match data well.

An extension of the model is also considered that aims at giving a first account of the effect of environmental fluctuations on large scale patterns. Analytic formulas are obtained, and comparisons to simulated data show again excellent agreement.

The conclusions drawn from the present work can help to shed a light on the effects

of spatial dispersal on large communities of living organisms and on the mathematical analysis of spatial stochastic processes. This could ultimately lead to the design of more effective conservation strategies, and to further unveil the delicate laws governing the coexistence of living organisms in complex natural systems.

Contents

Acknowledgements	ii
Abstract	iii
Contents	v
I Introduction	1
I.1 Biological evolution and natural selection	1
I.2 Neutral theory of molecular evolution	3
I.3 The neutral theory of Biodiversity and Biogeography	5
I.4 Spatial modelling of ecosystems	8
I.5 Criticality and scale invariance	13
II Mean-field and a phenomenological spatial model	19
II.1 Master equation and detailed balance	19
II.2 Birth Death mean field process	21
II.3 Stationary Solution of the BD process	23
II.4 Diffusion approximation with the Kramers-Moyal expansion	25
II.4.1 BD process with the Kramers-Moyal expansion	27

II.5	Diffusion approximation in the "critical limit"	28
II.6	Time dependent solution of the BD process	31
II.7	A Phenomenological Model	34
II.8	Pair Correlation of the Phenomenological model	37
II.9	The conditional probability distribution	41
II.10	Variance of the conditional distribution	46
II.11	Form invariance of the distribution of $N(R)$	48
III	A spatial stochastic model close to a critical point	53
III.1	Definition of the Spatial Birth-Death model and the violation of detailed balance	54
III.2	The Spatial Generating Function	59
III.3	Local mean abundance and two-points correlation function	60
III.4	The critical limit of the spatial generating function	62
III.5	Conditional generating function	66
III.6	Spatial continuous limit	68
III.7	Approximate solution at stationarity	71
III.7.1	A series expansion for $f(\cdot)$	73
III.7.2	Calculation of the approximate solution at stationarity	75
III.7.3	Evaluation of the accuracy of the method	78
III.8	Time-dependent spatial analysis	81

IV Simulation Schemes and Data Analysis	85
IV.1 Simulations of the process	85
IV.1.1 Doob-Gillespie Algorithm	86
IV.1.2 "Phenomenological" Algorithm	88
IV.2 Ecological descriptors and data analysis	93
IV.2.1 From $P(N R)$ to the SAR	96
IV.2.2 From the empirical two-points correlation to the RSA	96
IV.2.3 Analysis of two lowland tropical forest inventories	98
V Environmental noise model	107
V.1 Phenomenological model with environmental noise	109
V.1.1 Mean field model with environmental noise	109
V.1.2 Spatial model with environmental noise	113
V.2 Spatial generating function and two point correlation	114
V.3 An ansatz for the EN model	117
V.4 Simulation scheme in the EN model	119
V.5 Comparison of analytic solution and simulated data	120
VI Conclusions	123
Appendices	129
A Calculation of the moments	131
B An equality for $g(\cdot)$	135

C	Ansatz for $f(\mathbf{x})$ in the case of $ \mathbf{x} > R$	139
D	Model with independent dispersal	143
E	Time dependent analysis: calculations	149
F	Codes for simulations	153

Bibliography		174
---------------------	--	------------

Chapter I

Introduction

I.1 Biological evolution and natural selection

Species evolution by means of natural selection has been the great unifying principle in biology. The publication of the origin of species, in 1859 [51], opened the door to the hypothesis that changes of the environment, life-cycle 'strategies', interactions with other species, and kin or possibly group selection actively influence and shape the population size and structure of all species, including humans, over ecological time scales [95].

Darwin's theory introduced the idea that small, beneficial variations of traits may be accumulated within many generations, thus causing species to change and evolve over time (fig I.1.1). Understanding to what extent such mutations are a consequence of external influence, how the very own mechanism of adaptation manifests, and what are the key differences that maintain diversity in nature, have proved to be formidable problems. Quantitative theories able to make predictions and to explain causal connections are very rare in evolutionary studies, and this has elicited harsh criticism to the idea of species evolution itself.

At the other extreme, however, natural selection and adaptation are often invoked to ex-

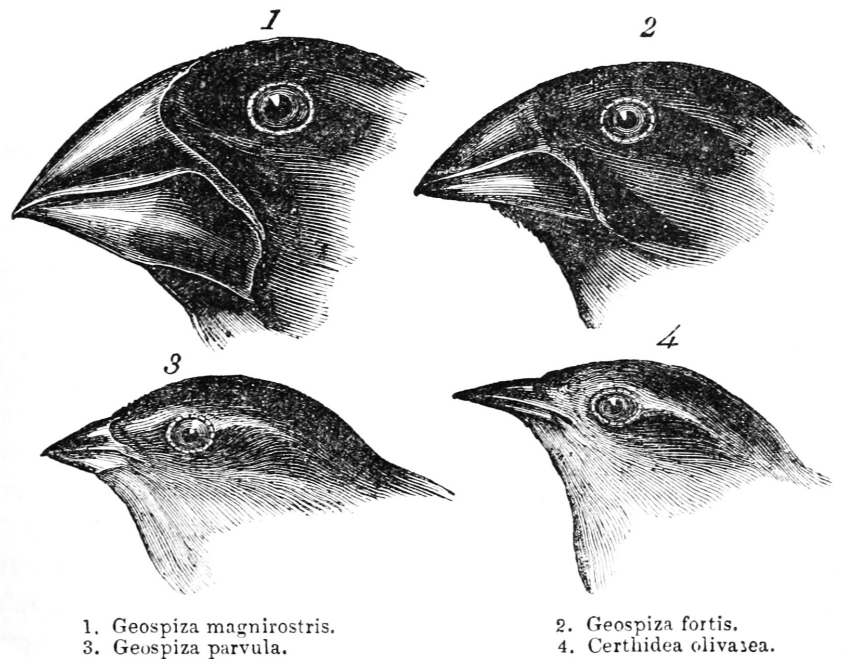


Figure I.1.1: **Darwin's finches**. The drawings represent four different species of passerine birds. The great variety of these species, together with that of tortoise, made Darwin raise doubts on the invariability of species, and put the seeds for his theory of natural selection. Image taken from [51]

plain the emergence of any physical mutation in living organisms, justifying any behaviour or observation in light of a specific, although often not better specified, evolutionary purpose [53].

Over the years the debate for a comprehensive theory of evolution has proceeded largely around extremes. In the early 1960s, for example, the scientific community seemed to have reached consensus over the idea that every biological character can be interpreted in light of adaptive evolution by natural selection, and that almost no mutation happens by pure chance. In such scheme, mutations are only a response to an external change in the environment. Famous is the quote by Ronald J. Fisher, that says "The rate of increase in the mean fitness of any organism at any time ascribable to natural selection acting through changes in gene frequencies is exactly equal to its genetic variance in fitness at that time" [66].

However, in that same period the advances in the sequencing of proteins made it possible to study amino-acid frequencies and distributions among related organisms. The results were shown to be incompatible with those of such neo-Darwinian selectionist theories: a very high rate of amino acid substitutions appeared to be uniformly distributed among diverse lineages of the same species, hence supporting the idea of an effective randomness in the recombination of genes (fig I.1.2).

I.2 Neutral theory of molecular evolution

If mutations were to happen only as a consequence of external changes, for example, a region with higher environmental instability would promote a higher variability in species, thus favouring diversity. The hypothesis that genetic variability is higher in unstable environments was then put under test: since the deep sea is the most stable and homogeneous habitat on earth, predictions would expect genetic diversity there to be very limited. On the contrary, it was demonstrated that many organisms living at the bottom of the deep sea have very high genetic variability [79].

Drawing from these and other observations, the Japanese biologist Kimura suggested that the great majority of molecular variations are selectively "neutral", i.e. they do not influence the fitness of organisms. Kimura made use of a rather new approach in mathematics at the time called 'diffusion models' [105, 62, 127].

While not denying that natural selection plays a central role in adaptive evolution, the neutral theory of molecular evolution assumes that only a small fraction of DNA changes produce an advantage over the individual or the species, while the great majority of mutations do not imply any significant variation at the phenotypic level, therefore leaving the rate of survival of a species unchanged.

Neutral theory generated a heated debate at the time of publications. The idea of an in-

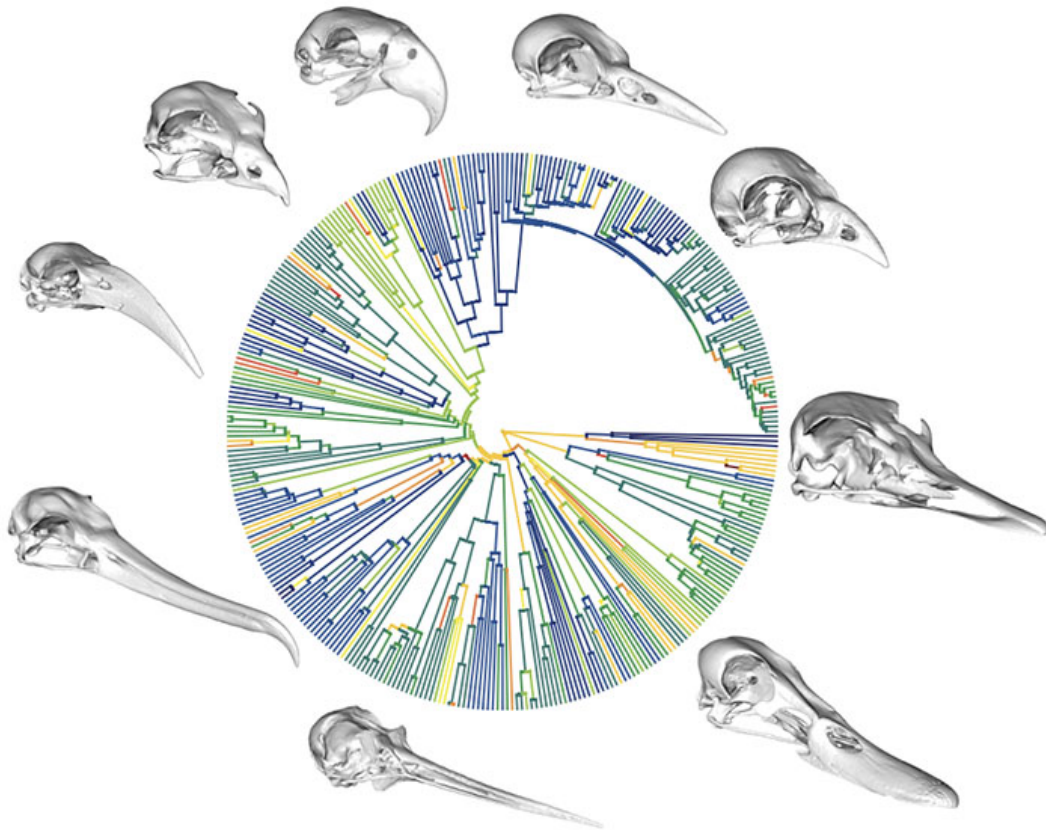


Figure I.1.2: **Evolution of the avian cranium.** Evolutionary tree of various types of bird's skulls, with each branch representing a different type. The colours represent the rate of evolution, i.e. how many variations of the phenotype have appeared over time (single variations that however are not signatures of a new species). The survey covered data on bird's skulls from a period of approximately 70 million years. Most of the species have evolved at a regular rate, with new species coexisting with older ones. Image from [63].

trinsic randomness in the genome recombination and in the genetic assembly of characteristics was disruptive for most biologists. However, the work by Kimura gave quantitative estimate of the rates of amino acid substitutions in many living organisms. The difficulty of teasing apart selection from randomness was eluded by considering those genes that code for the same protein, thus preserving the physical characteristics of an individual, its relationship to the environment and ultimately its adaptability.

The neutral theory of molecular evolution quantified the effect of randomness in the theory of evolution. However, the evidence that the force that regulates gene recombination is mostly random promoted the idea that such randomness could emerge also at the phenotypic level. As Kimura points out in his book: 'If a molecule or a part of a molecule is functionally less important, then the probability of a mutational change in it being selectively neutral (ie. selectively equivalent) is higher. In other words, the same job can be done equally well by a variety of amino acids. Thus, the rate of evolution in terms of mutant substitutions by random drift becomes high.'

Although the influence of external events plays a major role in determining the survival of a species over another, and species may react differently to alterations of their habitat, only some of such features may have developed for adaptation, while most of them may be arising by pure randomness in the recombination of genes.

I.3 The neutral theory of Biodiversity and Biogeography

When the neutral theory of molecular evolution was published, the idea of a fundamental equivalence in fitness of species was not completely new in ecology. Already in 1957 theories that are effectively neutral at the species level had started appearing, the most famous being 'the theory of island biogeography' by Robert H. MacArthur and Edward Osborne Wilson [116]. The observation of biodiversity in archipelagos of Melanesia and Florida had showed that fewer species live on islands than those living in areas of the same

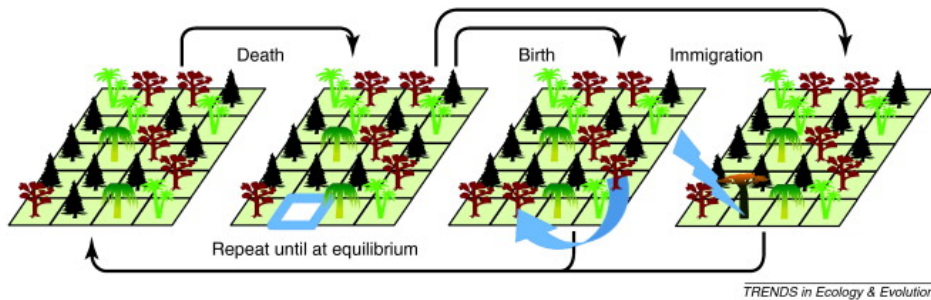


Figure I.3.1: **Unified neutral theory of biodiversity and biogeography.** Illustration of the model proposed by Hubbell. The ecosystem is saturated with exactly one individual in each site of a regular lattice. At each step an individual dies and is replaced by one individual of a species already present in the system (birth event) or by one of a new species (immigration event). Source [152].

size taken in the continent. A new model was therefore built, where insular species are maintained in an equilibrium between immigration from the mainland and local extinction. In this scenario, neutrality was expressed at the species level: species are considered altogether and are subject to the same stochastic rules. Differences in their physical appearance, group strategies and reciprocal interactions are completely neglected to retain only the effects of random dispersal and local extinction.

The success of MacArthur and Wilson's theory contrasted with what was the *status quo* of theoretical ecology. At the time of its publication, the greatest majority of theoretical ecologists believed that each species has a functional role and occupies a specific niche where it flourishes by consuming a specific set of resources. In this view, species coexist in an interactive equilibrium, and have evolved to be the best competitor in their own area and for a particular set of resources. However, the models arising from this viewpoint often rely on many parameters and are not deduced from first principles. One example is the so called 'Broken stick model' by MacArthur himself [115].

The theory of island biodiversity, instead, makes the implicit assumption that all of these effects are negligible compared to the effect of randomness in dispersal and in local extinction. In this new viewpoint, communities are open, non-equilibrium assemblages of

species largely dominated by random events. Species come and go, and their presence or absence is dictated by stochastic rules.

These two approaches have been seen as largely antithetical and mutually exclusive for a long time, and the heated debate on the superiority of one over the other has run on similar rails as the dualism among selectionism and neutralism for molecular evolution.

In 2001 Hubbell gathered some of the results of this debate in a monograph called 'The unified neutral theory of Biodiversity and Biogeography' in which he also presented a first unification [94].

The new theory aims at modelling species that are on a same trophic level, i.e. that compete for the same pool of limited resources. Typical examples of con-trophic species are plants in a forest or corals in a coral reef, because all of them place demands on similar resources like carbon, light and nitrate.

Neutral theories had been around for a long time. The elements of novelty of this new formulation resided in considering individuals, and not just species, to be identical. In this setting, organisms of the same community have identical per-capita probabilities of giving birth, dying, migrating and speciating regardless of the species they belong to. As the original neutral theory formulated by Kimura, this new theory postulates that fluctuations are the biggest factor in shaping the distribution of abundances, and deterministic effects stemming from fitness differences are completely neglected (although deterministic effects can still emerge in the dynamics).

The assumption of ecological neutrality raised many controversies because, at first look, it comes in sharp contrast with the classical concepts of niche theory and evolutionary balance. As Hubbell states in his book, 'niche differences are not essential to coexistence, if by "coexistence" we mean the persistence in sympatry of species for geologically significant lengths of time'.

Much of the misunderstanding may arise from what biologists mean by equilibrium and

coexistence. In the neutral theory an equilibrium arises between speciation, immigration and local extinction. In such framework all species turn out to be transient, despite having times to extinction of the order of millions to tens of millions of years (as emerges from the models).

Neutral theory has proved to describe several macro-ecological patterns through just very few adjustable parameters, and its simplicity has guaranteed mathematical and quantitative treatment. It has also provided valuable information in the cases where it has failed. It can be put under test in experiments as an actual scientific theory and it tells us what to expect when the observed macroecological patterns emerge as a consequence of randomness. As such, it is an effective null model for ecological patterns [4, 152, 153, 38, 5, 15, 22, 36, 104, 110, 122, 147].

The model described by Hubbell in 2001 analyzes the dynamical behavior of a meta-community composed of identically sized local communities. Each patch exchanges individuals with the meta-community, and the equilibrium abundance probability is calculated explicitly. However, no explicit spatial degree of freedom within the local communities is analysed, and individuals are considered to be well mixed. In order to analyse further the potentiality of neutral theory, it is necessary to extend such analysis to encompass spatial movement.

I.4 Spatial modelling of ecosystems

For analysing the spatial patterns of ecosystems, many different descriptors have been introduced over the years. Often described as "one of community ecology's few genuine laws" and one of the earliest to be introduced [8], the Species Area Relationship (SAR) relates the number of species of an ecosystem to the size of the sampled area. It is widely studied as a measure of spatial biodiversity, and implicitly quantifies the extent to which larger habitats support more species than smaller ones. From empirical observations, it is

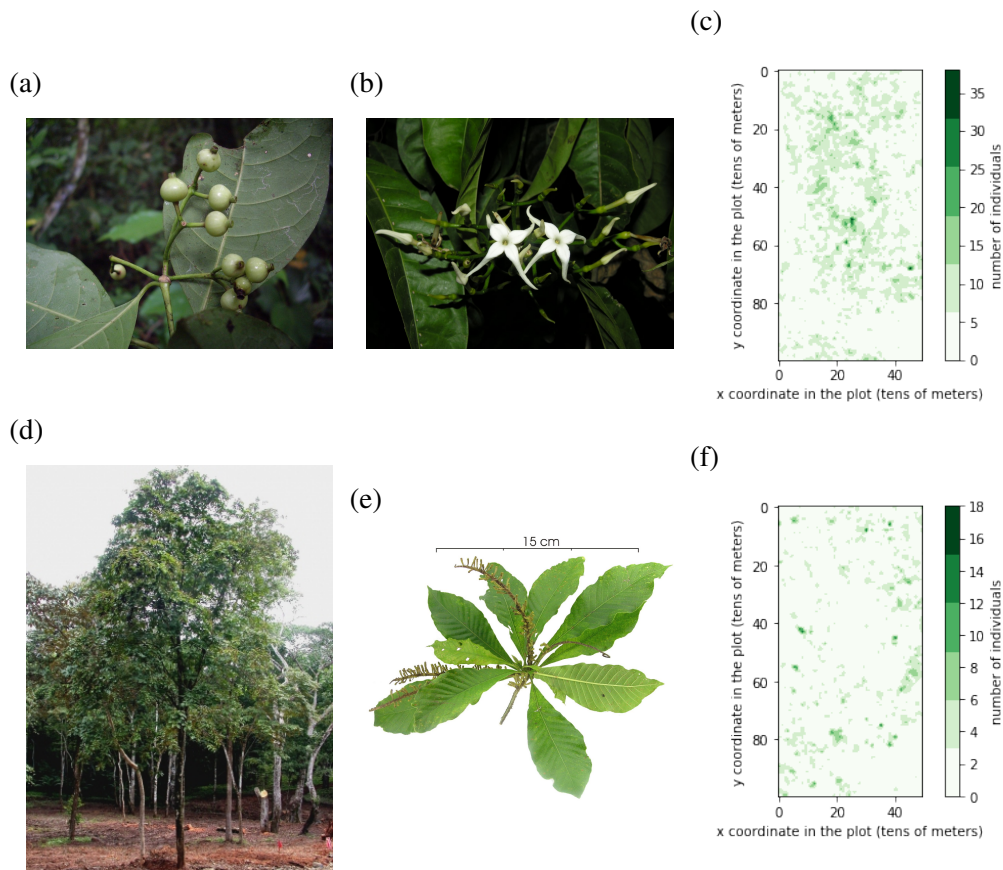


Figure I.3.2: **Spatial distribution of species in the BCI Panama plot** The figure reports pictures of two species of plants present in the Barro Colorado island forest reserve in Panama and the position of individuals within a 500×1000 meters plot. Figures (a), (b) and (c) refer to the species *Faramia Occidentalis*, and in particular (a) reports a picture of its immature fruits, (b) of its flowers and (c) of its geographical distribution. Figures (e), (f) and (g), instead, refer to the species *Alseis Blackiana*, and in particular (e) reports a picture of the whole tree, (f) of its flowers and leaves and (g) of its geographical distribution. Individuals of each species are not randomly distributed, and tend to be close to each other. More details on the Barro Colorado forest reserve and on its lowland forest inventory will be given in chapter IV. Pictures are taken from <http://hasbrouck.asu.edu/neotrop/>.

often found to display an inverted S shape in a log-log scaled plot, with a linear behavior at small and large areas, and similarly power law at intermediate scales [146, 145]. Such shape is ubiquitous in ecology, and has been seen also in systems with very different environmental and climatic characteristics [149]. Many models have also been seen to

display such qualitative behavior [67, 154, 56], even using different dispersal rules [150, 82]. Its robustness has been analysed also against different sampling strategies [88, 184], and in light of different speciation magnitudes [139].

Another important ecological descriptor of spatial patterns is the β -diversity, which measures the differences in species composition with distance. One way to define it (and the most used in empirical applications) is "the probability that two randomly chosen individuals at a certain distance are con-specific, i.e. belong to the same species" [113, 47]. For analysing the spatial turnover of species, the two point correlation function is also used, typically under the assumption of translational invariance [107]. The Relative Species abundance, instead, gives the probability that a randomly picked species has exactly n individuals in a certain area [6, 45, 44, 173, 175]. These three descriptors are not independent from each other, and hold important information about the dynamical properties of an ecosystem, such as the spatial and temporal scales of variation of the abundance of species, and the overall rate of speciation and migration into the ecosystem [78].

Well-mixed models neglect spatial degrees of freedom or include them only implicitly. They are conceptually and mathematically simple, and this is why they are so widely used [174]. However, there is empirical and theoretical evidence that spatial dispersal plays a crucial role in maintaining species diversity (fig I.3.2) [169, 59].

Spatially explicit models, intended as systems where individuals' spatial location and movement is analysed explicitly, instead are poorly understood, especially if compared to their well-mixed counterparts [121, 61, 38, 58, 60, 128]. Only in a few cases analytical formulas have been obtained, while the analysis has more frequently focused on computational approaches. This has hindered a full-understanding of the effect of spatial dispersal, e.g. on the stability or on the structural properties of ecosystems, ultimately limiting the range of applications of theoretical models.

In [183] the analysis of a stochastic patch-occupancy model has highlighted the presence of three distinct classes of stationary configurations. In the low-dispersal regime local

extinctions occur more quickly, on average, than the rate of immigration from adjacent patches. The system segregates spontaneously into independent spatial domains. At intermediate dispersal rates, immigrants arrive in patches more frequently than local extinction occurs, but the dispersal is not strong enough to synchronize local variations across the system. This is the most extinction-robust scenario. Patches are immediately recolonized after a local extinction. The high-dispersal regime covers the range of dispersal rates that lead to synchronized local dynamics across the entire meta-population. Here the system operates as a single, fully homogenized patch.

One of the most well-studied neutral models is the so called 'voter model with speciation', or multi-species voter model (MVM). It was originally developed for opinion dynamics [112, 34, 124, 125], and has since been expanded to many other areas such as epidemic diffusion and linguistics [143, 120].

In its original formulation, voters are placed on a network and each can choose among a set of q 'opinions'. In ecological applications, voters become individuals, they live on a regular lattice and their opinion corresponds to the species they belong to [111, 31]. At each time step, one site is chosen and the individual is removed, corresponding to a death event. Then, the empty site is filled with a certain probability by an individual of a new species, and this corresponds to a speciation event, while with complementary probability the new occupier is chosen to be from one of the existing species, thus accounting for birth events. The possible choices are often restricted to the species of individuals occupying nearest neighboring sites, thus introducing spatial dependence into the model. In general one can consider more complicated dispersal rules and enlarge the set of possible options by assigning different probabilities of colonization according to different distances.

The MVM is clearly a neutral model, as the microscopic dynamics is the same for all individuals. It is also a zero-sum process, because the total number of individuals is conserved. Within such model it is possible to calculate the β -diversity analytically, and the resulting functional form captures quite well the behavior of empirical data from different

forest censa [37]. However, no analytic formula has been derived for SAR or SAD, and over the years the analysis has been restricted to computational simulations or scaling assumptions [188]. The model displays the tri-phasic behavior of the SAR, thus holding further qualitative resemblance to field data. Different dispersal kernels have been analyzed [150] and numerical evidence has showed that SARs can be rescaled onto a universal function of only the area and the speciation rate [139].

In the MVM, the environment is saturated and every time a gap opens, following a death event, such place is immediately filled by a new individual. This is expected to be a good approximation of real dynamics in resource-rich ecosystems, while in sparser cases the environment is not always saturated and empty patches can exist. More recently a spatial neutral model was proposed where site occupancy is not bounded [133]. In the new model individuals die or reproduce with constant per capita rate, and when a birth event happens the newborn is located according to a dispersal distribution, thus introducing spatial effects into the system. Speciation events happen at a constant rate, thus preventing the system from reaching the trivial equilibrium state where all species have gone extinct. This model can be mapped into a field theory. An analytic result was obtained in [133], under the assumption that detailed balance and time invariance is satisfied. Despite being a guaranteed feature of the well-mixed model [100, 81], spatial dispersal breaks such temporal symmetry, and therefore conclusions based on this assumption are in fact unreliable [81]. Other extensions, or different approaches, have been attempted over the years, which however rely on non-rigorous simplifications or further assumptions [151, 135]

Finally, most of the stochastic models are analysed only at stationarity and neglect temporal fluctuations. Nonetheless, time correlations arise naturally in physical systems, and ultimately are of fundamental importance for preserving and monitoring endangered habitats [23, 163, 39, 42]. Statistical comparison of time-dependent patterns is usually much more difficult than the stationary analysis, because it requires more data and longer empirical time series, which are rarely available in ecology. Some success with a simple neutral

model was obtained in [13], but there is theoretical and empirical evidence that forest dynamics exhibits signatures of environmental stochasticity [108, 99, 40, 3]. Models based only on demographic stochasticity indeed tend to overestimate the expected times to extinction for abundant species. The difficulty of including environmental variability stems from the diverse nature and origin of such fluctuations [50, 91, 161], which, for example, can arise from variations in rainfall, temperature, fire outbreaks and pests.

I.5 Criticality and scale invariance

The theory of phase transitions was initially introduced with the goal of understanding the existence of permanent magnets (i.e. ferromagnetism). A pivotal role in such analysis was played by the Ising model: in its classic formulation random variables, the spins, can take only two possible values, $s = \pm 1$, at each site of a regular lattice. Local interactions promote their alignment, while thermal noise tends to randomize their orientations. The configuration at stationarity can be a disordered state for sufficiently high temperatures, while below a critical temperature interactions prevail and an ordered state arises in which the spins are aligned and the average magnetization is not zero [106, 100].

One can therefore recognise three broad classes of equilibrium configurations for spin systems. In the *supercritical* case the temperature is higher than the critical temperature and the system is in a disordered state. In the *subcritical* case the temperature is below the critical value and interactions promote the local alignment of spins (i.e. spin tend to have the same orientation, since energetically this is more stable), and in such case a net non-zero magnetisation can arise. The cases of a temperature exactly equal to the critical value are instead called '*critical*'.

In biological modelling, the notion of criticality has been used with rather different meanings depending on the context. In its classical formulation, it refers to a drastic shift in the behavior of a system following only minimal variations in its key features. A paradig-

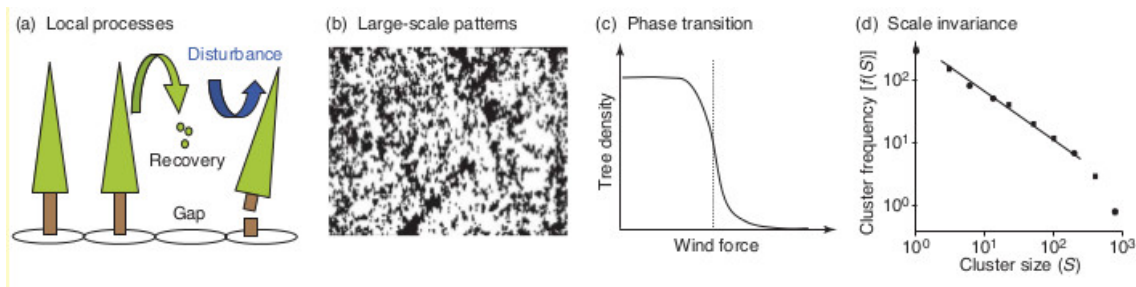


Figure I.5.1: **Criticality in ecosystems.** The figure shows some key concepts in the classic theory of criticality. In panel (a) local disturbance and recovery lead to the emergence of long-range correlations in the distribution of organisms, as showed in panel panel (b). The typical descriptors of the system, such as the density of trees, hence spontaneously poise themselves at a specific point where they can react promptly to such external forces (panel (c)), and it can be seen that this generates patterns with a complicated structure, which often display power-law distribution of abundances, as in panel (d). Source [137].

matic example is the brain, which has been observed to be poised at the boundary between a completely inactive and a fully epileptic state [137].

In models of communities of living organisms, individuals are born and die at certain rates, whose details depend on the system at hand (e.g. there may be interactions or environmental variations). If the average birth rate exceeds the average death rate, the total population of the system is going to increase without limit (or it increases until the carrying capacity is reached) because new individuals will appear faster than others disappear. Conversely, if the average birth rate is smaller than the average death rate (and if immigration and speciation effects are negligible) the system is going to deplete and the equilibrium distribution is that of an empty (or close to empty) system.

The statistical mechanics models that emerge from data of communities of living organisms, like trees in a forest, microbes in a water basin or humans in cities, often display birth and death per capita rates that are almost equal (if the carrying capacity is treated implicitly) [171]. One consequence of this observation is that the abundances of individuals are subject to very large fluctuations, and local occupation numbers appear correlated over large distances. In this regime spatial dispersal strongly influences large scale patterns.

Over the years different mechanisms have been deemed responsible for such behaviour. Large fluctuations may be triggered by fire outbreaks in a forest, disease spreads in bacterial communities or exceptional predation periods among animals. The ability to recover from such events is a key requirement for all living systems, and a basic robustness must be developed at least against the most frequent of such threats [137, 126] (fig I.5.1).

Recently, also arguments from information theory have been used to explain how a general adaptive mechanism for self-tuning to criticality can arise. In order to cope with the perceived signals, emanating from a given environmental source, an organism must retain information on the external inputs in the best possible way. Being able to better tune with such external conditions would provide it with a strong competitive advantage. There is mathematical proof that the optimal encoding parameters lay always around the peak of the generalized susceptibility, also known as 'Fisher information' [90, 89]. In such framework different complex sources can be best accounted for through small changes in the behavioural strategies.

The concept of criticality has been largely expanded over the years. Systems considered 'close to the critical point' have been compared with each other and commonalities have been highlighted. Among these it was discovered that critical systems often lack a characteristic spatial scale. Indeed, as the system approaches the critical point it is typical to find power-law distributions of individual abundances and an overall dis-homogeneity of spatial density. One of the paradigmatic examples is that of rainforests. The analysis of their biodiversity distributions often reveals a huge separation in abundances between rare and hyperdominant species, a phenomenon also known as 'Fisher paradox' [171]. Local abundances also appear to be correlated over large spatial scales.

Very often, the presence of a power law distribution has been used as a sufficient proof for considering a system as 'critical'. Power law distributions in adaptive systems have an old history, with first observations in the context of language dating back to 1913 [9, 96, 26]. The case of a power law with exponent minus two is often called Zipf law

[189]. Other examples have been found in the distribution of populations in cities, in that of family names and also of employees in firms [130]. Zipf laws have also been observed in mathematical systems where an unobserved variable (or variables) is present or when the system is affected by environmental variability [156, 126, 117]. Other scaling relationships, i.e. power-law probability distributions with different exponents, are also observed in river networks, in percolating systems [17], and in the number of species within a same genus from fossil records [118].

In search of scale invariant properties of ecological patterns, a model independent framework has been proposed in [187]. Two different sets of ecological data are analysed, one from a serpentine grassland and one from the Barro Colorado Island (BCI) forest stand, and despite the differences (e.g. in one case the SAR has a seemingly power-law behavior, in the other it shows deviations at all scales) both the BCI forest and the grassland show very good collapse into a unique, universal curve upon the tuning of just one parameter. Similar collapse was found in simulations of the MVM [188].

One of the main results that will be presented in this thesis is the proof that in a simple birth-death spatial model for ecosystems the distribution of the number of individuals is form-invariant at all scales when fluctuations are large. How and why such a choice has emerged in nature, and if it confers any evolutionary advantage to the species, will not be analysed, but analytical formulas will be derived that allow for the quantitative prediction of some spatial patterns in ecosystems. Further on, I also show how power law distributions arise when local fluctuations in the individuals' birth and death rates become non-negligible compared to demographic fluctuations.

This thesis is organised as follows. Chapter II introduces the general setting of birth-death Markov jump processes and analyses some examples, first in the mean-field case and later using a phenomenological spatial extension. Chapter III rigorously analyses a linear spatial stochastic birth death model for ecosystems in terms of an individual-based formulation of a metapopulation model. It shows how to calculate an accurate equa-

tion for the probability distribution of the number of individuals living in a certain area when the fluctuations are large. In chapter IV simulations of the process are considered. First, a new simulation scheme is introduced, which is optimised for the stationary distribution of stochastic differential equations, and then the results of simulated data are compared to analytic formulas. The same analytic results are used to make predictions of the abundance of individuals in real ecological datasets from two lowland tropical forest inventories. Chapter V concentrates on the effect of environmental fluctuations on spatial patterns of biodiversity. Analytic results are obtained and are compared to simulations of a phenomenological model. Finally, Chapter VI draws some conclusions, summarises the main findings and identifies the most promising research questions that can benefit from the results of this thesis.

Chapter II

Mean-field and a phenomenological spatial model

Hubbel's neutral theory seeks to capture the influence of speciation, extinction, dispersal and ecological drift on the macro-scale patterns of ecosystems. In its simplest formulation, it also assumes that individuals are independent and demographically alike on a per capita basis. Obviously, this remains an approximation and there is clear evidence that species behave differently even within the same taxa [57]. Nonetheless, neutral theory is simple enough to allow for a tractable null theory of community assembly. This chapter will focus on the mathematical analysis of the distributions that emerge from neutral dynamics in a simple birth-death process within a well-mixed setting and on a first, phenomenological, spatial extension.

II.1 Master equation and detailed balance

I will denote by \mathbf{c} the configuration of an ecosystem. Throughout this thesis \mathbf{c} will take different forms: at first it will be a vector with the total abundances of the different species.

Later on, it will include the local abundances of each individual in the spatial setting. In the spirit of simplification 'Markovian' dynamics will also be assumed.

Indicating by $p(\mathbf{c}, t | \mathbf{c}_0, t_0)$ the probability that the configuration \mathbf{c} is seen at time t given that the configuration at time t_0 was \mathbf{c}_0 (abbreviated $p(\mathbf{c}, t)$), its time evolution (with time independent jump rates) will be given by the following master equation (ME)

$$\frac{\partial p(\mathbf{c}, t)}{\partial t} = \sum_{\mathbf{c}'} \left[T(\mathbf{c} | \mathbf{c}') p(\mathbf{c}', t) - T(\mathbf{c}' | \mathbf{c}) p(\mathbf{c}, t) \right] \quad (\text{II.1.1})$$

where $T(\mathbf{c}' | \mathbf{c})$ is the transition rate from \mathbf{c} to \mathbf{c}' [100, 68]. If stationarity can be reached, the probability distribution becomes independent of t for $t \rightarrow \infty$. I will denote the equilibrium distribution by $P(\mathbf{c})$.

Together with the initial conditions and the boundary conditions, the function $T(\mathbf{c}' | \mathbf{c})$ determines the dynamics of the stochastic process. Among the many possible choices for $T(\mathbf{c}' | \mathbf{c})$, there are some that satisfy a very interesting property, called detailed balance (DB), i.e.

$$T(\mathbf{c} | \mathbf{c}') P(\mathbf{c}') - T(\mathbf{c}' | \mathbf{c}) P(\mathbf{c}) = 0 \quad (\text{II.1.2})$$

Substituting eq (II.1.2) into eq (II.1.1), it is immediate to observe that a probability distribution that satisfies detailed balance is also a stationary solution of the ME. On the other hand, not all stationary distributions satisfy detailed balance.

It is possible to show that a necessary and sufficient condition for the validity of DB is that for any cycle in the space of configurations (i.e. the space where \mathbf{c} is defined), the probability of moving through it in one direction is equal to the probability of moving in the opposite direction [100, 186]. More precisely, DB is satisfied if and only if for any choice of a closed path $\{\mathbf{c}_1, \dots, \mathbf{c}_m, \mathbf{c}_1\}$, with m an arbitrary number, the following holds

$$T(\mathbf{c}_1 | \mathbf{c}_2) T(\mathbf{c}_2 | \mathbf{c}_3) \cdots T(\mathbf{c}_m | \mathbf{c}_1) = T(\mathbf{c}_1 | \mathbf{c}_m) T(\mathbf{c}_m | \mathbf{c}_{m-1}) \cdots T(\mathbf{c}_2 | \mathbf{c}_1) \quad (\text{II.1.3})$$

This condition is called Kolmogorov criterion, and corresponds to the time-reversibility condition. In fact, it states that a process that moves in one direction in the space of configurations is equally as probable as a process that goes in the opposite direction.

In the following chapters, I show that detailed balance is violated in processes where spatial diffusion is coupled to auto-catalytic reactions (such as a birth event proportional to the local number of individuals) [81].

The models presented in the following paragraph instead preserve DB. This allows for a much easier mathematical treatment, and for the analytic calculation of the stationary distribution.

II.2 Birth Death mean field process

This paragraph introduces two non-spatial, well-mixed neutral models for ecosystems. The states of the system are denoted by $\mathbf{c} = (n_1, \dots, n_S) = \mathbf{n}$, where n_i indicates the abundances of species $i = 1, \dots, S$ and S denotes the total number of species in the system.

In nature, a single individual parent may give birth to several individuals at a time, and many individuals may die altogether. For simplicity, here only a one step processes will be considered, where at each infinitesimal time step δt only one birth or death event can happen.

The jump rates here are renamed as $T((n_1, \dots, n_\alpha + 1, \dots)|\mathbf{n}) = b_\alpha(\mathbf{n})$, i.e. $b_\alpha(\mathbf{n})$ is the birth rate for species α when the system is in state \mathbf{n} , and $T((n_1, \dots, n_\alpha - 1, \dots)|\mathbf{n}) = d_\alpha(\mathbf{n})$ is instead the death rate for species α when this latter is in state \mathbf{n} .

In general, the birth and death rates of one species can depend on all other species through interactions. If the model is neutral, they become symmetric functions of the n_i and do not depend on the species label. If one further assumes that species are independent from each

other, it is also possible to completely neglect interactions, so that each species becomes disentangled from the dynamics of the others.

With these simplifications in mind, one is left with $b_\alpha(\mathbf{n}) = b_n$ and $d_\alpha(\mathbf{n}) = d_n$, with n labelling the abundance of the generic species. The probability distribution of the process, which before was denoted $p(\mathbf{c}, t)$, will now drop its dependence on all other species and will retain only one (i.e. therefore the α label will be dropped). Denoting it with $p_n(t)$, its evolution is described by the following master equation

$$\frac{\partial p_n(t)}{\partial t} = p_{n+1}(t)d_{n+1} + p_{n-1}(t)b_{n-1} - p_n(t)(b_n + d_n) \quad (\text{II.2.1})$$

and boundary conditions need to be chosen for $n = 0$.

Note that, in this scenario, each species abundance can be considered as an independent realizations of the process.

In order to specify the model, one needs to define the jump rates. In a context where individuals are completely neutral the birth and death per capita rates (i.e. d_n/n and b_n/n) are constant.

This assumption is just a first simplification. In empirical datasets, it is often observed that rare species have a mild per-capita reproductive advantage over more abundant ones. Over the years many hypothesis have been formulated on how this arises. One hypothesis is that host-specific pathogens or predators act in the vicinity of the maternal parent. This spatially structured effect suppresses the most abundant species allowing more uncommon ones to spread. Another hypothesis considers that species respond in a species-specific manner to the fluctuating environment, and the external conditions influence inter-species and intra-species interactions in such a way as to favour a higher diversity [14].

The following paragraphs analyse two different choices for the birth-death per capita rates. The main difference among them is the way they take into consideration boundary conditions and the rare-species reproductive advantage.

II.3 Stationary Solution of the BD process

The choice of boundary conditions for eq (II.2.1) is not always straightforward and often depends on the type of applications at hand. The use of absorbing boundary conditions at $n = 0$ leads to a stationary distribution where all species have gone extinct. Questions related to population extinction are important problems in mathematical biology, but, as we are here chiefly interested in the long-time coexistence of multiple species, reflecting boundary conditions are preferred. These latter often mimic the rare species advantage mentioned in the previous paragraph. In such case $b_n > 0$ and $d_n = 0$ when $n = 0$, and imposing that the left hand side of eq (II.2.1) is zero it is easy to calculate that $P_n = \lim_{t \rightarrow \infty} p_n(t)$ for $n = 1, 2, 3, \dots$ takes the form

$$P_n = P_0 \prod_{i=0}^{n-1} \frac{b_i}{d_{i+1}} \quad (\text{II.3.1})$$

with P_0 being the probability of $n = 0$ and it can be determined from normalisation conditions.

Here, I analyse two choices of birth-death rates which have been the subject of intense research in theoretical ecology [14, 133, 13, 178, 176]. Both of them introduce a mild reproductive advantage for rare species at the individual level, which effectively acts as a reflecting boundary condition.

The first choice [177] is the following

$$b_n = b n + \nu \delta_{n,0} \quad d_n = r n \quad (\text{II.3.2})$$

where b , r and ν are positive constants. The stationary probability distribution is readily obtained to be

$$P_n = P_0 \frac{\nu x^n}{r^n n!}$$

where $x = b/r$ is assumed to be smaller than one for normalisation purposes (i.e. $r > b$). Denoting with S the total empirical number of species in the ecosystem and with Φ_n the number of species with n individuals at equilibrium, from eq (II.3.1) for $n > 0$ one also gets

$$\langle \Phi_n \rangle = SP_0 \prod_{i=0}^{n-1} \frac{b_i}{d_{i+1}} = \theta \frac{x^n}{n}$$

where $x = b/r < 1$ and $\theta = SP_0\nu/r$. This is the celebrated Fisher log-series distribution, i.e. the distribution Ronald Fisher proposed to describe the empirical abundance of species in real ecosystems. It was seen experimentally for the first time as early as in 1943 [14].

Another choice of rates, different from that implemented in eq (II.3.2), considers instead the following

$$b_n = b n + b_0 \quad d_n = r n \quad (\text{II.3.3})$$

In the rest of this thesis, I will refer to the birth-death model defined by these rates and by the master equation (II.2.1) as the BD (for birth-death) model. The constant term b_0 can be readily interpreted as an immigration or speciation coefficient, or a sum of both. Once again, the stationary distribution can be calculated explicitly from eq (II.3.1), and leads to the following negative binomial distribution

$$P_n = \binom{n + \frac{b_0}{b} - 1}{n} x^n (1 - x)^{\frac{b_0}{b}} \quad (\text{II.3.4})$$

where $x = b/r$ as before.

This probability distribution displays an internal mode for $\frac{b_0}{b} > 1$, and allows to describe a much larger set of abundance distributions. Indeed, it is often observed empirically that the effect of immigration is not negligible, and that the relative species abundance displays a unimodal behavior.

The study of discrete probability distributions has provided a first look into the properties of the birth death process, but to proceed further in the analysis and gain deeper insight

one needs to introduce more sophisticated mathematical techniques.

II.4 Diffusion approximation with the Kramers-Moyal expansion

In this paragraph I describe one of the most common and broadly used 'diffusion' approximations: the so called 'Kramers-Moyal expansion'.

Markovian dynamics will be considered, as defined in eq (II.1.1), with the configurations of the system being the total abundances of species, $\mathbf{n} = (n_1, \dots, n_S)$, with n_α the abundance of the α -th species and S the total number of species. For simplicity the ecosystem is assumed to be always saturated with N individuals in total, although this hypothesis comes in contrast with that of independence of species. Nonetheless, in the regime of large N (compared to the abundance of each species) the two assumptions are compatible with each other. It is also the most commonly accepted approach in the literature for neutral models of ecosystems [14].

As before, only one individual can be born at each time step δt . Neutral dynamics and the independence of species will also be assumed. In such framework, I use the following notation: $\mathcal{W}^+(n)$ is the (time independent) rate with which one individual is added to a species when its abundance is n , and equivalently $\mathcal{W}^-(n)$ is the rate of removing one individual to species α when the species has n individuals.

The master equation that describes the probability distribution of the abundance of a species at time t is therefore

$$\begin{aligned} \frac{\partial p(n, t)}{\partial t} = & \mathcal{W}^-(n+1)p(n+1, t) + \mathcal{W}^+(n-1)p(n-1, t) \\ & - \mathcal{W}^+(n)p(n, t) - \mathcal{W}^-(n)p(n, t) \end{aligned}$$

I make the assumption that $\mathcal{W}^+(\cdot)$ and $\mathcal{W}^-(\cdot)$ are only functions of $x = n/N$. With a slight abuse of notation, I will indicate by $p(x, t)$ the probability that $n = xN$ (i.e. I change the name of the variable at the argument of $p(x, t)$). The result is the following equation

$$\begin{aligned} \frac{\partial p(x, t)}{\partial t} = & \mathcal{W}^-\left(x + \frac{1}{N}\right) p\left(x + \frac{1}{N}, t\right) + \mathcal{W}^+\left(x - \frac{1}{N}\right) p\left(x - \frac{1}{N}, t\right) \\ & - \mathcal{W}^-(x) p(x, t) - \mathcal{W}^+(x) p(x, t) \end{aligned}$$

In an ecosystem, one expects the total number of individuals to be very large. The equation above suggests a Taylor expansion of $\mathcal{W}^+(\cdot)$, $\mathcal{W}^-(\cdot)$ and $p(\cdot)$ around x for small $\varepsilon = \frac{1}{N}$, at least far from the boundaries. This is known as the Kramers-Moyal expansion [68].

Considering terms up to second order in $N \rightarrow \infty$ yields the following

$$\begin{aligned} \frac{\partial p(x, t)}{\partial t} = & -\frac{1}{N} \frac{\partial}{\partial x} [A(x)p(x, t)] \\ & + \frac{1}{2N^2} \frac{\partial^2}{\partial x^2} [B(x)p(x, t)] + \mathcal{O}(N^{-3}) \end{aligned} \quad (\text{II.4.1})$$

where

$$\begin{aligned} A(x) &= \mathcal{W}^+(x) - \mathcal{W}^-(x) \\ B(x) &= \mathcal{W}^+(x) + \mathcal{W}^-(x) \end{aligned}$$

and, truncating eq (II.4.1) at $\mathcal{O}(N^{-2})$, the result is the Fokker-Planck equation of the system. Retaining only the first order in N , one recovers the deterministic evolution of the system, also called Liouville equation, i.e.

$$\frac{\partial p(x, t)}{\partial t} = -\frac{1}{N} \frac{\partial}{\partial x} [A(x)p(x, t)] + \mathcal{O}(N^{-1}) \quad (\text{II.4.2})$$

If the initial condition is expressed in terms of a delta, i.e. $p(x, 0) = \delta(x - x_0)$, with x_0 a

constant, the abundances solve the following deterministic equation

$$\dot{x}(t) = A(x, t)$$

For simplicity of notation, it is normally preferred to scale back to the initial variable naming, i.e. to replace $xN \rightarrow n$. This is a slight abuse of notation, and it is important not to forget that with n we in fact indicate a continuous variable at this point.

II.4.1 BD process with the Kramers-Moyal expansion

In this section, the Kramers-Moyal expansion is applied to the birth death process with rates as in eq (II.3.3). The procedure is not rigorous, but nonetheless it represents one of the most common approaches in the literature [16, 13] and it serves as a term of comparison with a more rigorous approach, that will be introduced in the next paragraph.

In the context of the model defined by eq (II.3.3), the Fokker-Planck equation at (II.4.1) reads

$$\frac{\partial p(x, t)}{\partial t} = -\frac{\partial}{\partial n} \left[(b_0 - \mu n) p(n, t) \right] + \sigma^2 \frac{\partial^2}{\partial n^2} \left[(n + \epsilon) p(n, t) \right] \quad (\text{II.4.3})$$

where I have introduced the following constants

$$\mu = r - b \quad \sigma^2 = \frac{r + b}{2} \quad \epsilon = \frac{b_0}{r + b}$$

It is easy to verify that the equilibrium solution of such equation has the following form

$$p(n, t \rightarrow \infty) = P(n) = P_0 (n + \epsilon)^{\frac{b_0 + \mu \epsilon}{\sigma^2} - 1} e^{-\frac{\mu n}{\sigma^2}} \quad (\text{II.4.4})$$

where P_0 is a normalization constant. If one further considers $\sigma^2 \gg \mu$, the following is

obtained

$$P(n) = \left(\frac{\mu}{\sigma^2}\right)^{\frac{b_0}{\sigma^2}} \frac{n^{\frac{b_0}{\sigma^2}-1} e^{-\frac{\mu n}{\sigma^2}}}{\Gamma(b_0/\sigma^2)} \quad (\text{II.4.5})$$

which is a gamma distribution of shape b_0/σ^2 and scale σ^2/μ .

Transforming the initial discrete equation into a partial differential equation has clearly led to many advantages. However, in this approach one does not have the control over the regimes of parameters where eq (II.4.5) is a good approximation of the full stationary probability distribution.

The following paragraph shows a more rigorous approach to obtain an equally insightful diffusion approximation.

II.5 Diffusion approximation in the "critical limit"

When a system is close to the critical point, the fluctuations in the abundance of individuals become very large. In this paragraph, I will make use of this observation and consider a limit in the parameters' values that will determine a diffusion approximation of the BD model.

Starting from the birth-death master equation, eq (II.2.1), substituting the rates at eq (II.3.3) one obtains

$$\frac{\partial p_n(t)}{\partial t} = p_{n+1}(t) r (n+1) + p_{n-1}(t) [b (n-1) + b_0] - p_n(t) [(b+r)n + b_0]$$

I introduce the following parameter $\varepsilon = \frac{r-b}{r}$ and rescale the number of individuals as $n = \tilde{n} \frac{r}{r-b} = \tilde{n}/\varepsilon$, i.e.

$$\begin{aligned} \frac{\partial p_{\tilde{n}}(T)}{\partial T} = & p_{\tilde{n}+\varepsilon}(T) \frac{1}{\varepsilon^2} (\tilde{n} + \varepsilon) + p_{\tilde{n}-\varepsilon}(T) \left[\frac{g}{r\varepsilon^2} (\tilde{n} - \varepsilon) + \frac{b_0}{\mu} \right] + \\ & - p_{\tilde{n}}(T) \left[\frac{g+r}{r\varepsilon^2} \tilde{n} + \frac{b_0}{\mu} \right] \end{aligned}$$

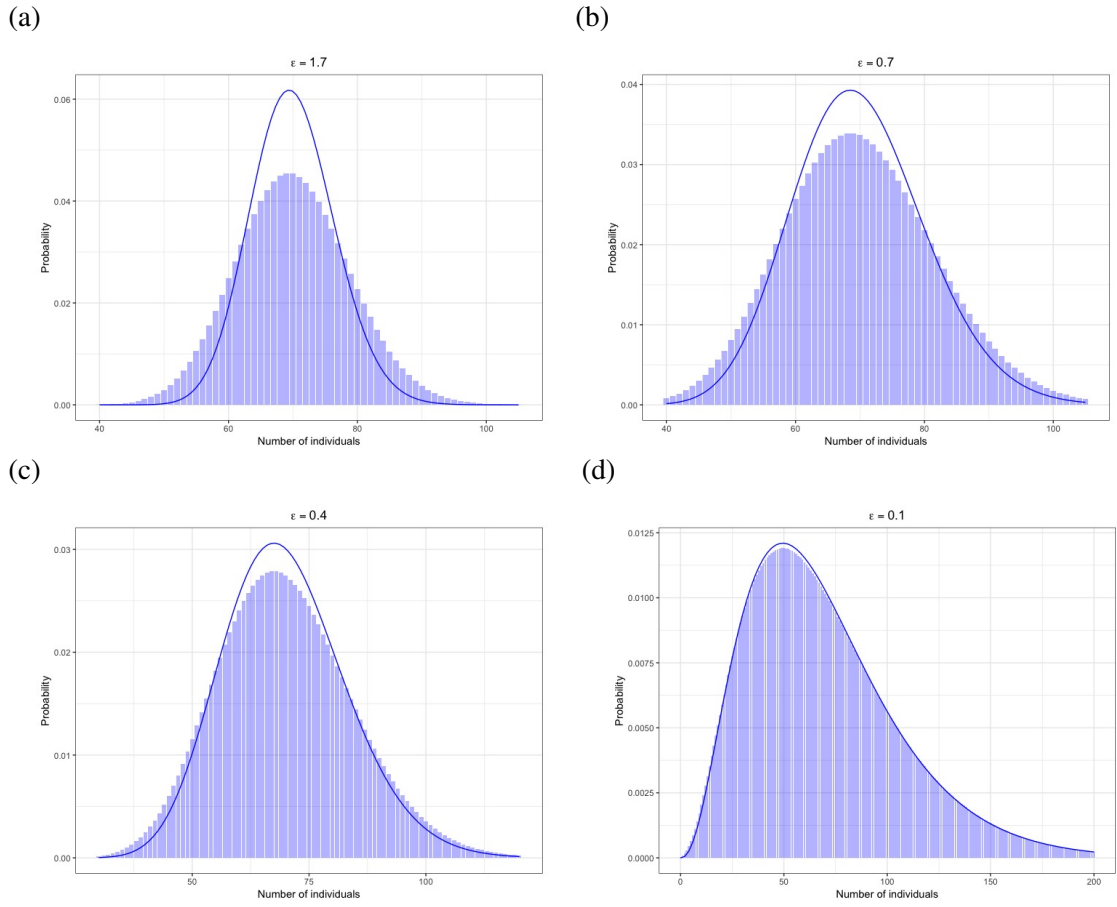


Figure II.5.1: **Diffusion approximation in the critical limit.** The figure compares the negative binomial distribution at eq (II.3.4) (histograms) and the gamma distribution at eq (II.5.3) (blue line). In plot (a) parameters are $b_0 = 70$, $b = 0.1$ and $r = 1.1$, in plot (b) $b_0 = 70$, $b = 1$ and $r = 2$, in plot (c) $b_0 = 70$, $b = 2$ and $r = 3$ and in plot (d) $b_0 = 70$, $b = 20$ and $r = 21$. In the titles the value of $\epsilon = \frac{2(r-b)}{r+b}$ is reported. Note that as it becomes small the two distributions come closer to each other.

where $t = \mu T$, with $\mu = r - b$. Expanding up to second order in ϵ and noticing that $b/r = 1 - \epsilon$ the following holds

$$\begin{aligned} \frac{\partial p_{\tilde{n}}(T)}{\partial T} = & \left(p_{\tilde{n}}(T) + \frac{\partial p}{\partial \tilde{n}}(T) \epsilon + \frac{\partial^2 p}{\partial \tilde{n}^2}(T) \epsilon^2 + \mathcal{O}(\epsilon^3) \right) \frac{1}{\epsilon^2} (\tilde{n} + \epsilon) + \\ & + \left(p_{\tilde{n}}(T) - \frac{\partial p}{\partial \tilde{n}}(T) \epsilon + \frac{\partial^2 p}{\partial \tilde{n}^2}(T) \epsilon^2 + \mathcal{O}(\epsilon^3) \right) \left[\frac{1 - \epsilon}{\epsilon^2} (\tilde{n} - \epsilon) + \frac{b_0}{\mu} \right] + \\ & - p_{\tilde{n}}(T) \left[\frac{2 - \epsilon}{\epsilon^2} \tilde{n} + \frac{b_0}{\mu} \right] \end{aligned}$$

and so, rearranging, one obtains

$$\begin{aligned} \frac{\partial p_{\tilde{n}}(T)}{\partial T} &= p_{\tilde{n}}(T) + \tilde{n} \frac{\partial p}{\partial \tilde{n}}(T) - \frac{b_0}{r} \frac{\partial p_{\tilde{n}}}{\partial \tilde{n}}(T) + \tilde{n} \frac{\partial^2 p}{\partial \tilde{n}^2}(T) = \\ &= - \frac{\partial}{\partial \tilde{n}} \left[\left(\frac{b_0}{\mu} - \tilde{n} \right) p_{\tilde{n}} \right] + \frac{\partial^2}{\partial \tilde{n}^2} (\tilde{n} p_{\tilde{n}}) + \mathcal{O}(\varepsilon) \end{aligned}$$

As before, for simplicity I rescale back to n , i.e. $\tilde{n}/\varepsilon \rightarrow n$, where now n is to be considered as a continuous variable. The final result is the following Fokker-Planck equation

$$\frac{\partial p(n, T)}{\partial T} = - \frac{\partial}{\partial n} \left[\left(\frac{b_0}{\mu} - n \right) p(n, t) \right] + \frac{r}{\mu} \frac{\partial^2}{\partial n^2} [n p(n, t)]$$

For consistency with the previous notation, I rewrite the coefficient r/μ considering that

$$\frac{r}{\mu} = \frac{1}{\varepsilon} = \frac{r + b + (r - b)}{2\mu} = \frac{r + b}{2\mu} + \frac{1}{2}$$

Therefore as $\varepsilon \rightarrow 0$ the term $1/2$ is negligible and $\frac{r}{\mu} = \frac{r+b}{2\mu} = \frac{\sigma^2}{\mu}$.

In the final form, the Fokker-Planck equation for $p_n(t)$ (which I now write $p(n, t)$) in the limit of $\varepsilon \rightarrow 0$ reads

$$\frac{\partial p(n, t)}{\partial t} = - \frac{\partial}{\partial n} \left[(b_0 - \mu n) p(n, t) \right] + \sigma^2 \frac{\partial^2}{\partial n^2} [n p(n, t)] \quad (\text{II.5.1})$$

which in the Itô prescription is associated to the following Langevin equation

$$\dot{n}(t) = b_0 - \mu + \sigma \sqrt{n} \xi(t) \quad (\text{II.5.2})$$

with $\xi(t)$ being a zero mean, gaussian white noise with autocorrelation $\langle \xi(t) \xi(t') \rangle = 2\delta(t - t')$.

The stationarity solution is calculated imposing that the left hand side of eq (II.5.1) is zero. It is hence easy to calculate that $P(n)$, the stationary probability distribution of the

model, is a gamma distribution, and takes the following explicit form

$$P(n) = \left(\frac{\mu}{\sigma^2}\right)^{\frac{b_0}{\mu}} \frac{n^{\frac{b_0}{\sigma^2}-1} e^{-\frac{\mu n}{\sigma^2}}}{\Gamma(b_0/\sigma^2)} \quad (\text{II.5.3})$$

which indeed is equal to that calculated in eq (II.4.5). The variance of this distribution is equal to $\frac{b_0}{\mu} \frac{\sigma^2}{\mu}$ and hence the limit for $\sigma^2/\mu \rightarrow \infty$ is also a limit for large fluctuations. This justifies why, in the following, we will refer to such limit as the "critical limit".

Considering further the limit of small immigration, $\frac{b_0}{\sigma^2} \ll 1$, the continuous approximation of the Fisher log-series is obtained, i.e.

$$P(n) \propto n^{\frac{b_0}{\sigma^2}-1} e^{-\frac{\mu n}{\sigma^2}} = n^{-1} x^n$$

and hence $P(n, t \rightarrow \infty) \propto \frac{x^n}{n}$ with $x = e^{-\frac{\mu}{\sigma^2}}$. This can be therefore considered as the probability distribution in the limit of small immigration, conditional of the species not having gone extinct (i.e. conditional on not having reached the absorbing $n = 0$ point).

II.6 Time dependent solution of the BD process

The models analysed so far are simple enough to admit a closed-formula solution even for the discrete stationary solution, as calculated. In such cases, the diffusion approximation seems superfluous. Things change when more complicated systems are considered, or when one wants to calculate the time-dependent evolution of the process. Discrete equations are notoriously more difficult to treat, while the analysis of PDEs can rely on a plethora of powerful mathematical techniques.

The solution of the differential equation in (II.5.1) can be calculated analytically even at any time t . This is done by introducing the Laplace transform of $p(n, t)$, and solving the equation in the space of moments. Imposing reflecting boundary conditions at each time

t , and for initial conditions of the type $p(n, 0) = \delta(n - n_0)$, with $n_0 > 0$ a constant, after some non banal and rather involved calculations (for details see [13]), one obtains

$$p(n, t|n_0, 0) = \left(\frac{\mu}{\sigma^2}\right)^{\frac{b_0}{\sigma^2}} n^{\frac{b_0}{\sigma^2}-1} e^{\frac{n\mu}{\sigma^2}} \frac{[(\mu/\sigma^2)^2 n_0 n e^{-\mu t}]^{\frac{1}{2}-\frac{b_0}{2\sigma^2}}}{1 - e^{-\mu t}} \times \quad (\text{II.6.1})$$

$$\times \exp\left[-\frac{(\mu/\sigma^2)(n + n_0)e^{-\mu t}}{1 - e^{-\mu t}}\right] I_{\frac{b_0}{\sigma^2}-1}\left[\frac{(2\mu/\sigma^2)\sqrt{n_0 n e^{-\mu t}}}{1 - e^{-\mu t}}\right]$$

where $I_\nu(\cdot)$ is a modified Bessel function of the first kind.

Since $I_\nu(z) \approx (z/2)^\nu/\Gamma(\nu + 1)$ as $z \rightarrow 0^+$, it is easy to calculate that, in the limit $t \rightarrow \infty$, one indeed re-obtains the stationary solution as in eq (II.5.3).

From equation (II.5.1), one can also easily calculate the time evolution of the average number of individuals: multiplying on both sides by n and integrating from zero to infinity one gets

$$\frac{\partial}{\partial t}\langle n \rangle(t) = b_0 - \mu\langle n \rangle(t)$$

which, setting $\langle n \rangle(t = 0) = n_0$, yields

$$\langle n \rangle(t) = \frac{b_0}{\mu} + \left(n_0 - \frac{b_0}{\mu}\right) e^{-\mu t} \quad .$$

Similarly, multiplying eq (II.5.1) by n^2 and integrating one gets the equation for the second moment $\langle n^2 \rangle$

$$\frac{\partial}{\partial t}\langle n^2 \rangle(t) = 2\langle n \rangle(t)b_0 - 2\mu\langle n^2 \rangle(t) + 2\sigma^2\langle n \rangle(t)$$

which is solved by

$$\langle n^2 \rangle(t) = \left(\frac{b_0}{\mu}\right)^2 + \frac{\sigma^2 b_0}{\mu \mu} + 2\left(\frac{b_0}{\mu} + \frac{\sigma^2}{\mu}\right)\left(n_0 - \frac{b_0}{\mu}\right)\left(e^{-\mu t} - e^{-2\mu t}\right) - \frac{\sigma^2 b_0}{\mu \mu} e^{-2\mu t}$$

As $t \rightarrow \infty$, this expression converges to $\langle n^2 \rangle(t) = \left(\frac{b_0}{\mu}\right)^2 + \frac{b_0 \sigma^2}{\mu \mu}$ (I will henceforth omit the

time dependence at $\langle \cdot \rangle$ when considering stationary values, i.e. $\langle \cdot \rangle = \langle \cdot \rangle(t \rightarrow \infty)$, and the variance of the equilibrium distribution is the same as that of eq (II.5.3), as it should.

Another important pattern for applications is the so called 'turnover distribution'. It measures the rate at which individuals leave the system and are replaced by new individuals. In ecology, it reflects the continuous reassembly through immigration, emigration and local extinction.

The species turnover distribution (STD) measures the probability that the ratio of abundances of a species separated by a time interval t , $n(t)/n(0)$, is equal to m , i.e.

$$\begin{aligned} STD(m, t) &= \left\langle \delta\left(\frac{n}{n_0} - m\right) \right\rangle = \\ &= \int_0^\infty dn_0 \int_0^\infty dn p(n, t|n_0, 0) p(n_0) \delta\left(m - \frac{n}{n_0}\right) \end{aligned} \quad (\text{II.6.2})$$

Under stationary conditions, i.e. considering that $p(n_0)$ is the stationary distribution of eq (II.5.3) and $p(n, t|n_0, 0)$ is given by eq (II.6.1), it takes the following explicit form [13]

$$\begin{aligned} STD(m, t) &= A \frac{m+1}{m} \frac{(e^{\mu t})^{\frac{b_0}{2\sigma^2}}}{1 - e^{-\mu t}} \left(\frac{\sinh(\mu t/2)}{m}\right)^{\frac{b_0}{\sigma^2} + 1} \times \\ &\quad \times \left(\frac{4m^2}{(m+1)^2 e^{\mu t} - 4m}\right)^{\frac{b_0}{\sigma^2} + \frac{1}{2}} \end{aligned} \quad (\text{II.6.3})$$

where A is a normalization constant. Notice that this distribution depends only on two parameters, i.e. b_0/σ^2 and μ .

The models considered so far have analysed well-mixed environments, where the spatial degrees of freedom are neglected in order to focus on the internal dynamics of the community. In the following paragraph, I consider a first extension of the analysis and incorporate spatial diffusion in a phenomenological way.

II.7 A Phenomenological Model

Well-mixed models are conceptually and mathematically simple, and are a good first framework for testing the hypothesis of neutral theory. However, such a simplistic approach cannot account for the spatial turnover of species, the increase in species richness with the sampled area, and for the overall key factors determining species coexistence [169].

In spatially extended systems, one expects that individuals of the same species are found close-by rather than further apart. For example, in the case of trees this is a consequence of the limitation of seed dispersal onto the ground.

In this paragraph, I consider a natural, yet not rigorous, extension of the BD model. This work has been peer reviewed and published, and is available as reported in [138].

The set of (continuous) abundances of individuals are here defined at each site of a regular d -dimensional lattice. Space is thus subdivided into voxels, each with $2d$ nearest neighbours, and within each voxel individuals are considered well-mixed and treated as point-like particles which undergo the demographic birth-death dynamics described in the previous paragraph.

By indicating with a the length of the voxel side (equivalently the lattice spacing), we assume that a is much smaller than all the other macroscopic length scales of interest, including the spatial correlation scale of the system.

Inspired by the Langevin equation of the mean field system, eq (II.5.2), I hence consider the following set of stochastic differential equations

$$\dot{n}_i = D\Delta_i n_i(t) + b_0 - \mu n_i(t) + \sigma\sqrt{n_i(t)}\xi_i(t) \quad (\text{II.7.1})$$

where $n_i(t)$ is the (continuous) number of individuals in site i at time t , $\xi_i(t)$ is a zero mean Gaussian white noise with correlations $\langle \xi_i(t)\xi_j(t') \rangle = \delta_{i,j}\delta(t-t')$, D is the diffusion

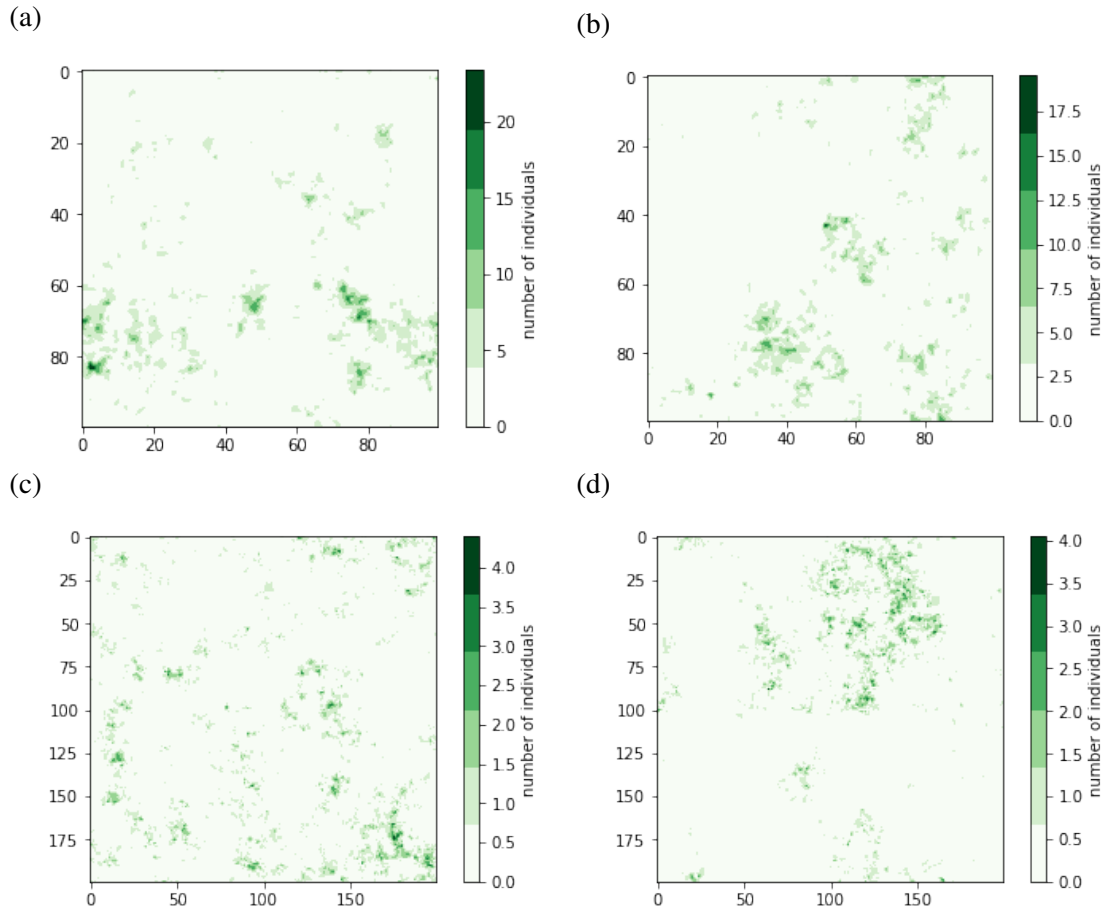


Figure II.7.1: **Snapshots of the phenomenological model** The figure reports four configurations of the phenomenological model defined by eq (II.7.2). Panels (a) and (b) refer to a system with parameters $D = 20$, $b_0 = 0.1$, $\mu = 0.1$, $\sigma = 10$. Panels (c) and (d) instead refer to a systems with parameters $D = 100$, $b_0 = 0.01$, $\mu = 0.1$, $\sigma = 10$. More details on how these snapshots were calculated will be given in Chapter IV.

coefficient that regulates the spatial correlations among sites and Δ_i the discrete Laplace operator defined as

$$\Delta_i n_i(t) = \sum_{j:|i-j|=1} [n_j(t) - n_i(t)]$$

Equation (II.7.1) has been considered without any derivation. Such heuristic model will be revisited in terms of a metapopulation model, and formulated as an individual-based system in the next chapters. At this stage, it must be considered only as an intuitive (and non-rigorous) spatial extension of the BD model, which nonetheless will allow for some useful insight.

Reactions taking place inside each voxel are supposed to be the main source of stochasticity in the system defined at eq (II.7.1). As a consequence, upon switching off the birth and death events and leaving only spatial diffusion (i.e. putting $b, r, b_0 = 0$), the resulting process is purely deterministic (indeed $\sigma, \mu = 0$) and the stochasticity due to the random hopping of individuals is completely neglected (i.e. one does not observe the random walk on the mesh).

This may appear as an inconsistency of the approach, since eq (II.7.1) is supposed to be a continuous approximation of a *stochastic* birth death process in space. In Chapter III a rigorous procedure will be undertaken which will clarify this point. In this paragraph, instead, I will focus on the properties (e.g. the local mean and two point correlation) of the random field defined by eq (II.7.1).

By indicating with $\{n\} = \{n_1, n_2, \dots, n_i, \dots\}$ the configuration of abundances on the lattice, with n_i being the (continuous) number of individuals in site i , in the Itô prescription the probability density function of $p(\{n\}, t)$ satisfies the following Fokker-Planck equation

$$\begin{aligned} \partial_t p(\{n\}, t) = & - \sum_i \frac{\partial}{\partial n_i} \left[\left(D \Delta_i n_i(t) + b_0 - \mu n_i \right) p(\{n\}, t) \right] + \\ & + \sigma^2 \sum_i \frac{\partial^2}{\partial n_i^2} [n_i^2 p(\{n\}, t)] \end{aligned} \quad (\text{II.7.2})$$

where the sums are over all the sites of the lattice. Similarly to the mean field case, by multiplying on both sides for n_k and integrating one obtains the mean number of individuals per site, which at stationarity reads $\langle n_k \rangle = \frac{b_0}{\mu}$. The calculation of the spatial two-point correlation and variance is a bit more involved and is analysed in the following paragraphs. See figure II.7.1 for the representation of some configurations of the random field.

II.8 Pair Correlation of the Phenomenological model

The diffusion term in equation (II.7.1) correlates the sites in the lattice with each other. For calculating the two point correlation function, defined as $\langle n_l n_k \rangle$, I first multiply equation (II.7.2) by $n_l n_k$ and integrate over all values of n in each site. The equation I obtain is the following

$$\frac{\partial}{\partial t} \langle n_l n_k \rangle(t) = D[\Delta_l \langle n_l n_k \rangle(t) + \Delta_k \langle n_l n_k \rangle(t)] + 2b_0 \langle n \rangle(t) - 2\mu \langle n_l n_k \rangle(t) + 2\sigma^2 \langle n \rangle(t) \delta_{l,k}$$

In order to focus on stationary patterns, I drop the term at LHS and indicate with $\langle n_l n_k \rangle$ the stationary two point correlation (i.e. $\langle n_l n_k \rangle(t \rightarrow \infty)$). For notation purposes, I also introduce the following function $G_{l,k} = \langle n_l n_k \rangle - \langle n_l \rangle \langle n_k \rangle = \langle n_l n_k \rangle - \langle n \rangle^2$, which is defined at stationarity. Substituting into the equation one gets

$$D(\Delta_i G_{i,j} + \Delta_j G_{i,j}) - 2\mu G_{i,j} + 2\sigma^2 \langle n \rangle \delta_{i,j} = 0 \quad (\text{II.8.1})$$

I now introduce a system of Cartesian coordinates and indicate with \mathbf{x} the d -dim position vector of a site. I hence make the substitution $i \rightarrow \mathbf{x}$ and $j \rightarrow \mathbf{y}$, and notice that the coordinates of the sites lay at multiples of a . I further introduce a Fourier series expansion, which, since we are considering an infinite lattice and the system is homogeneous, is

written as

$$\mathcal{G}(\mathbf{p}) = \sum_{\mathbf{x}, \mathbf{y}} e^{i\mathbf{p}\cdot(\mathbf{x}-\mathbf{y})} G_{\mathbf{x}, \mathbf{y}}$$

Multiplying eq (II.8.1) by $e^{i\mathbf{k}\cdot(\mathbf{x}-\mathbf{y})}$ and summing over all \mathbf{x}, \mathbf{y} , the following is obtained

$$\frac{D}{a^2} \mathcal{G}(\mathbf{p}) \left[\sum_{k=1}^d \left(e^{ip_k a} + e^{-ip_k a} - 2 \right) \right] - \mu \mathcal{G}(\mathbf{p}) + 2\sigma^2 \langle n \rangle = 0$$

where p_k is the k -th component of vector \mathbf{p} . This leads to

$$\mathcal{G}(\mathbf{p}) = \frac{\sigma^2 b_0}{\mu^2} \frac{1}{1 + \frac{2D}{\mu a^2} \sum_{k=1}^d (1 - \cos(p_k a))}$$

In order to obtain $G_{\mathbf{x}, \mathbf{y}}$ one needs to anti-transform $\mathcal{G}(\mathbf{p})$ via the following

$$G_{\mathbf{x}, \mathbf{y}} = \left(\frac{a}{2\pi} \right)^d \int_{\mathcal{C}} d\mathbf{p} \mathcal{G}(\mathbf{p}) e^{-i\mathbf{p}\cdot(\mathbf{x}-\mathbf{y})}$$

which stems from the definition of $\mathcal{G}(\mathbf{p})$. Here, \mathcal{C} is the hypercubic d -dimensional primitive unit cell of size $2\pi/a$. Therefore

$$G_{\mathbf{x}, \mathbf{y}} = \left(\frac{a}{2\pi} \right)^d \frac{\sigma^2 b_0}{\mu^2} \int_{\mathcal{C}} d\mathbf{p} \frac{e^{-i\mathbf{p}\cdot(\mathbf{x}-\mathbf{y})}}{1 + \frac{2D}{\mu a^2} \sum_{k=1}^d (1 - \cos(p_k a))}$$

This integral can be solved explicitly using Watson's integrals. In the one dimensional case $G_{x,y}$ reduces to the following simple exponential

$$G_{x,y} = C k^{|x-y|/a} \tag{II.8.2}$$

where k and C are positive constants that can be calculated from eq (II.8.1). Indeed, imposing that the equation is solved for $x \neq y$ one gets

$$\frac{D}{a^2} (k + 1/k - 2) - \mu = 0$$

and hence

$$k = 1 + \frac{\mu a^2}{2D} - \frac{\mu a^2}{2D} \sqrt{1 + \frac{4D}{\mu a^2}}$$

From these relationships, one also deduces the correlation length of the system (indicated with λ in the following). Indeed, upon re-writing eq (II.8.2) as $G_{x,y} = C e^{\frac{|x-y|}{a} \log(k)}$ one can observe that $\lambda = -a/\log(k)$, and that it converges to $\sqrt{D/\mu}$ as $a \rightarrow 0$. At the same time for $x = y$ in eq (II.8.1) one gets

$$C 2 \frac{D}{a^2} (k-1) - \mu C + \sigma^2 \langle n \rangle = 0$$

which leads to

$$C = \frac{\sigma^2 b_0}{\mu} \frac{1}{\mu} \left(1 + \frac{4D}{\mu a^2}\right)^{-1/2}$$

In more general terms, one can obtain a good deal of simplification by taking the continuous spatial limit, $a \rightarrow 0$. To accommodate such limit, one first needs to rescale parameters as

$$\bar{D} = D a^2 \quad \bar{b}_0 = \frac{b_0}{a^d}$$

Considering the first order terms in the limit of $a \rightarrow 0$, I will indicate with $\bar{G}(\mathbf{x}, \mathbf{y})$ the leading order term of $G_{x,y}$ in the continuous spatial limit (i.e. $a \rightarrow 0$). The result is

$$\begin{aligned} \bar{G}(\mathbf{x}, \mathbf{y}) &= \frac{1}{(2\pi)^d} \frac{\sigma^2 b_0}{\mu^2} \int_{\mathbb{R}^d} d\mathbf{p} \frac{e^{i\mathbf{p}(\mathbf{x}-\mathbf{y})}}{1 + \frac{D}{\mu} \mathbf{p}^2} \\ &= \frac{\bar{\rho}^2 \langle n \rangle^2}{(2\pi \bar{\lambda})^2} \left(\frac{|\mathbf{x} - \mathbf{y}|}{\bar{\lambda}} \right)^{1-\frac{d}{2}} K_{1-\frac{d}{2}} \left(\frac{|\mathbf{x} - \mathbf{y}|}{\bar{\lambda}} \right) \end{aligned} \quad (\text{II.8.3})$$

where $K_\nu(\cdot)$ is the modified Bessel function of the second kind and of order ν [1], \mathbf{x} and \mathbf{y} are vector of coordinates and

$$\bar{\lambda} = \sqrt{\frac{\bar{D}}{\mu}} \quad , \quad \bar{\rho} = \sqrt{\frac{\sigma^2}{\bar{b}_0}}$$

For applications and for comparison to empirical datasets, a very important quantity is the Pair Correlation Function (PCF), which is defined as

$$g_{\mathbf{x},\mathbf{y}} = \frac{\langle n_{\mathbf{x}}n_{\mathbf{y}} \rangle}{\langle n \rangle^2} \quad (\text{II.8.4})$$

The reason why one prefers this ratio over the simpler two-point correlation $\langle n_{\mathbf{x}}n_{\mathbf{y}} \rangle$ is that in a first approximation it is independent of the lattice side a .

Since $g_{\mathbf{x},\mathbf{y}} = 1 + \mathcal{G}_{\mathbf{x},\mathbf{y}}/\langle n \rangle^2$, by indicating with $\bar{g}(\mathbf{x},\mathbf{y})$ the leading order term for $g_{\mathbf{x},\mathbf{y}}$ in the continuous spatial limit, in the two dimensional case the PCF reduces to

$$\bar{g}(\mathbf{x},\mathbf{y}) = 1 + \frac{1}{2\pi} \left(\frac{\bar{\rho}}{\bar{\lambda}} \right)^2 K_0 \left(\frac{r}{\bar{\lambda}} \right) \quad (\text{II.8.5})$$

where $r = |\mathbf{x} - \mathbf{y}|$.

The regimes of large and small spatial correlation are particularly important. From the properties of the Bessel function $K_\nu(x)$, it is easy to obtain

$$\bar{g}(x, y) = \begin{cases} -\frac{1}{2\pi} \left(\frac{\bar{\rho}}{\bar{\lambda}} \right)^2 \log \left(\frac{r}{\bar{\lambda}} \right) & \text{for } \frac{r}{\bar{\lambda}} \rightarrow 0 \\ \frac{1}{2\sqrt{2\pi}} \sqrt{\frac{\bar{\lambda}}{r}} \left(\frac{\bar{\rho}}{\bar{\lambda}} \right)^2 e^{-\frac{r}{\bar{\lambda}}} & \text{for } \frac{r}{\bar{\lambda}} \rightarrow \infty \end{cases}$$

Therefore, the correlation decays exponentially at large distances while it increases arbitrarily (logarithmically) at small distances. Departing from the continuous spatial limit, these considerations are valid only when the condition $|\mathbf{x} - \mathbf{y}| \gg a$ holds. In the discrete system, the logarithmic divergence for $r \ll \bar{\lambda}$ is not observed. At scales comparable to the lattice spacing a , one should use the discrete two-point correlation function obtained before.

II.9 The conditional probability distribution

Ecological spatial patterns try to describe quantitatively the biodiversity present in specific areas of an ecosystem. Smaller areas have been seen to sustain fewer species than larger ones, and individuals of a same species have a higher probability to be found close-by rather than farther apart. As observed in the previous paragraphs, in a neutral framework where species are independent the observed number of individuals for each one of them can be considered as independent realisations of the same stochastic process. However, even in this simplified framework the scaling of the probability distribution with the size of the area can not be easily calculated [14].

For understanding how biodiversity changes with scale, in the models I will analyse in this thesis I will focus on the number of individuals present in a circular area \mathcal{V} (or ball in higher dimensions, or segment in one dimension) of radius R . In the discrete spatial system I therefore define the following random variable

$$N_{\mathcal{V}} = \sum_{i \in \mathcal{V}} n_i \quad .$$

which indeed accounts for the total number of individuals living in \mathcal{V} . Since calculations turn out to be easier in the continuous spatial framework, I rescale the parameters as done in previous sections and take the limit of the lattice side $a \rightarrow 0$, i.e.

$$N_{\mathcal{V}} = \sum_{i \in \mathcal{V}} n_i \rightarrow N(R) = \int_{\mathcal{V}} n(\mathbf{x}) d\mathbf{x}$$

where now $n(\mathbf{x})$ is a density of individuals. I hence indicate with V the Lebesgue measure of the area (or volume, or length depending on the dimension) of the d -dimensional ball, i.e.

$$V = \frac{\pi^{d/2}}{\Gamma\left(\frac{d}{2} + 1\right)} R^d$$

In order to calculate the mean value $\langle N_{\mathcal{V}} \rangle$ at stationarity, I multiply by $\sum_{j \in \mathcal{V}} n_j$ equation (II.7.2) and then integrate. Since I have assumed that the model is homogeneous, I find the following

$$\langle N(R) \rangle = \frac{\bar{b}_0 V}{\mu} \quad (\text{II.9.1})$$

The calculation of the second moment of the equation can be calculated similarly. First, I multiply twice eq (II.7.2) for $N_{\mathcal{V}}$ and then I integrate over all the values of $\{n\}$. Alternatively, I first proceed with calculating the function $\langle n(x)N(R) \rangle$ and then integrate over $x \in \mathcal{V}$.

It is worth remarking that all the analysis carried out below, which is related to the "phenomenological model", will be of fundamental importance also in the next chapters. In fact, similar equations are found also in the analysis of the spatial model analysed in chapter III.

As a first step, I sum for $i \in \mathcal{V}$ on both sides of eq (II.8.1). Considering the continuous spatial limit I obtain the following equation at stationarity

$$\begin{aligned} \frac{\bar{D}}{\mu} \int_{\mathcal{V}} d\mathbf{y} \nabla_{\mathbf{y}}^2 \langle n(\mathbf{x})n(\mathbf{y}) \rangle + \frac{\bar{D}}{\mu} \nabla_{\mathbf{x}}^2 \langle n(\mathbf{x})N_{\mathcal{V}} \rangle - 2 \langle n(\mathbf{x})N_{\mathcal{V}} \rangle + \\ + 2 \frac{\bar{b}_0 \bar{b}_0 V}{\mu \mu} + 2 \frac{\sigma^2 \bar{b}_0}{\mu \mu} \Theta(R - |x|) = 0 \end{aligned} \quad (\text{II.9.2})$$

where $|x|$ is the radial distance of point \mathbf{x} from the center of \mathcal{V} and $\Theta(z)$ is the Heaviside step function, which takes value $\Theta(z) = 1$ for $z \geq 0$ and $\Theta(z) = 0$ for $z < 0$.

As calculated in the previous section, $\langle n(\mathbf{x})n(\mathbf{y}) \rangle$ is a function only of the distance among \mathbf{x} and \mathbf{y} . Assuming that the system is homogeneous, the following holds

$$\nabla_{\mathbf{y}}^2 \langle n(\mathbf{x})n(\mathbf{y}) \rangle = \nabla_{\mathbf{x}}^2 \langle n(\mathbf{x})n(\mathbf{y}) \rangle$$

Therefore, equation (II.9.2) reduces to

$$\bar{\lambda}^2 \nabla_{\mathbf{x}}^2 \langle n(\mathbf{x})N_{\mathcal{V}} \rangle - \langle n(\mathbf{x})N_{\mathcal{V}} \rangle + \langle n \rangle \langle N(R) \rangle + \frac{\sigma^2}{\mu} \langle n \rangle \Theta(R - |\mathbf{x}|) = 0 \quad (\text{II.9.3})$$

Equation (II.9.3) must be solved separately for $R \leq |\mathbf{x}|$ and $R \geq |\mathbf{x}|$. Boundary conditions at $|\mathbf{x}| = R$ and the continuity of the spatial derivative of $\langle n(\mathbf{x})N_{\mathcal{V}} \rangle$ in $|\mathbf{x}|$ will fix the values of the integration constants. In Appendix A, I show the details of these long, but otherwise straightforward, calculations. Here I only report the results.

For $|\mathbf{x}| \leq R$ one obtains

$$\langle n(\mathbf{x})N(R) \rangle = \langle n \rangle \langle N(R) \rangle + \frac{\sigma^2}{\mu} \langle n \rangle \Psi\left(\frac{|\mathbf{x}|}{\lambda}, \frac{R}{\lambda}\right) \quad (\text{II.9.4})$$

where

$$\Psi\left(\frac{|\mathbf{x}|}{\lambda}, \frac{R}{\lambda}\right) = 1 - \left(\frac{|\mathbf{x}|}{R}\right)^{1-\frac{d}{2}} \frac{K_{\frac{d}{2}}\left(\frac{R}{\lambda}\right) I_{\frac{d}{2}-1}\left(\frac{|\mathbf{x}|}{\lambda}\right)}{I_{\frac{d}{2}-1}\left(\frac{R}{\lambda}\right) K_{\frac{d}{2}}\left(\frac{R}{\lambda}\right) + K_{\frac{d}{2}-1}\left(\frac{R}{\lambda}\right) I_{\frac{d}{2}}\left(\frac{R}{\lambda}\right)} \quad (\text{II.9.5})$$

Note that I have defined the function $\Psi\left(\frac{|\mathbf{x}|}{\lambda}, \frac{R}{\lambda}\right)$ only for $|\mathbf{x}| \leq R$.

Instead for the case of $|\mathbf{x}| \geq R$ one obtains

$$\begin{aligned} \langle n(\mathbf{x})N(R) \rangle = & \langle n \rangle \langle N(R) \rangle + \\ & + \frac{\sigma^2}{\mu} \langle n \rangle \left(\frac{|\mathbf{x}|}{R}\right)^{1-\frac{d}{2}} \frac{I_{\frac{d}{2}}\left(\frac{R}{\lambda}\right) K_{\frac{d}{2}-1}\left(\frac{|\mathbf{x}|}{\lambda}\right)}{I_{\frac{d}{2}-1}\left(\frac{R}{\lambda}\right) K_{\frac{d}{2}}\left(\frac{R}{\lambda}\right) + K_{\frac{d}{2}-1}\left(\frac{R}{\lambda}\right) I_{\frac{d}{2}}\left(\frac{R}{\lambda}\right)} \end{aligned} \quad (\text{II.9.6})$$

These two functions give the correlation between the number of individuals at a point \mathbf{x} and the sum of individuals in \mathcal{V} . Notice that, in both cases, the correlation decreases as $|\mathbf{x}|$ increases. Moreover, as $|\mathbf{x}| \rightarrow \infty$, one gets $\langle n(\mathbf{x})N(R) \rangle = \langle n(\mathbf{x}) \rangle \langle N(R) \rangle$, and hence the abundances in \mathbf{x} and those in \mathcal{V} become uncorrelated.

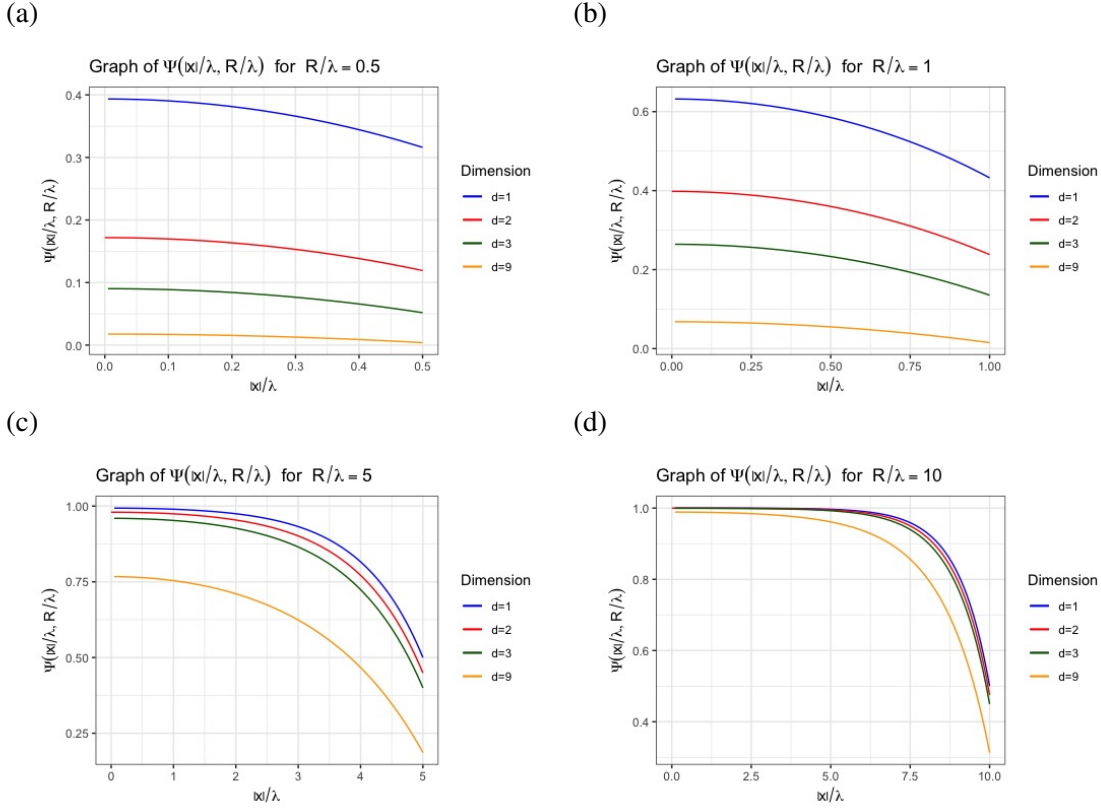


Figure II.9.1: **Plots of $\Psi\left(\frac{|\mathbf{x}|}{\lambda}, \frac{R}{\lambda}\right)$** The figure reports the plot of the function $\Psi\left(\frac{|\mathbf{x}|}{\lambda}, \frac{R}{\lambda}\right)$ as calculated in equation (II.9.5). Panel (a) has $R/\bar{\lambda} = 0.5$, panel (b) $R/\bar{\lambda} = 1$, panel (c) $R/\bar{\lambda} = 5$ and panel (d) $R/\bar{\lambda} = 10$. As $R/\bar{\lambda} \rightarrow 0$, $\Psi(\cdot)$ tends to zero uniformly. Instead, for $R/\bar{\lambda} \rightarrow \infty$, $\Psi(\cdot)$ tends to one uniformly, regardless of the dimension.

One consideration, that will become very important later on, regards the limit of such functions for small and large correlation length.

From the properties of the Bessel functions, in the limit of large argument $z \rightarrow \infty$ it is well-known that the following holds [1]

$$I_\nu(z) = \frac{e^z}{\sqrt{2\pi z}} \left(1 + \mathcal{O}(1/z)\right) \quad K_\nu(z) = \sqrt{\frac{\pi}{2z}} e^{-z} \left(1 + \mathcal{O}(1/z)\right) \quad (\text{II.9.7})$$

and note that the limit is independent of the order ν .

Fixing $|\mathbf{x}|$, R and all the other parameters and using the relationship at eq (II.9.7), it is

easy to show that for $\bar{\lambda}/R \rightarrow 0$

$$\Psi\left(\frac{|\mathbf{x}|}{\bar{\lambda}}, \frac{R}{\bar{\lambda}}\right) = 1 + \mathcal{O}\left[e^{-\frac{R-|\mathbf{x}|}{\bar{\lambda}}}\left(\frac{|\mathbf{x}|}{R}\right)^{1-d}\right]$$

and therefore for $\bar{\lambda}/R \rightarrow 0$

$$\langle n(\mathbf{x})N(R) \rangle \rightarrow \langle n \rangle \langle N(R) \rangle + \frac{\sigma^2}{\mu} \langle n \rangle \quad \text{for } |\mathbf{x}| < R$$

At the same time, from a direct calculation, it is also immediate to show that, in the same limit

$$\langle n(\mathbf{x})N(R) \rangle \rightarrow \langle n \rangle \langle N(R) \rangle \quad \text{for } |\mathbf{x}| > R$$

The case of $\bar{\lambda}/R \rightarrow \infty$ is more involved. After careful calculation (or via a software for algebraic calculus, e.g. Wolfram Mathematica), it is possible to show that fixing $|\mathbf{x}|$, R and all the other parameters and for $|\mathbf{x}| < R$ the following equations hold

$$\Psi\left(\frac{|\mathbf{x}|}{\bar{\lambda}}, \frac{R}{\bar{\lambda}}\right) = \begin{cases} \frac{R}{\bar{\lambda}} + \mathcal{O}((\bar{\lambda}/R)^2) & \text{for } d = 1 \\ -\frac{1}{2} \left(\frac{R}{\bar{\lambda}}\right)^2 \log\left(\frac{R}{\bar{\lambda}}\right) + \mathcal{O}((\bar{\lambda}/R)^2) & \text{for } d = 2 \\ \frac{1}{3} \left(\frac{R}{\bar{\lambda}}\right)^2 + \mathcal{O}((\bar{\lambda}/R)^3) & \text{for } d = 3 \end{cases} \quad (\text{II.9.8})$$

and, at first order, it is $\mathcal{O}((R/\bar{\lambda})^2)$ for $d > 3$. Notice that, in any dimension, Ψ tends to zero as $\bar{\lambda}/R \rightarrow \infty$ (fig II.9.1).

II.10 Variance of the conditional distribution

From eq (II.9.4), it is straightforward to calculate the second moment of the distribution. In fact, the following equation obviously holds

$$\int_{\mathcal{V}} d\mathbf{x} \langle n(\mathbf{x})N(R) \rangle = \langle N(R)^2 \rangle$$

Once again, the details of the calculations are reported in Appendix A. The result is the following

$$\langle N^2(R) \rangle = \langle N(R) \rangle^2 + \frac{\sigma^2}{\mu} \langle N(R) \rangle \psi\left(\frac{R}{\bar{\lambda}}\right) \quad (\text{II.10.1})$$

where I have defined the following function for ease of notation

$$\psi\left(\frac{R}{\bar{\lambda}}\right) = 1 - \frac{d \bar{\lambda}}{R} \frac{K_{\frac{d}{2}}\left(\frac{R}{\bar{\lambda}}\right) I_{\frac{d}{2}}\left(\frac{R}{\bar{\lambda}}\right)}{I_{\frac{d}{2}-1}\left(\frac{R}{\bar{\lambda}}\right) K_{\frac{d}{2}}\left(\frac{R}{\bar{\lambda}}\right) + I_{\frac{d}{2}}\left(\frac{R}{\bar{\lambda}}\right) K_{\frac{d}{2}-1}\left(\frac{R}{\bar{\lambda}}\right)} \quad (\text{II.10.2})$$

By definition $\text{Var}(N_{\mathcal{V}}) = \langle N_{\mathcal{V}}^2 \rangle - \langle N_{\mathcal{V}} \rangle^2$. In this case, therefore, one can immediately obtain the variance of the random variable $N(R)$, which reads

$$\text{Var}(N_{\mathcal{V}}) = \frac{\sigma^2}{\mu} \langle N(R) \rangle \psi\left(\frac{R}{\bar{\lambda}}\right) = \langle N(R) \rangle \Sigma(R) \quad (\text{II.10.3})$$

where I have also introduced the following function

$$\Sigma(R) = \frac{\sigma^2}{\mu} \psi\left(\frac{R}{\bar{\lambda}}\right) \quad (\text{II.10.4})$$

Fixing R , and considering the small correlation regime, i.e. $\bar{\lambda}/R \rightarrow 0$, from the properties of the Bessel functions, eq (II.9.7), one obtains

$$\psi\left(\frac{R}{\bar{\lambda}}\right) = 1 + \mathcal{O}\left(\frac{\bar{\lambda}}{R}\right)$$

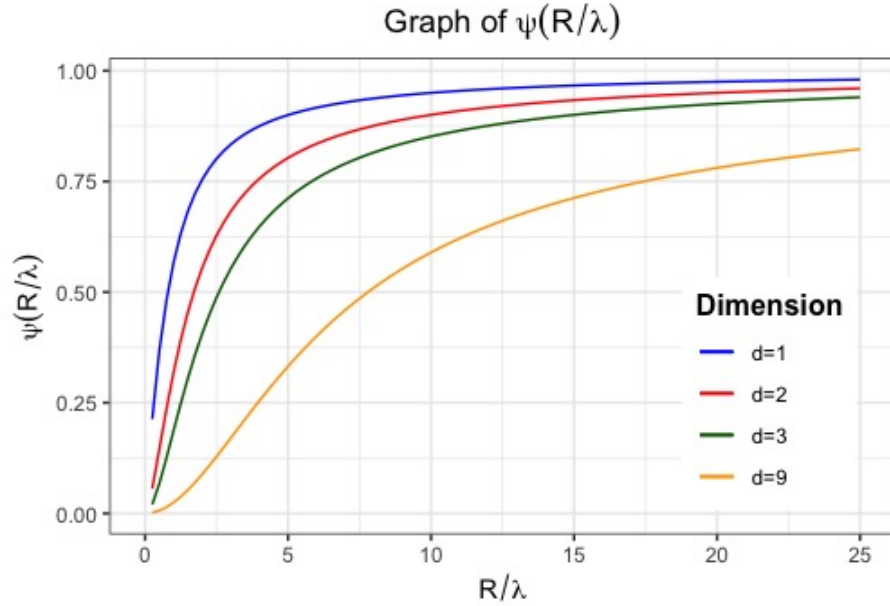


Figure II.10.1: **Plots of $\psi(R/\bar{\lambda})$.** The figure is a plot of function $\psi(R/\bar{\lambda})$ as calculated in eq II.10.2. The function tends to zero for $R/\bar{\lambda} \rightarrow 0$, while it tends to one for $R/\bar{\lambda} \rightarrow \infty$, regardless of the dimension. As a consequence, the ratio between the standard deviation and the average value of $N(R)$ tends to zero for $R/\bar{\lambda} \rightarrow \infty$, as is expected by the fact that when R is large compared to the correlation length $\bar{\lambda}$, $N(R)$ represents the sum of many, patch-wise independent random variables.

and therefore $\Sigma(R) = \frac{\sigma^2}{\mu}$ in the limit $\bar{\lambda}/R \rightarrow 0$.

The case of small argument is more involved. Upon fixing R and all the other parameters at first order in $\bar{\lambda}/R \rightarrow \infty$ one obtains

$$\psi\left(\frac{R}{\bar{\lambda}}\right) = \begin{cases} \frac{R}{\bar{\lambda}} + \mathcal{O}\left(\left(\frac{R}{\bar{\lambda}}\right)^2\right) & \text{for } d = 1 \\ -\frac{1}{2}\left(\frac{R}{\bar{\lambda}}\right)^2 \log\left(\frac{R}{\bar{\lambda}}\right) + \mathcal{O}\left(\left(\frac{R}{\bar{\lambda}}\right)^2\right) & \text{for } d = 2 \\ \frac{2}{5}\left(\frac{R}{\bar{\lambda}}\right)^2 + \mathcal{O}\left(\left(\frac{R}{\bar{\lambda}}\right)^3\right) & \text{for } d = 3 \end{cases} \quad (\text{II.10.5})$$

and it is $\mathcal{O}\left(\left(\frac{R}{\bar{\lambda}}\right)^2\right)$ for $d > 3$. Also, notice that $\psi\left(\frac{R}{\bar{\lambda}}\right) \rightarrow 0$ for $\bar{\lambda}/R \rightarrow \infty$ in any dimension d (fig II.10.1).

These considerations will become of fundamental importance in the next chapters and

will be the pivotal relationships for calculating the probability distribution of $N(R)$.

On the other hand, one fundamental result is readily obtained from eq (II.10.3) . It links the variance of $N(R)$ to its average. Empirical observations have often found that in ecosystems a power law relationship emerges, such as

$$\text{Var}(N_\nu) \propto \langle N(R) \rangle^\varphi$$

with φ typically assuming values between one and two [97, 166]. This relationship is known with the name of Taylor's law.

Considering all the parameters to be fixed, and focusing on variations of the radius R , in the two dimensional case one obtains $\text{Var}(N_\nu) \propto \langle N(R) \rangle^2 \log(\langle N(R) \rangle)^{1/2}$, i.e. $\text{Var}(N_\nu) \propto \langle N(R) \rangle^2 \log(\langle N(R) \rangle)$ for $R/\bar{\lambda} \ll 1$, while $\text{Var}(N_\nu) \propto \langle N(R) \rangle$ for $R/\bar{\lambda} \gg 1$. So for areas of radius much smaller than the correlation length the model is characterised by $\varphi = 2$ with logarithmic corrections, while in the case of areas much larger than $\bar{\lambda}$ one observes $\varphi = 1$.

It has been proved that Taylor's law can emerge from a much more general class of stochastic processes, for example when the dynamical rates of the model are affected by environmental variability [97]. In the case of the phenomenological extensions of the BD model the previous arguments have proved that a change in the scaling exponent φ is expected as a consequence of diffusivity in a spatially extended system.

II.11 Form invariance of the distribution of $N(R)$

In the context of self organised criticality, the invariance of the functional form of the probability distribution is often associated with the occurrence of power laws. In theoretical ecology, the analysis of empirical data have shown that some spatial patterns have a different type of scaling collapse: the relative species abundance (RSA) at different scales

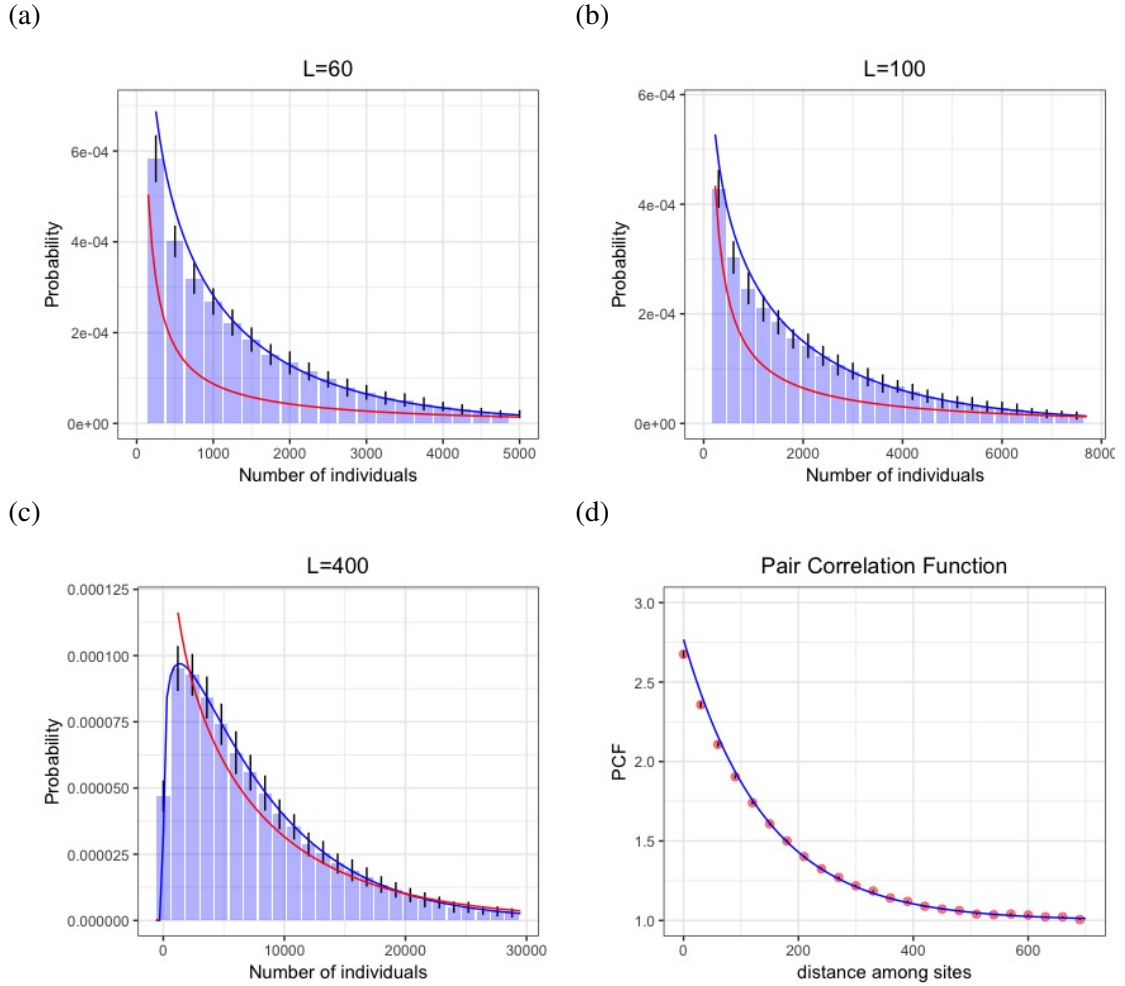


Figure II.10.2: **Comparison of simulated data** of eq (II.7.1) at stationarity with the theoretical prediction of eq (II.11.1) in dimension 1. Histograms represent simulated data, with the black segments indicating errors at two standard deviations. The blue line is the prediction from eq (II.11.1), while the red line is the gamma distribution in the mean field regime, i.e. as in eq (II.11.1) but assuming no spatial dispersal (and so $\text{Var}(N_V) = \sigma^2/\mu$). The parameters of the model are $D = 200$, $b_0 = 0.2$, $\mu = 0.01$ and $\sigma = 10$, and so $\lambda = 141$. Panel (a) refers to a segment of length 60 sites, panel (b) to one of length 100, and panel (c) 400. Panel (d) instead compares the pair correlation function from simulated data with the theoretical formula calculated in eq (II.8.4). The lattice has a total of 1000 sites. The agreement is surprisingly good at all the analysed scales. More details on the simulation scheme and on how errors and histograms were calculated will be given in chapter IV.

can be overlaid on top of each other by the judicious choice of the correct “scaling variables”. The functional shape thus obtained is far from being a power law [187, 142, 14].

Inspired by these observations, one can assume that, at stationarity, the probability distribution of the number of individuals living in a certain area maintains the same functional form across all scales. This assumption does not necessarily mean that the probability distribution is scale invariant, but that changes of the size of the area can be encoded only in the change of the parameters of the distribution. The appropriate scaling of the parameters can be calculated, for example, by matching the moments of the distribution at all scales if they can be calculated independently.

More precisely, in the case of the phenomenological model defined by eq (II.7.1) one obvious choice is to assume that the random variable $N(R)$ is distributed as a gamma distribution, i.e. it has the same form as the stationary solution of the BD model calculated at eq (II.5.3). The parameters of the distribution have to be chosen so that they match at *all scales* the moments of $N(R)$ calculated at eq (II.9.1) and (II.10.3).

I here assume that

$$P(N|R) = \frac{1}{\beta(R)} \frac{(N/\beta(R))^{\alpha(R)-1}}{\Gamma(\alpha(R))} e^{-N/\beta(R)} \quad (\text{II.11.1})$$

with $\Gamma(\cdot)$ a gamma function. I calculate $\alpha(R)$ and $\beta(R)$ so that they match the correct mean and variance of the system. From the properties of the gamma distribution one finds that

$$\alpha(R) = \frac{\langle N(R) \rangle^2}{\text{Var}(N(R))} \quad \beta(R) = \frac{\text{Var}(N(R))}{\langle N(R) \rangle}$$

Of course, this is just an assumption and there is no mathematical evidence at this stage that this is true, nor to what extent this is verified. However, comparing this analytical shape with simulations of the model (for which more details will be given in chapter IV) one observes a surprisingly good match for a wide range of different parameters. Examples are reported in Fig II.10.2 for the one dimensional case and in Fig II.11.1 for

the two dimensional case. Such results can be justified with a higher mathematical rigour in the context of an individual based model of meta-communities, and this is indeed going to be the focus of much of the rest of this thesis.

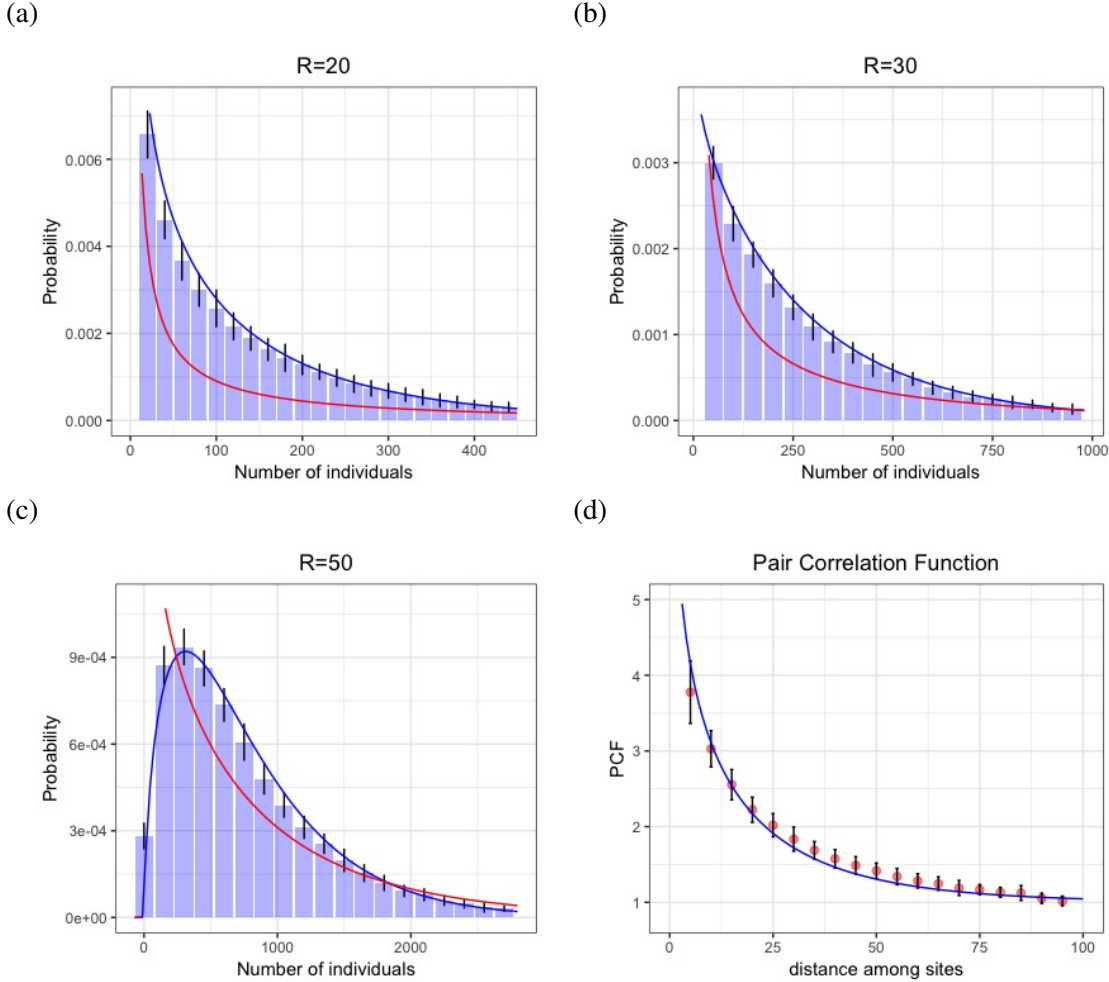


Figure II.11.1: **Comparison of simulated data** of eq (II.7.1) at stationarity with the theoretical prediction of eq (II.11.1) in dimension two. Histograms represent simulated data, with the black segments indicating errors at two standard deviations. The blue line is the prediction made using eq (II.11.1), while the red line is the gamma distribution in the mean field regime, i.e. as in eq (II.11.1) but assuming no spatial dispersal (and so $\text{Var}(N_\gamma) = \sigma^2/\mu$). The parameters of the model are $D = 100$, $b_0 = 0.01$, $\mu = 0.1$ and $\sigma = 10$, and hence $\lambda = 32$. Panel (a) refers to an area of radius $R = 20$, panel (b) to one of radius $R = 30$, and panel (c) to $R = 50$. Panel (d) instead compares the pair correlation function from simulated data with the theoretical formula calculated in eq (II.8.4). The lattice has a total of 40,000 sites positioned in a two dimensional lattice of 200 sites per side. The agreement is surprisingly good at all the analysed scales. More details on the simulation scheme and on how errors and histograms were calculated will be given in chapter IV.

Chapter III

A spatial stochastic model close to a critical point

Despite the lack of rigorous mathematical derivation, the phenomenological model presented in the previous chapter has some interesting mathematical properties, e.g. the two-point correlation function and the variance of the conditional probability distribution can be calculated analytically. Moreover, direct simulations of the spatially explicit Langevin equation have showed that the functional form of the stationary distribution can be form invariant (i.e. the shape of the probability distribution does not change across spatial scales).

Motivated by these results, in this chapter I will introduce and analyse a spatial metacommunity model where local communities are located on a d -dimensional regular graph (or lattice). Within each site individuals are treated as diluted, well-mixed point-like particles undergoing a linear birth-death process equal to that of the BD model defined in chapter II. However, now individuals can also jump from one site to another, thus coupling the dynamics of the local communities to each other and explicitly endowing the model with spatial degrees of freedom. Movement is considered at the microscopic level within a non-phenomenological individual based formulation. It will be proved that this model

violates microscopic detailed balance and therefore there is no time invariance at stationarity. Its simplicity, however, allows to calculate important macroscopic patterns, and in the regime of large fluctuations further analytic results can be achieved.

The first part defines the model and proves that detailed balance is broken. Then the generating function of the process is introduced and it is showed that it satisfies a set of ordinary differential equations. Studying the populations living within an arbitrary spheric sub-volume an analytical formula for the distribution of abundances is calculated in what is referred to as the "critical limit".

III.1 Definition of the Spatial Birth-Death model and the violation of detailed balance

The model is defined by the following birth-death dynamics: each individual dies at a constant death rate r and gives birth at a constant rate b . The newborn individual remains in the same local community with probability γ ($0 \leq \gamma \leq 1$), whereas it hops onto one of the $2d$ nearest neighbours with probability $1 - \gamma$. All communities are also colonized by external individuals at a constant immigration rate b_0 . This prevents the system from reaching the absorbing state (i.e. an empty system with zero individuals).

The set of points belonging to the lattice, of linear size a , is denoted by \mathbb{L} . Let X_i , $i \in \mathbb{L}$, indicate an individual living in site i . The reactions defining the model's dynamics can be

cast into the following form



where j indicates a nearest neighbor of site i . Notice that in this model spatial movement, determined by reaction (III.1.2), is always coupled to birth, so that only newborn individuals can move. Also, birth in one place does not entail death of an individual in another place. This choice mimics the natural behaviour of trees, that once germinated in a place do not change their position (while their seeds can move to other locations). Nonetheless, the results that will be presented in this chapter are not specific of this choice: equivalent results can be obtained for a model where movement is independent of birth events, which is the typical case, for example, of bacteria or animals like breeding birds. Appendix D illustrates such case and demonstrates that the analysis of that model and of the "seed dispersal" model just defined lead to very similar results in the considered regimes.

In order to avoid extinction or demographic explosion as time grows, it will always be assumed that $b_0 > 0$ and $0 < b < r$. Indeed from direct observation of ecological data the regime which is physically more interesting has $b_0 \ll b$ and $b \simeq r$.

I indicate with n_i the number of individuals in site i . Assuming perfect mixing within every site, when the configuration of the system is $\{n\} = \{n_i : i \in \mathbb{L}\}$ the birth and death

rates in site i , i.e. $\mathcal{W}_i^+(\{n\})$ and $\mathcal{W}_i^-(\{n\})$, read respectively

$$\begin{aligned}\mathcal{W}_i^+(\{n\}) &= \frac{b(1-\gamma)}{2d} \sum_{j:|j-i|=1} n_j + b\gamma n_i + b_0 \\ \mathcal{W}_i^-(\{n\}) &= r n_i \quad .\end{aligned}\tag{III.1.5}$$

The rate \mathcal{W}_i^+ is therefore determined by three terms: the first represents seeds dispersal and ultimately couples local communities to each other, the second accounts for birth events happening in site i , and the b_0 term accounts for immigration events from the outside. The rate \mathcal{W}_i^- instead is determined by death events happening in site i .

In eq (III.1.5) rates are linear, which is crucial for the mathematical analysis. More realistic model would include non-linearities arising e.g. from a carrying capacity, selection effect etc. However, in this analysis we are interested in the dynamics near criticality and therefore consider what is arguably the simplest (minimal) non-trivial spatially-explicit model exhibiting criticality.

Figure III.1.1 schematically illustrates the main features of the model just described. For ease of notation I define the following constant

$$D := \frac{b(1-\gamma)}{2d}$$

In the rest of this thesis this model will be referred to as the 'spatial birth death' model, and abbreviated as SBD.

Indicating with $P(\{n\}, t)$ the probability to find the system in the configuration $\{n\}$ at

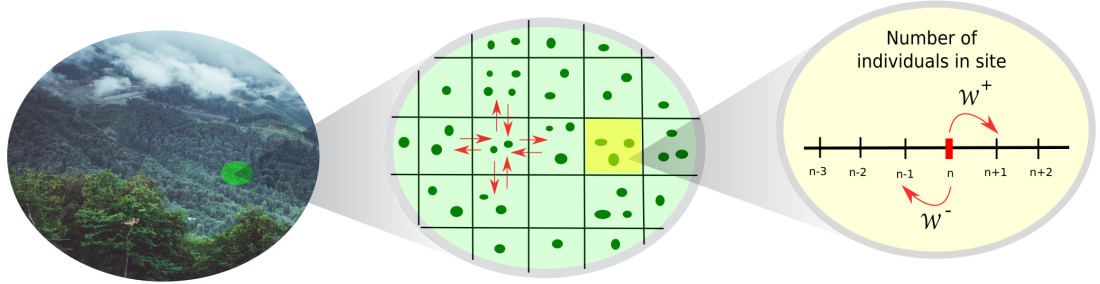


Figure III.1.1: **Illustration of the model.** Individual trees are represented by dark green circles within local communities which are located on a regular graph (or lattice). Each individual may die or give birth to an offspring with constant per capita rates. New individuals remain in the community of the parent with probability γ or hop onto one of the $2d$ nearest neighbours with probability $1 - \gamma$. All communities are also colonized by external individuals at a constant immigration rate b_0 . The dynamics of local abundances of individuals is therefore determined by the jump rates \mathcal{W}_i^+ and \mathcal{W}_i^- defined in eq (III.1.5).

time t the following master equation then holds

$$\begin{aligned} \frac{\partial}{\partial t} P(\{n\}, t) = \sum_{i \in \mathbb{L}} \left\{ \mathcal{W}_i^+(\{\dots, n_i - 1, \dots\}) P(\{\dots, n_i - 1, \dots\}, t) + \right. & \quad \text{(III.1.6)} \\ & - \mathcal{W}_i^+(\{n\}) P(\{n\}, t) + \\ & + \mathcal{W}_i^-(\{\dots, n_i + 1, \dots\}) P(\{\dots, n_i + 1, \dots\}, t) + \\ & \left. - \mathcal{W}_i^-(\{n\}) P(\{n\}, t) \right\} \end{aligned}$$

where the dots represent that all other occupation numbers remain as in $\{n\}$ and it is intended that $P(\cdot) = 0$ whenever any of the entrances is negative.

Solving the model would involve calculating the probability $P(\{n\}, t)$ for every time t , which depends on an infinite set of variables, $\{n\}$. This is a very complicated mathematical problem, which so far has not been possible to solve.

In the language of chemical kinetics the reaction (III.1.1) represents an autocatalytic production and, coupled to spatial diffusion, is responsible for the violation of detailed balance [81]. As showed in chapter II, detailed balance is satisfied if and only if the probability to go along any closed path in the space of configurations does not depend on the

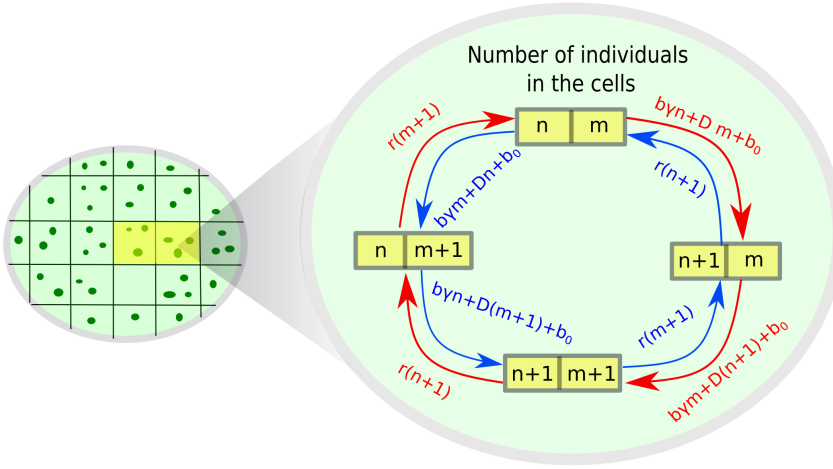


Figure III.1.2: **Violation of detailed balance** The picture represents a closed path in the space of configurations of the process which has different probabilities depending on the direction of the journey. It starts by taking two neighboring sites, which initially have n and m individuals respectively. The probability to jump into the other states of the path are reported and the arrows indicate the direction. In the clockwise direction (red arrows) the probability is $[b\gamma n + Dm + b_0][b\gamma m + D(n+1) + b_0][r(n+1)][r(m+1)]$. In the anti-clockwise path (blue arrows) the total probability is $[b\gamma m + Dn + b_0][b\gamma n + D(m+1) + b_0][r(m+1)][r(n+1)]$. In general, i.e. for $b \neq 0$, $r \neq 0$, $D \neq 0$, $D \neq b$ and $m \neq n$, the two probabilities are not equal, and therefore time invariance does not hold.

direction that one chooses (this is known as the Kolmogorov criterion [100, 68]). Figure III.1.2 shows a counterexample for the model at hand, i.e. it shows a path that has different probabilities depending on the direction of the journey.

The violation of detailed balance has important implications: from the conceptual point of view it determines that the process is irreversible, even at stationarity. From the mathematical point of view there is no practical method to explicitly compute the stationary distribution. since the local dynamics are coupled at all scales.

In order to make analytic progress, a diffusion approximation will be considered, similar to that introduced in the mean field system. The local abundances n_i will be transformed into continuous random variables \tilde{n}_i by means of a rescaling by means of a rescaling and by considering the near-critical regime dominated by large fluctuations, the afore-

mentioned "critical limit". Unlike the case of chapter II, however, a slightly different approach will be adopted, which involves the rescaling of the generating function of the model and the assumption that the generating function is analytical in a neighborhood of the complex origin.

III.2 The Spatial Generating Function

In the study of stochastic processes the generating function (sometimes called 'moment generating function') provides the basis for an alternative route to analytical results compared with working directly with probability density functions or cumulative distribution functions.

The spatial generating function in this thesis is defined as follows

$$\zeta(\{H\}, t) = \langle e^{\sum_{k \in \mathbb{L}} n_k H_k} \rangle = \sum_{\{n\}} e^{\sum_{k \in \mathbb{L}} n_k H_k} p(\{n\}, t) \quad (\text{III.2.1})$$

where $H_i \leq 0$ for every $i \in \mathbb{L}$. This function generates the moments of the random variables $\{n\}$ in the sense that through partial derivatives one can calculate them directly. For example the in-site mean and pair correlation can be calculated from this simple relationships

$$\begin{aligned} \frac{\partial}{\partial H_i} \zeta(\{H\}, t) \Big|_{\{H\}=0} &= \langle n_i \rangle \\ \frac{\partial^2}{\partial H_i \partial H_j} \zeta(\{H\}, t) \Big|_{\{H\}=0} &= \langle n_i n_j \rangle \end{aligned}$$

and, accordingly, the m -point correlation function is calculated via partial-differentiating m times.

Multiplying through by $e^{\sum_{k \in \mathbb{L}} n_k H_k}$ both sides of eq (III.1.6) and summing over all possible

values of $\{n_i : i \in \mathbb{L}\}$ one obtains the following equation for the dynamics of $\zeta(\{H\}, t)$

$$\begin{aligned} \frac{\partial}{\partial t} \zeta(\{H\}, t) = \sum_{i \in \mathbb{L}} \left\{ (e^{H_i} - 1) \left[D \sum_{j:|i-j|=1} \frac{\partial \zeta}{\partial H_j} \right. \right. \\ \left. \left. + b\gamma \frac{\partial \zeta}{\partial H_i} + b_0 \zeta \right] + r(e^{-H_i} - 1) \frac{\partial \zeta}{\partial H_i} \right\} \end{aligned} \quad (\text{III.2.2})$$

The full solution to equation (III.2.2) is beyond reach. However, one can gain a lot of information about the process by looking into the moments of the distribution, in particular the mean number of individuals and the spatial correlation between pair of sites.

III.3 Local mean abundance and two-points correlation function

The equation for the mean number of individuals in site k can be obtained by taking the partial derivative of both sides of eq.(III.2.2) with respect to H_k and then setting $\{H\} = 0$. The result is the following linear equation

$$\frac{\partial \langle n_k \rangle}{\partial t} = \frac{b(1-\gamma)}{2d} \Delta_k \langle n_k \rangle - \mu \langle n_k \rangle + b_0$$

Considering stationarity and exploiting the homogeneity of the model one readily obtains $\langle n \rangle = \frac{b_0}{\mu}$. The correlation between sites k and l , i.e. $\langle n_k n_l \rangle$, can instead be calculated by partial-differentiating with respect to H_k and H_l on both sides of eq.(III.2.2) and subsequently setting $\{H\} = 0$. In this case one gets

$$\begin{aligned} \frac{\partial}{\partial t} \langle n_k n_l \rangle = D \left(\Delta_k \langle n_k n_l \rangle + \Delta_l \langle n_k n_l \rangle \right) + \\ - 2\mu \langle n_k n_l \rangle + 2b_0 \langle n \rangle + \delta_{k,l} \left(2\sigma^2 \langle n \rangle + b_0 \right) \end{aligned} \quad (\text{III.3.1})$$

where the usual notation is considered and we have defined

$$\sigma^2 := \frac{r+b}{2} . \quad (\text{III.3.2})$$

Similarly to what was done in chapter II, a d -dim system of Cartesian coordinates is now introduced. With the substitution $i \rightarrow \mathbf{x}$ and $j \rightarrow \mathbf{y}$, with \mathbf{x} and \mathbf{y} the vectors of coordinates, the stationary solution of eq.(III.3.1) is directly calculated by considering the Fourier series expansion of $\langle n_{\mathbf{x}} n_{\mathbf{y}} \rangle$, following the same procedure used to solve eq (II.8.1). The final expression reads

$$\begin{aligned} \langle n_{\mathbf{k}} n_{\mathbf{l}} \rangle &= \langle n \rangle^2 + \langle n \rangle^2 \rho^2 \left(1 + \frac{\mu}{2\sigma^2} \right) \times \\ &\times \left(\frac{a}{2\pi} \right)^d \int_{\mathcal{C}} d\mathbf{p} \frac{e^{i\mathbf{p} \cdot (\mathbf{k}-\mathbf{l})}}{1 + 2\lambda^2 \sum_{i=1}^d (1 - \cos(p_i a))} \end{aligned} \quad (\text{III.3.3})$$

where p_i is the i -th Cartesian component of the d -dim vector \mathbf{p} and \mathcal{C} is the hypercubic primitive unit cell of size $2\pi/a$. In line with the notation used in previous paragraphs, I have also introduced

$$\lambda := \sqrt{\frac{\bar{D}}{\mu}} \quad \text{and} \quad \rho := \sqrt{\frac{\sigma^2}{b_0}} ,$$

One approach could be to solve eq (III.3.3) analytically, but it is possible to obtain a good deal of simplification by considering a continuous spatial limit. The first step is to rescale the occupation numbers at sites \mathbf{x} and \mathbf{y} as $n_{\mathbf{x}} = n(\mathbf{x})a^d, n_{\mathbf{y}} = n(\mathbf{y})a^d$, with $n(\mathbf{x}), n(\mathbf{y})$ densities of individuals in \mathbf{x} and \mathbf{y} . Parameters need to be rescaled as well, i.e.

$$\bar{\lambda} := \sqrt{\frac{\bar{D}}{\mu}} \quad \bar{\rho} := \sqrt{\frac{\sigma^2}{b_0}} ,$$

where $\bar{D} = Da^2$ and $\bar{b}_0 = b_0/a^d$ are constant for $a \rightarrow 0$. Notice that the notations are analogous to those used for the phenomenological model of chapter II, and the reason

will appear evident in the following.

In this context, I indicate with $\langle n \rangle$ the average density of individuals, which at stationarity is equal to \bar{b}_0/μ . Finally, the integral at eq (III.3.3) simplifies, and dividing through by $\langle n \rangle^2$ on both sides of eq (III.3.3) one arrives at the following result

$$\frac{\langle n(\mathbf{x})n(\mathbf{y}) \rangle}{\langle n \rangle^2} = 1 + \frac{\bar{\rho}^2}{(2\pi\bar{\lambda}^2)^{d/2}} \left(1 + \frac{\mu}{2\sigma^2}\right) \times \quad (\text{III.3.4})$$

$$\times \left(\frac{|\mathbf{x} - \mathbf{y}|}{\bar{\lambda}}\right)^{\frac{2-d}{2}} K_{\frac{2-d}{2}}\left(\frac{|\mathbf{x} - \mathbf{y}|}{\bar{\lambda}}\right)$$

where $|\mathbf{x} - \mathbf{y}|$ is the distance between the sites located at \mathbf{x} and \mathbf{y} , and K_ν is the modified Bessel function of the second kind of order ν [109, 1].

The Bessel function K_ν decays exponentially fast for large arguments, and therefore for $|\mathbf{x} - \mathbf{y}| \gg \bar{\lambda}$ the abundances in \mathbf{x} and \mathbf{y} become uncorrelated.

Comparing this expression to that of the two point correlation function for the phenomenological model, one observes a striking similarity at all terms. The only difference is the term $\frac{\mu}{2\sigma^2}$ in the parenthesis. This implies that in systems where $\frac{\mu}{2\sigma^2} \rightarrow 0$ the two point correlation in the SBD model and in the phenomenological model converge to the same function.

In the next section I will demonstrate that not only all the moments, but the two models themselves converge in the limit of $\frac{\mu}{\sigma^2} \rightarrow 0$ (the so called "critical limit").

III.4 The critical limit of the spatial generating function

Large fluctuations in the abundance of individuals are a common trait of many real world, spatially extended communities of living organisms [176, 178, 78, 185, 89]. In mathematical terms this observation can lead to interesting new approaches that have the potential to simplify the analysis without losing touch with real world applications.

As done in the previous chapter for the BD process, I consider the parameter $\varepsilon = \frac{2(r-b)}{r+b} = \mu/\sigma^2$. I also assume the following scaling: $\frac{b_0}{\mu}\varepsilon = \mathcal{O}(1)$ as $\varepsilon \rightarrow 0^+$.

The parameter ε indicates how close the system is to the critical point, independently of all the other spatial degrees of freedom. In order to fix even the scaling of spatial diffusion, one needs to consider the independent parameter $\eta = \frac{D}{\sigma^2}$. I make the assumption that $\eta = \mathcal{O}(\varepsilon)$ as $\varepsilon \rightarrow 0^+$, and since $\eta/\varepsilon = \lambda^2$ this implies $\lambda = \mathcal{O}(1)$. In this way spatial dispersal and demographic fluctuations will be of the same order in the limit.

Other choices for the scaling of the parameters would end up in more trivial frameworks. If $\eta = o(\varepsilon)$ patterns emerging from spatial diffusion are negligible over demographic fluctuations, and one returns to a mean field system, while $\eta = \mathcal{O}(1)$ would result in spatial dispersal dominating over local birth-death dynamics.

I hence assume that the generating function $\zeta(\{H\}, t)$ is analytic at $H_i = 0$ for any i and that the most important contribution to the equation of $\zeta(\{H\}, t)$ comes from a negative real neighborhood of the origin with thickness $\mathcal{O}(\varepsilon)$. This is tantamount to introducing the change of variables $H_i = \varepsilon S_i$ into eq (III.2.2) and to expanding in powers of ε , assuming $S_i = \mathcal{O}(1)$ and $S_i \leq 0$. These assumptions yield the following equation

$$\begin{aligned} \frac{\partial}{\partial t} \zeta(\{H\}, t) = \sum_{i \in \mathbb{L}} \left\{ \left[\varepsilon S_i + \frac{\varepsilon^2}{2} S_i^2 + \mathcal{O}(\varepsilon^3) \right] \left[\frac{D}{\varepsilon} \sum_{j: |i-j|=1} \frac{\partial \zeta}{\partial S_j} \right. \right. \\ \left. \left. + \frac{b\gamma}{\varepsilon} \frac{\partial \zeta}{\partial S_i} + b_0 \zeta \right] + \frac{r}{\varepsilon} \left[-\varepsilon S_i + \frac{\varepsilon^2}{2} S_i^2 + \mathcal{O}(\varepsilon^3) \right] \frac{\partial \zeta}{\partial S_i} \right\} \end{aligned}$$

Retaining only the leading order in ε (with the scaling assumptions for the parameters considered above) the following is obtained

$$\frac{\partial}{\partial t} \zeta(\{S\}, t) = \sum_{i \in \mathbb{L}} \sigma^2 S_i \left\{ \eta \Delta_i \frac{\partial \zeta}{\partial S_i} - \varepsilon \frac{\partial \zeta}{\partial S_i} + \frac{\varepsilon}{\rho^2} \zeta + \varepsilon S_i \frac{\partial \zeta}{\partial S_i} \right\} . \quad (\text{III.4.1})$$

Finally, rescaling time as $T := \mu t$ and, with a slight abuse of notation, going back to the

original notation $S_i \rightarrow H_i \varepsilon$ one finds:

$$\frac{\partial \zeta}{\partial T} = \sum_{i \in \mathbb{L}} H_i \left\{ \lambda^2 \Delta_i \frac{\partial \zeta}{\partial H_i} - \frac{\partial \zeta}{\partial H_i} + \langle n \rangle \zeta + \frac{\sigma^2}{\mu} H_i \frac{\partial \zeta}{\partial H_i} \right\}, \quad (\text{III.4.2})$$

Here ζ indicates the generating function of a set of *continuous* random variables n_i and the H_i are the conjugated variables.

From the continuous generating function $\zeta(\{H\}, t)$ one can calculate the probability $p(\{n\}, t)$ via the corresponding inverse Laplace transform

$$p(\{n\}, t) = \prod_{k \in \mathbb{L}} \left(\frac{1}{2\pi} \int_{-\infty}^{\infty} e^{i n_k H_k} dH_k \right) \zeta(\{iH\}, t)$$

where $\{iH\} = \{iH_1, \dots, iH_k, \dots\}$, i.e. it is the set of variables $\{H\}$ each multiplied by the complex unity i .

Multiplying eq (III.4.2) by $\prod_{k \in \mathbb{L}} \left(\frac{1}{2\pi} \int_{-\infty}^{\infty} e^{i n_k H_k} dH_k \right)$ and integrating by parts one obtains the following Fokker Planck equation for the continuous variables n_i

$$\begin{aligned} \frac{\partial}{\partial T} P(\{n\}, T) = \sum_{i \in \mathbb{L}} \left\{ \frac{\partial}{\partial n_i} \left[- \left(\lambda^2 \Delta_i n_i - n_i + \langle n \rangle \right) P(\{n\}, T) \right] + \right. \\ \left. + \frac{\sigma^2}{\mu} \frac{\partial^2}{\partial n_i^2} \left[n_i P(\{n\}, T) \right] \right\} \end{aligned} \quad (\text{III.4.3})$$

which, in the Itô prescription, is equivalent to the following set of Langevin equations

$$\frac{d}{dT} n_i = \lambda^2 \Delta_i n_i - n_i + \langle n \rangle + \frac{\sigma}{\sqrt{\mu}} \sqrt{n_i} \xi_i(T) \quad \text{for } i \in \mathbb{L}$$

with $\langle \xi_i(T) \xi_j(T') \rangle = 2\delta_{i,j} \delta(T - T')$ or, with the change of variable $t = T/\mu$ (notice that $\xi_i(T) = \xi_i(t)/\sqrt{\mu}$)

$$\frac{d}{dt} n_i = \dot{n}_i = D \Delta_i n_i - \mu n_i + b_0 + \sigma \sqrt{n_i} \xi_i(t) \quad \text{for } i \in \mathbb{L} \quad (\text{III.4.4})$$

where ξ_i is a zero-mean Gaussian white noise of covariance $\langle \xi_i(t) \xi_j(t') \rangle = 2\delta_{i,j} \delta(t - t')$.

This is the first important result of this thesis: in the limit of small $\varepsilon = \mu/\sigma^2$ the SBD model converges to the phenomenological model introduced in the previous chapter, and their dynamics is defined by the Fokker Planck equation in (III.4.3). This procedure is not equivalent to the naïve Kramers-Moyal expansion of eq.(III.1.6), nor to Van Kampen's system size expansion [100], as demonstrated in Chapter II. In fact, in the first case the parameter that regulated the expansion is not properly specified, and conclusions stemming from this approach are often non-rigorous. In the system size expansion technique, instead, one assumes that the system is populated by a very large number of individuals and that fluctuations are small, but as we have observed, the case of eq (III.4.3) is exactly the opposite, since fluctuations are dominant. The procedure analysed in this section is therefore a diffusive approximation of the process in the parameter regimes that have been identified.

Assuming that σ^2/μ is large has important consequences on the features of the model. Indeed, as calculated in chapter II, in such regime the fluctuations of the number of individuals living over a certain area diverge, a feature that is typical of systems poised at the critical point. For such reason, in the rest of this thesis the limit of $\sigma^2/\mu = 1/\varepsilon \rightarrow \infty$ will be referred to as the 'critical limit' [137].

The diffusive approximation just outlined yields a much simpler set of dynamical equations for the SBD model, but still there are no known methods to solve eq (III.4.3). Nonetheless, the knowledge of the details of each single local occupation number is definitely an over-abundance of information in real-world applications.

In the following I therefore focus on the conditional probability distribution of the system, which describes the number of individuals present in a certain area (or volume, or segment). Differently from the procedure used in chapter II, which focused directly on the Fokker-Planck equation, here the dynamical equations will be calculated from the spatial generating function.

III.5 Conditional generating function

Consistently with the notation of the previous chapter, \mathcal{V} indicates the set of sites or communities belonging to a d -dim volume of measure $|\mathcal{V}| = V$ and $N(V, t) = \sum_{i \in \mathcal{V}} n_i(t)$ indicates the total number of individuals present in \mathcal{V} at time t .

Indicating with $p(N|V, t)$ the conditional probability of $N_{\mathcal{V}}$ the conditional generating function will be denoted by

$$Z(h|V, t) = \langle e^{hN(V, t)} \rangle = \int_0^{\infty} dN e^{hN} p(N|V, t)$$

with $h \leq 0$.

It is immediate to observe that $Z(h|V, t)$ can be easily calculated from ζ by imposing that the set of variables $\{H\} = \{H_i : i \in \mathbb{L}\}$ take the following values

$$H_i = \begin{cases} h & \text{if } i \in \mathcal{V} \\ 0 & \text{if } i \notin \mathcal{V} \end{cases} \quad (\text{III.5.1})$$

Indeed

$$\zeta(\{H\}) = \langle e^{\sum_k H_k n_k} \rangle \rightarrow Z(h) = \langle e^{N_{\mathcal{V}} h} \rangle$$

Imposing the conditions (III.5.1) to eq (III.4.2) one also finds the equation for the dynamics of $Z(h)$ (within the critical limit), i.e.

$$\begin{aligned} \frac{\partial}{\partial T} Z(h|V, T) = h \left[\lambda^2 \sum_{i \in \mathcal{V}} \Delta_i f(i, h, V, T) - \frac{\partial Z}{\partial h} + \right. \\ \left. + \langle n \rangle V Z \right] + \frac{\sigma^2}{\mu} h^2 \frac{\partial Z}{\partial h} \end{aligned} \quad (\text{III.5.2})$$

where $f(i, h, V, T) = \langle n_i e^{hN} \rangle$ and where the following identity has been used

$$\sum_{i \in \mathcal{V}} \langle n_i e^{hN} \rangle = \frac{\partial Z}{\partial h}(h|V, T) \quad . \quad (\text{III.5.3})$$

The function $f(\cdot)$ is in general unknown and can not be easily obtained from first principles. The equation that describes its dynamics can nonetheless be calculated from eq (III.4.2).

In order to do so, first one needs to partial differentiate on both sides by H_k , thus obtaining

$$\begin{aligned} \frac{\partial^2 \zeta}{\partial T \partial H_k} = & \sum_{i \in \mathbb{L}} \delta_{i,k} \left\{ \lambda^2 \Delta_i \frac{\partial \zeta}{\partial H_i} - \frac{\partial \zeta}{\partial H_i} + \langle n \rangle \zeta + 2 \frac{\sigma^2}{\mu} H_i \frac{\partial \zeta}{\partial H_i} \right\} + \\ & \sum_{i \in \mathbb{L}} H_i \left\{ \lambda^2 \Delta_i \frac{\partial^2 \zeta}{\partial H_i \partial H_k} - \frac{\partial^2 \zeta}{\partial H_i \partial H_k} + \langle n \rangle \frac{\partial \zeta}{\partial H_k} + \frac{\sigma^2}{\mu} H_i \frac{\partial^2 \zeta}{\partial H_i \partial H_k} \right\} \quad . \end{aligned}$$

where $\delta_{i,k}$ is a Kronecker delta function. Then one needs to impose conditions as in eq (III.5.1). It is important to notice that, depending on whether $k \in \mathcal{V}$ or not, $H_k = h$ or $H_k = 0$, and therefore different equations are obtained depending on k .

For $k \in \mathcal{V}$ one finds the following

$$\begin{aligned} \frac{\partial}{\partial T} f(k, h, V, T) = & \lambda^2 \Delta_k f(k, h) - f(k, h) + \frac{b_0}{\mu} Z + \\ & + h \left[\lambda^2 \sum_{i \in \mathcal{V}} \Delta_i g(i, k, h) - \frac{\partial}{\partial h} f(k, h) + \langle n \rangle V f(k, h) \right] + \\ & + 2 \frac{\sigma^2}{\mu} h f(k, h) + \frac{\sigma^2}{\mu} h^2 \frac{\partial}{\partial h} f(k, h) \end{aligned} \quad (\text{III.5.4})$$

while for $k \notin \mathcal{V}$ one has

$$\begin{aligned} \frac{\partial}{\partial T} f(k, h, V, T) = & \lambda^2 \Delta_k f(k, h) - f(k, h) + \frac{b_0}{\mu} Z + \\ & + h \left[\lambda^2 \sum_{i \in \mathcal{V}} \Delta_i g(i, k, h) - \frac{\partial}{\partial h} f(k, h) + \langle n \rangle V f(k, h) \right] + \\ & + \frac{\sigma^2}{\mu} h^2 \frac{\partial}{\partial h} f(k, h) \end{aligned} \quad (\text{III.5.5})$$

where $g(i, k, h, V, T) := \langle n_i n_k e^{hN} \rangle$ and the following identity has been used

$$\sum_{i \in \mathcal{V}} \langle n_i n_k e^{hN} \rangle = \frac{\partial}{\partial h} f(k, h, V, T) \quad . \quad (\text{III.5.6})$$

Eq.(III.5.4) connects the dynamics of $f(\cdot)$ with that of $Z(\cdot)$ and of a newly defined function $g(\cdot)$. Since $g(\cdot)$ is unknown this approach seems to be inconclusive: proceeding on calculating the equations for $g(\cdot)$ would yield an equation depending on the three point function, leading to an open hierarchy of equations.

In the continuous spatial limit one can prove that the mathematical treatment simplifies considerably and further analytical insight can be achieved.

III.6 Spatial continuous limit

The presence of the term $\Delta_i g(i, x, h, t)$ in equations (III.5.4) and (III.5.5) complicates considerably their analytical treatment. In order to solve them and calculate $f(\cdot)$ one first needs to obtain a closed set of equations to relate $\Delta_i g(i, x, h, t)$ only to $f(x, h, t)$ and $Z(h, t)$.

Appendix B shows the proof that as a approaches zero and becomes negligible with respect to any other characteristic length of the system (such as the characteristic radius of \mathcal{V}) one has that $\Delta_i g(i, j, h, t) = \Delta_j g(i, j, h, t)$. Therefore, as a/R becomes small it is

possible to show that the following identity holds

$$\sum_{i \in \mathcal{V}} \Delta_i g(i, j, h, V, T) = \frac{\partial}{\partial h} \Delta_j f(j, h, V, T) \quad (\text{III.6.1})$$

The next step for introducing a spatial continuous limit in equations (III.5.4) and (III.5.5) is to consider the following rescaling of the parameters

$$\bar{\lambda} = \frac{\bar{D}}{\mu} = \lambda a \quad b_0 = a^d \bar{b}_0$$

with $\bar{D} = D a$ and \bar{b}_0 constant as $a \rightarrow 0$. Then the density of individuals at point \mathbf{x} is introduced so that $n_{\mathbf{x}} = a^d n(\mathbf{x})$. Lastly, one defines $N(V, t) = \int_{\mathcal{V}} d\mathbf{x} n(\mathbf{x}, t)$ and, with a slight abuse of notation, $f(\mathbf{x}, h, V, T) = \langle n(\mathbf{x}) e^{hN} \rangle$ (in fact the average is now taken over the *continuous* range of values of $n(\mathbf{x})$).

With such considerations eq (III.5.2) becomes

$$\begin{aligned} \frac{\partial}{\partial T} Z(h|V, T) = h \left[\bar{\lambda}^2 \int_{\mathcal{V}} d\mathbf{x} \nabla_{\mathbf{x}}^2 f(\mathbf{x}, h, T) - \frac{\partial Z}{\partial h} + \right. \\ \left. + \langle n \rangle V Z \right] + \frac{\sigma^2}{\mu} h^2 \frac{\partial Z}{\partial h} \end{aligned} \quad (\text{III.6.2})$$

In the limit $a \rightarrow 0$ and exploiting the appropriate scaling relationships at eq (III.6.1) also the following equality holds

$$\bar{\lambda}^2 \int_{\mathcal{V}} d\mathbf{x} \nabla_{\mathbf{x}}^2 g(\mathbf{x}, \mathbf{y}, h, V, T) = \bar{\lambda}^2 \frac{\partial}{\partial h} \nabla_{\mathbf{y}}^2 f(\mathbf{y}, h, V, T)$$

In this spatial continuous limit the equation for $f(\mathbf{y})$ in the case of $\mathbf{y} \in \mathcal{V}$ (i.e. equation

III.5.4), becomes

$$\begin{aligned} \frac{\partial}{\partial T} f(\mathbf{y}, h, V, T) = & \bar{\lambda}^2 \nabla_{\mathbf{y}}^2 f(\mathbf{y}, h) - f(\mathbf{y}, h) + \langle n \rangle Z + \\ & + h \left[\bar{\lambda}^2 \frac{\partial}{\partial h} \nabla_{\mathbf{y}}^2 f(\mathbf{y}, h) - \frac{\partial}{\partial h} f(\mathbf{y}, h) + \langle n \rangle V f(\mathbf{y}, h) \right] + \\ & + \frac{\sigma^2}{\mu} \frac{\partial}{\partial h} \left[h^2 f(\mathbf{y}, h) \right] \end{aligned} \quad (\text{III.6.3})$$

For the case $\mathbf{y} \notin \mathcal{V}$, i.e. eq (III.5.5), instead one finds

$$\begin{aligned} \frac{\partial}{\partial T} f(\mathbf{y}, h, V, T) = & \bar{\lambda}^2 \nabla_{\mathbf{y}}^2 f(\mathbf{y}, h) - f(\mathbf{y}, h) + \langle n \rangle Z + \\ & + h \left[\bar{\lambda}^2 \frac{\partial}{\partial h} \nabla_{\mathbf{y}}^2 f(\mathbf{y}, h) - \frac{\partial}{\partial h} f(\mathbf{y}, h) + \langle n \rangle V f(\mathbf{y}, h) \right] + \\ & + \frac{\sigma^2}{\mu} h^2 \frac{\partial}{\partial h} f(\mathbf{y}, h) \end{aligned} \quad (\text{III.6.4})$$

These two equations depend on $f(\cdot)$ and $Z(h)$, and, together with eq (III.6.2), form a closed set of equations (in fact we have removed the explicit dependence on $g(\cdot)$). Notice that $f(\mathbf{x}, h, V, T)$ is not always a continuous function. For example, in the regime of small diffusivity, i.e. $\bar{\lambda} = 0$, one can calculate from eq (III.6.3) and eq (III.6.4) that

$$\begin{aligned} f(\mathbf{x}, V, h, T) = & \frac{1}{V} \frac{\partial Z}{\partial h} \quad \text{for } \mathbf{x} \in \mathcal{V} \\ f(\mathbf{x}, V, h, T) = & \langle n \rangle Z \quad \text{for } \mathbf{x} \notin \mathcal{V} \end{aligned}$$

These equalities could also be calculated considering that for $\bar{\lambda} = 0$ each site is independent and each meta-population undergoes a simple birth death process, so that indeed $n(\mathbf{x}) = N(R)/V$ for $\mathbf{x} \in \mathcal{V}$ and $n(\mathbf{x})$ is independent of $N(R)$ for $\mathbf{x} \notin \mathcal{V}$. This of course leads again to

$$\begin{aligned} \langle n(\mathbf{x}) e^{hN_{\mathcal{V}}} \rangle = & \frac{1}{V} \langle N_{\mathcal{V}} e^{hN_{\mathcal{V}}} \rangle \quad \text{for } \mathbf{x} \in \mathcal{V} \\ \langle n(\mathbf{x}) e^{hN_{\mathcal{V}}} \rangle = & \langle n(\mathbf{x}) \rangle \langle e^{hN_{\mathcal{V}}} \rangle \quad \text{for } \mathbf{x} \notin \mathcal{V} \end{aligned}$$

Focusing on the case of \mathcal{V} being a d -dimensional ball of radius R and indicating now $N_{\mathcal{V}}$ as $N(R)$, equation (III.6.3) will describe $f(\mathbf{x})$ for $|\mathbf{x}| < R$, while eq (III.6.4) will be valid for $|\mathbf{x}| \geq R$.

Notice that with this choice the mean and variance of the random variable $N(R)$ are exactly equal to those calculated in chapter II, i.e. $\langle N(R) \rangle = \bar{b}_0 V / \mu$ and the variance is exactly equal to that reported in eq (II.10.3). Indeed, by putting $h = 0$ in equations (III.6.3) and (III.6.4) one recovers eq (II.9.2). These results will also be of focal importance in the next paragraph to calculate an approximate analytical form for $f(\mathbf{x})$, which will turn out to be very accurate for any parameter choice in the vicinity of the critical point.

III.7 Approximate solution at stationarity

Equations (III.6.2) and (III.6.3) constitute a closed set of equations for $Z(h)$ and $f(\mathbf{x})$ in the case $\mathbf{x} \in \mathcal{V}$. It is easy to see from the definition of $f(\cdot)$ that the following equations must hold for any h and any T :

$$\int_{\mathcal{V}} f(\mathbf{x}, V, h, T) d\mathbf{x} = \frac{\partial Z}{\partial h}(h|V, T) \quad (\text{III.7.1})$$

The previous chapter focused on calculating the first and second moments of $N(R)$, as well as the correlation function $\langle n(\mathbf{x})N(R) \rangle$. I here recall the main results, which are $\langle N(R) \rangle = \bar{b}_0 V / \mu$, and

$$\begin{aligned} \langle n(\mathbf{x})N(R) \rangle &= \langle n \rangle \langle N(R) \rangle + \frac{\sigma^2}{\mu} \langle n \rangle \Psi\left(\frac{|\mathbf{x}|}{\lambda}, \frac{R}{\lambda}\right) \quad \text{for } |\mathbf{x}| < R \\ \langle N_{\mathcal{V}}^2 \rangle &= \langle N(R) \rangle^2 + \frac{\sigma^2}{\mu} \langle N(R) \rangle \psi\left(\frac{R}{\lambda}\right) \end{aligned}$$

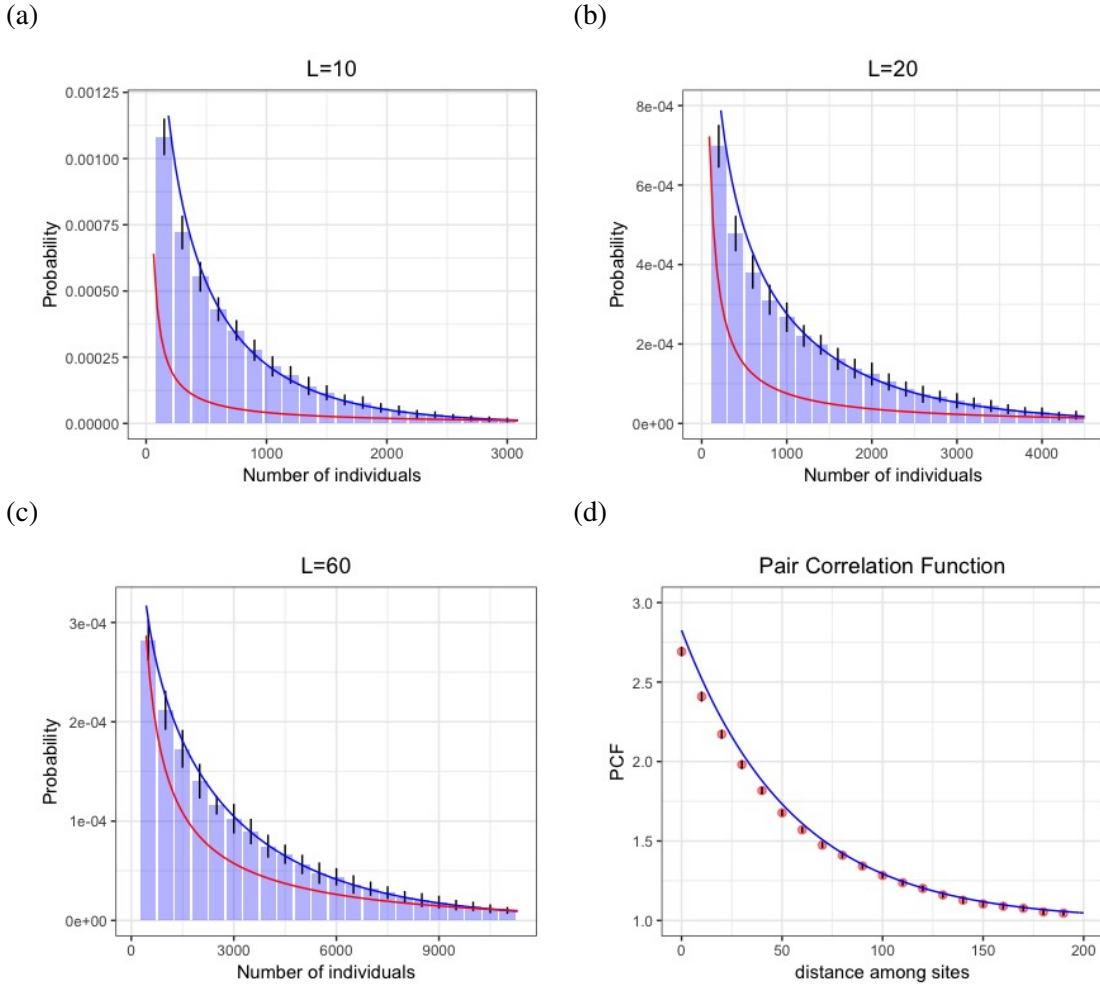


Figure III.6.1: **Comparison of simulated data** of eq (III.1.6) at stationarity with the theoretical prediction of eq(III.7.15) in dimension one. Histograms are simulated data, with the black segments indicating errors at two standard deviations. The blue line is the prediction made using eq (III.7.15), while the red line is the gamma distribution in the mean field regime, i.e. as in eq (III.7.15) but assuming no spatial dispersal (and so $\Sigma(R) = \sigma^2/\mu$). The parameters of the model are $D = 30$, $b_0 = 0.5$, $\mu = 0.01$ and $\sigma = 10$. Panel (a) refers to a segment of length 10 sites, panel (b) to one of length 20, and panel (c) 60. Panel (d) instead compares the pair correlation function from simulated data with the theoretical formula calculated in eq (II.8.4). The lattice has a total of 400 sites, and periodic boundary conditions were imposed. More details on the simulation scheme and on how errors and histograms are calculated will be given in Chapter IV.

where

$$\Psi\left(\frac{|\mathbf{x}|}{\bar{\lambda}}, \frac{R}{\bar{\lambda}}\right) = 1 - \left(\frac{|\mathbf{x}|}{R}\right)^{1-\frac{d}{2}} \frac{K_{\frac{d}{2}}\left(\frac{R}{\bar{\lambda}}\right) I_{\frac{d}{2}-1}\left(\frac{|\mathbf{x}|}{\bar{\lambda}}\right)}{I_{\frac{d}{2}-1}\left(\frac{R}{\bar{\lambda}}\right) K_{\frac{d}{2}}\left(\frac{R}{\bar{\lambda}}\right) + K_{\frac{d}{2}-1}\left(\frac{R}{\bar{\lambda}}\right) I_{\frac{d}{2}}\left(\frac{R}{\bar{\lambda}}\right)} \quad (\text{III.7.2})$$

and

$$\psi\left(\frac{R}{\bar{\lambda}}\right) = 1 - \frac{d \bar{\lambda}}{R} \frac{K_{\frac{d}{2}}\left(\frac{R}{\bar{\lambda}}\right) I_{\frac{d}{2}}\left(\frac{R}{\bar{\lambda}}\right)}{I_{\frac{d}{2}-1}\left(\frac{R}{\bar{\lambda}}\right) K_{\frac{d}{2}}\left(\frac{R}{\bar{\lambda}}\right) + I_{\frac{d}{2}}\left(\frac{R}{\bar{\lambda}}\right) K_{\frac{d}{2}-1}\left(\frac{R}{\bar{\lambda}}\right)} \quad (\text{III.7.3})$$

To gain a better idea of the behaviour of these functions, which will be of pivotal importance in the following, the reader is referred to figures II.10.1 and II.9.1 in chapter II. In that context, these quantities were obtained from the phenomenological model, but as we have demonstrated in the previous section, the SBD model and the phenomenological model converge in the critical limit, and so do the moments of the conditional probability distribution.

III.7.1 A series expansion for $f(\cdot)$

In this section I want to outline how it is possible to obtain an analytic approximation of the function $f(\mathbf{x}, V, h)$ at stationarity. This will be then used to calculate an approximate distribution for the conditional distribution of the SBD model in the critical limit (equivalently, for the phenomenological model of chapter II).

As a starting point $f(\mathbf{x}, V, h, T)$ will be re-written in terms of a series expansion such as

$$f(\mathbf{x}, V, h, T) = \frac{1}{V} \frac{\partial Z}{\partial h} \left[\sum_{i=0}^{\infty} h^i A_i(\mathbf{x}, V, T) \right] \quad (\text{III.7.4})$$

where A_i are functions that must be appropriately calculated. Imposing that

$$f(\mathbf{x}, V, h, T) \Big|_{h=0} = \langle n(T) \rangle$$

i.e. that $f(\mathbf{x}, V, h, T)|_{h=0} = \langle N(R, T) \rangle / V$ by homogeneity, one readily finds that $A_0(\mathbf{x}) = 1$ and so

$$f(\mathbf{x}, V, h, T) = \frac{1}{V} \frac{\partial Z}{\partial h} \left[1 + \sum_{i=1}^{\infty} h^i A_i(\mathbf{x}, V, T) \right] \quad (\text{III.7.5})$$

From the conditions in eq (III.7.1), one further observes that the following equality must always be satisfied

$$\int_{\mathcal{V}} A_i(\mathbf{x}, V, T) d\mathbf{x} = 0 \quad \text{for } i = 1, 2, \dots \quad (\text{III.7.6})$$

Following the definition of $f(\mathbf{x}, V, h, T)$ one also has

$$\frac{\partial^m}{\partial h^m} f(\mathbf{x}, h) \Big|_{h=0} = \langle n(\mathbf{x}, T) N(R, T)^m \rangle$$

Making use of these relations it is possible to calculate implicitly the value of each of the functions A_i in the expansion. For example by partial-differentiation of eq (III.7.5) and taking $h = 0$ one obtains

$$\langle n(\mathbf{x}) N(R, T) \rangle = \frac{1}{V} \langle N(R, T)^2 \rangle + \langle n(T) \rangle A_1(\mathbf{x}, T)$$

which (implicitly) yields the following expression for $A_1(\mathbf{x}, T)$

$$A_1(\mathbf{x}, T) = \frac{1}{\langle n(T) \rangle} \left(\langle n(\mathbf{x}, T) N(R, T) \rangle - \frac{1}{V} \langle N(R, T)^2 \rangle \right) \quad (\text{III.7.7})$$

At stationarity the T dependence is dropped and, from the results of previous sections and of Chapter II, $A_1(\mathbf{x})$ can be written explicitly. After some easy algebraic calculations, and substituting equations (II.9.4) and (II.10.1) the following expression is obtained

$$A_1(\mathbf{x}) = \frac{\sigma^2}{\mu} \left[\Psi\left(\frac{|\mathbf{x}|}{\lambda}, \frac{R}{\lambda}\right) - \psi\left(\frac{R}{\lambda}\right) \right] \quad (\text{III.7.8})$$

In theory one could continue with the calculation of the moments of $N(R)$ and proceed to writing the explicit equations for each of the $A_i(\cdot)$. However a good deal of simplification

can be obtained by truncating the expansion in eq (III.7.5) to only the second term. This yields the following approximate expression for $f(\mathbf{x}, h)$

$$f(\mathbf{x}, h) = \frac{1}{V} \frac{\partial Z}{\partial h} \left[1 + hA_1(\mathbf{x}) \right] \quad (\text{III.7.9})$$

Of course this is just an approximation and at this stage there is no saying how big is the error that one introduces by truncating the expansion. A proper evaluation of the accuracy of this method is undertaken in section III.7.3. Before the evaluation of the accuracy, the next section will focus on the explicit calculation of the conditional generating function.

III.7.2 Calculation of the approximate solution at stationarity

Substituting eq (III.7.9) into eq (III.6.3), and noticing that

$$\nabla_{\mathbf{x}}^2 A_1(\mathbf{x}) = \frac{1}{\langle n \rangle} \nabla_{\mathbf{x}}^2 \langle n(\mathbf{x})N(R) \rangle \quad (\text{III.7.10})$$

which follows directly from eq (III.7.7), one immediately obtains the following equation

$$\frac{\bar{\lambda}^2 h}{V \langle n \rangle} \int_{\mathcal{V}} d\mathbf{x} \nabla_{\mathbf{x}}^2 \langle n(\mathbf{x})N(R) \rangle \frac{\partial Z}{\partial h} - \frac{\partial Z}{\partial h} + \langle n \rangle V Z + \frac{\sigma^2}{\mu} h \frac{\partial Z}{\partial h} = 0 \quad (\text{III.7.11})$$

I here recall that $\langle n(\mathbf{x})N(R) \rangle$ satisfies the following equation (see eq (II.9.3))

$$\bar{\lambda}^2 \nabla_{\mathbf{x}}^2 \langle n(\mathbf{x})N(R) \rangle - \langle n(\mathbf{x})N(R) \rangle + \langle n \rangle \langle N(R) \rangle + \frac{\sigma^2}{\mu} \langle n \rangle \Theta(|\mathbf{x}| - R) = 0 \quad (\text{III.7.12})$$

which in turn gives

$$\begin{aligned} \bar{\lambda}^2 \int_{\mathcal{V}} d\mathbf{x} \nabla_{\mathbf{x}}^2 \langle n_{\mathbf{x}}N(R) \rangle &= \langle N(R)^2 \rangle - \langle N(R) \rangle^2 - \frac{\sigma^2}{\mu} \langle N(R) \rangle = \\ &= \langle N(R) \rangle \Sigma(R) - \frac{\sigma^2}{\mu} \langle N(R) \rangle \end{aligned} \quad (\text{III.7.13})$$

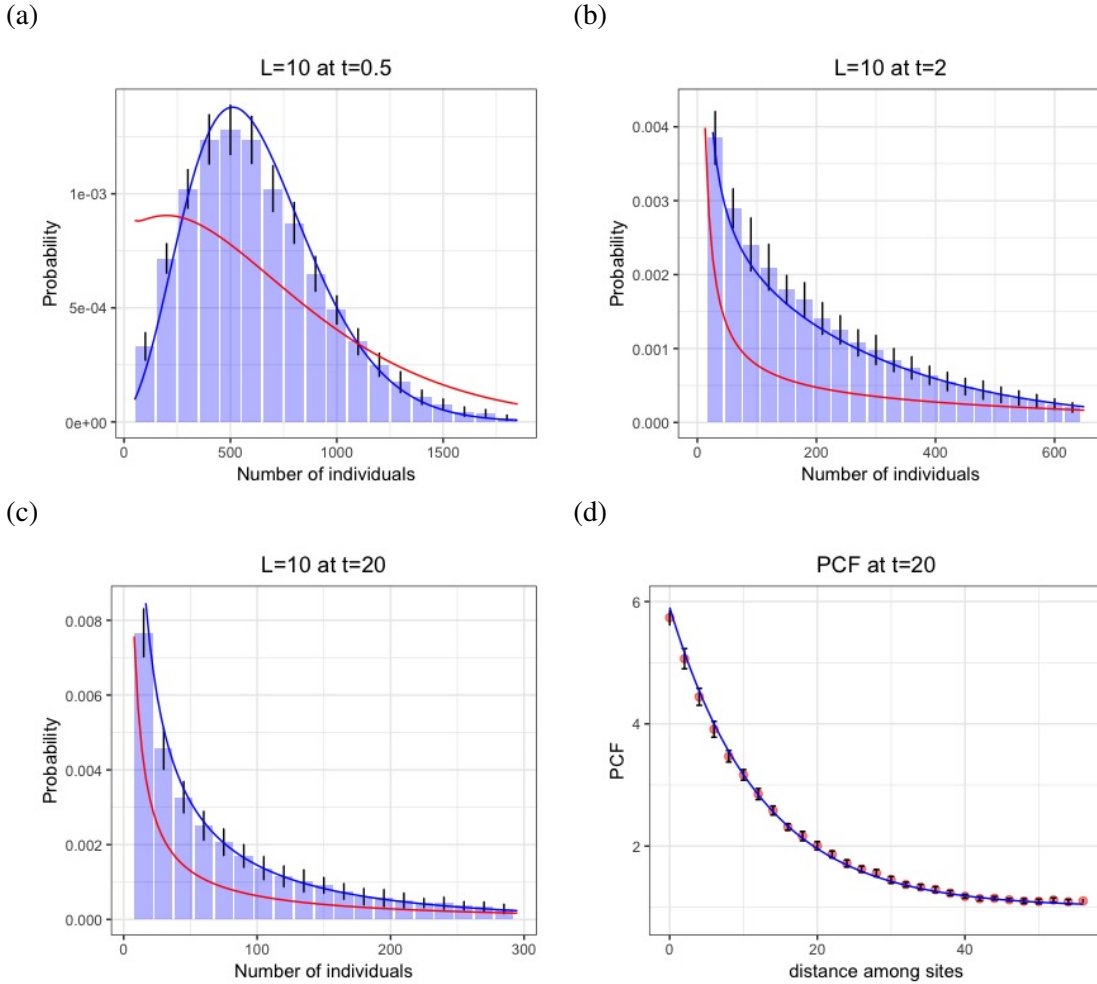


Figure III.7.1: **Comparison of simulated data** of eq (III.1.6) with the theoretical prediction of eq (III.8.3) at different times in dimension one. Histograms are simulated data, with the black segments indicating errors at two sigmas. The blue line is the prediction made by using eq III.8.3, while the red line is the mean field solution, i.e. eq (III.8.3) with $\Sigma(R) = \sigma^2/\mu$. The parameters of the model are $D = 150$, $b_0 = 5$, $b = 300$ and $d = 301$. Panel (a) refers to $T = 0.5$, panel (b) to $T = 2$, and panel (c) to $T = 20$. Panel (d) instead compares the pair correlation function from simulated data at stationarity with the theoretical formula calculated in eq (II.8.4). The lattice has a total of 200 sites. More details on the simulation scheme and on how errors and histograms were calculated will be given in Chapter IV

where the relationship $\Sigma(R) = \frac{\langle N^2(R) \rangle - \langle N(R) \rangle^2}{\langle N \rangle}$ has been used (it stems from eq (II.10.3) and eq (II.10.4)).

Substituting the LHS of eq (III.7.13) into equation (III.7.11) one arrives at the following

$$\left(1 - h \Sigma(R)\right) \frac{\partial Z}{\partial h} = \langle n \rangle V Z \quad (\text{III.7.14})$$

This equation is easily solved in h , and imposing normalisation conditions, i.e. that $Z(h) \Big|_{h=0} = 1$, the following explicit formula for $Z(h)$ is obtained

$$Z(h|V) = \left(1 - h \Sigma(R)\right)^{-\frac{\langle N \rangle}{\Sigma(R)}}$$

Inverting $Z(h|V)$ (using the inverse Laplace transform) yields the probability distribution for N at stationarity, i.e.

$$P(N|R) = \left(\frac{1}{\Sigma(R)}\right)^{\frac{\langle N(R) \rangle}{\Sigma(R)}} \frac{N^{\frac{\langle N(R) \rangle}{\Sigma(R)} - 1} e^{-\frac{N}{\Sigma(R)}}}{\Gamma\left(\frac{\langle N(R) \rangle}{\Sigma(R)}\right)}. \quad (\text{III.7.15})$$

which is a gamma distribution and is exactly equal to the one that was heuristically assumed in Chapter II as the stationary conditional probability distribution of the phenomenological model, i.e. eq (II.11.1). This result is not trivial and does not only represent a perturbation of the mean-field regime. The simplicity of this equation is in striking contrast with the complexity of the SBD model, and in fact it is a good approximation of $P(N|R)$ only in some regimes of parameters, i.e. the critical regime described before.

In equation (III.7.15) one can observe that changes of the spatial scale are encoded in the appropriate scaling of the parameters. Since $\Sigma(R) = \frac{\sigma^2}{\mu}$ as $\bar{\lambda} \rightarrow 0$ one also re-obtains the mean field solution in such limit. On the other hand the fact that $\Sigma(R) \rightarrow 0$ as $\bar{\lambda} \rightarrow \infty$ leads to $Z(h|V) = e^{\langle N(R) \rangle h}$, and the probability distribution reduces to a delta function centered at the mean population $\langle N(R) \rangle$.

Figure III.6.1 compares the simulations of the Markov birth death process with rates in eq (III.1.5) at stationarity and the conditional probability density function just obtained at eq (III.7.15). The match is surprisingly good at all scales.

III.7.3 Evaluation of the accuracy of the method

In order to calculate the accuracy of such approach and to estimate the error that one introduces truncating the expansion at eq (III.7.5) as in eq (III.7.9) one possibility is to substitute the expression for $f(\cdot)$ at eq (III.7.9) into eq (III.5.4) at stationarity. This way it is possible to give explicit calculation of the terms that do not cancel out.

Substituting eq (III.7.9) into eq (III.6.3) one obtains

$$\begin{aligned} \frac{\partial}{\partial T} \frac{1}{V} \frac{\partial Z}{\partial h} [1 + hA_1(\mathbf{x})] &= \bar{\lambda}^2 \nabla_{\mathbf{x}}^2 \frac{1}{V} \frac{\partial Z}{\partial h} [1 + hA_1(\mathbf{x})] - \frac{1}{V} \frac{\partial Z}{\partial h} [1 + hA_1(\mathbf{x})] + \langle n \rangle Z + \\ &+ h \left\{ \bar{\lambda}^2 \frac{\partial}{\partial h} \nabla_{\mathbf{x}}^2 \frac{1}{V} \frac{\partial Z}{\partial h} [1 + hA_1(\mathbf{x})] - \frac{\partial}{\partial h} \frac{1}{V} \frac{\partial Z}{\partial h} [1 + hA_1(\mathbf{x})] + \right. \\ &+ \langle n \rangle V \frac{1}{V} \frac{\partial Z}{\partial h} [1 + hA_1(\mathbf{x})] \left. \right\} + \\ &+ \frac{\sigma^2}{\mu} \frac{\partial}{\partial h} \left\{ h^2 \frac{1}{V} \frac{\partial Z}{\partial h} [1 + hA_1(\mathbf{x})] \right\} \end{aligned} \quad (\text{III.7.16})$$

At stationarity (i.e. putting all time derivatives to zero), taking eq (III.7.10) and substituting the LHS of eq (III.7.13) into eq (III.7.16), the following equation is obtained

$$\begin{aligned} \frac{\partial}{\partial h} \left\{ h \left[- \left(1 - h\Sigma(R) \right) \frac{\partial Z}{\partial h} + \langle n \rangle V Z \right] \right\} + \\ + A_1(\mathbf{x}, R) \left\{ \frac{\partial}{\partial h} \left[\frac{\sigma^2}{\mu} h^3 \frac{\partial Z}{\partial h} \right] + h^2 \langle n \rangle V \frac{\partial Z}{\partial h} \right\} = 0 \end{aligned} \quad (\text{III.7.17})$$

One can immediately observe that retaining only terms up to $\mathcal{O}(h)$ for h small this equation reduces to the h -partial derivative of eq (III.7.14), and hence is solved by the probability density function at eq (III.7.15). The limit of small h is tantamount to considering a large population approximation.

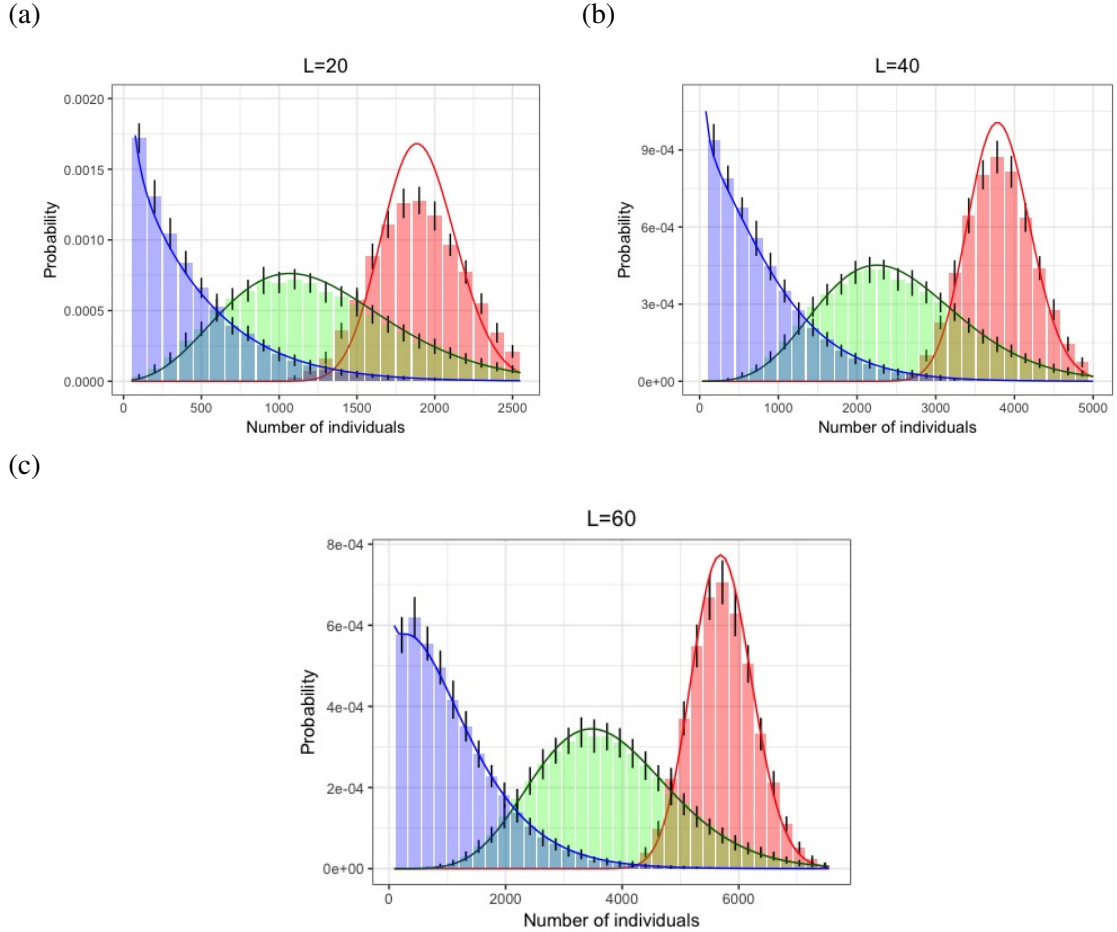


Figure III.7.2: **Comparison of simulated data** of eq (III.1.6) with the theoretical prediction of eq (III.8.3) at different times in dimension one and for different segment length. Histograms are data simulated with Doob-Gillespie algorithm, with the black segments indicating errors at two standard deviations. the different colors represent different times, with red indicating $T = 0.05$, green $T = 0.5$ and blue $T = 2$. The parameters here are $D = 150$, $b_0 = 5$, $b = 600$ and $d = 601$ (hence $\gamma = 1/2$). Panel (a) refers to a segment of length 20 sites, panel (b) to one of length 40 sites, and panel (c) 60 sites. The lattice has a total of 400 sites. More details on the simulation scheme and on how errors and histograms were calculated are given in chapter IV

Another important case where the equation is satisfied is for $A_1(\mathbf{x}, R) = 0$. As seen in eq (III.7.8), $A_1(\mathbf{x}, R)$ can be written in terms of $\Psi(\cdot)$ and $\psi(\cdot)$ as follows

$$A_1(\mathbf{x}, R) = \frac{\sigma^2}{\mu} \left[\Psi\left(\frac{|\mathbf{x}|}{\bar{\lambda}}, \frac{R}{\bar{\lambda}}\right) - \psi\left(\frac{R}{\bar{\lambda}}\right) \right]$$

As was showed in the previous chapter (and in figures II.10.1 and II.9.1) fixing $|\mathbf{x}|$ and R and taking $\bar{\lambda} \rightarrow 0$ the following asymptotic expansions are found

$$\begin{aligned} \Psi\left(\frac{|\mathbf{x}|}{\bar{\lambda}}, \frac{R}{\bar{\lambda}}\right) &= 1 + \mathcal{O}\left[e^{-\frac{R-|\mathbf{x}|}{\bar{\lambda}}}\left(\frac{|\mathbf{x}|}{R}\right)^{1-d}\right] \\ \psi\left(\frac{R}{\bar{\lambda}}\right) &= 1 + \mathcal{O}\left(\frac{\bar{\lambda}}{R}\right) \end{aligned}$$

Therefore for $|\mathbf{x}| < R$ their difference indeed vanishes and $A_1(\mathbf{x}, R) \rightarrow 0$. At the same time one can verify that Ψ and ψ both tend to zero as $\bar{\lambda} \rightarrow \infty$ (see eq (II.9.8) and eq (II.10.5), and figures II.10.1 and II.9.1). even in this regime one therefore obtains $A_1(\mathbf{x}, R) \rightarrow 0$.

The analysis of equation (III.7.17) has highlighted that there exists at least two parameter regimes where the error that is introduced truncating the expansion (III.7.5) as in eq (III.7.9) tends to zero. Together with such regimes it was also shown that for large populations, i.e. if one retains terms up to $\mathcal{O}(h)$ as $h \rightarrow 0$, the neglected terms are of higher order.

The interplay of these two effects makes it possible to approximate the conditional distribution of the model with eq (III.7.15) with very high accuracy for many choices of parameters close to the critical point. Intuitively, as the system stirs away from the mean field case ($\bar{\lambda} = 0$) one needs to consider slightly larger populations and the approximation is still good. By increasing $\bar{\lambda}$, one reaches the maximum of $A_1(x, R)$ and the approximation deteriorates (though it can still be very accurate), but as soon as $\bar{\lambda}$ is increased the approximation yields again better results, and moving towards the regimes of very large

$\bar{\lambda}$ it keeps improving. These intuitions are confirmed by simulations in all the expected cases.

In Appendix C a similar process is undertaken for $f(\mathbf{x})$ for the case $|\mathbf{x}| > R$ for solving eq III.6.4. An implicit form is obtained and consistency equations are found. However, this case turns out to be involved, and it is not possible to find an approximation whose functional form is independent of the spatial scale, as instead was possible for $|\mathbf{x}| < R$.

III.8 Time-dependent spatial analysis

The study of stationary patterns has revealed that there is a surprising parallelism between the mean field probability distribution and the conditional distribution in the spatially extended model, in that the functional form of the conditional probability distribution turns out to be scale invariant and to coincide with the mean field distribution. It is now natural to wonder what is the relationship among them as the system moves away from stationarity. In particular, is it still true that, approximately, the spatial conditional distribution retains the mean field shape? And if so, how do parameters vary with scale?

In appendix E, I consider an ansatz for the functional form of $f(\mathbf{x}, h, V, T)$ which allows for some analytic treatment. The results that are obtained reflect the intuition that if the conditional probability distribution is form invariant at stationarity, then this must hold true also close to the stationary regime (i.e. for $t \gg \mu$). In this section I will only give an overview of the results of such analysis, which is not fully rigorous and has to be considered as an approximation for $t \gtrsim \mu$. Nonetheless it gives an insightful look into the spatial evolution of the SBD model.

For values of $T = \mu t$ that are not too small (see appendix E) the Fokker-Planck equation

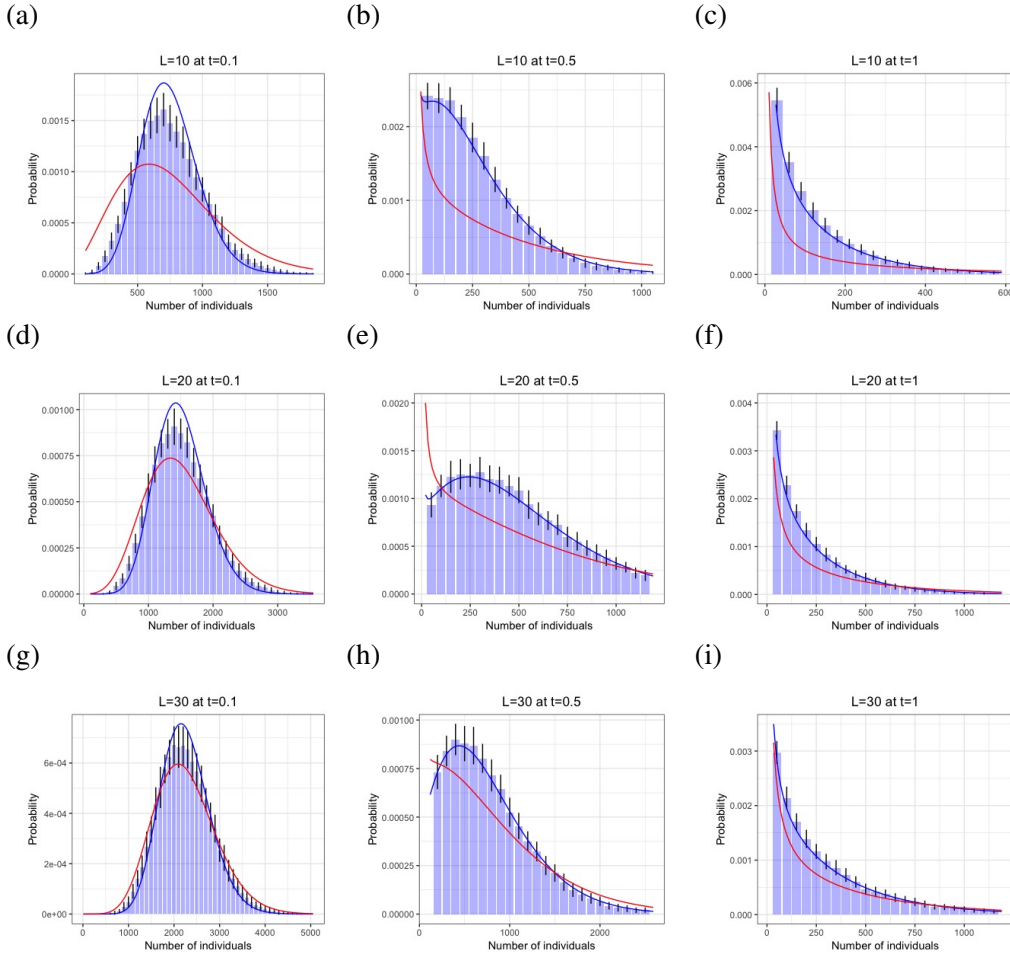


Figure III.7.3: **Comparison of simulated data** of eq (III.1.6) with the theoretical prediction of eq (III.8.3) at different times in dimension one. Histograms are simulated data, with the black segments indicating errors at two standard deviations. The blue line is the prediction of eq (III.8.3), while the red line is the mean field solution, i.e. eq (III.8.3) with $\Sigma(R) = \sigma^2/\mu$. The parameters of the model are $D = 500$, $b_0 = 10$, $b = 1200$ and $r = 1203$. Length of the segments and times are reported in the titles of the plots. Notice that for small t the analytical solution (blue line) does not give accurate results, but also that already for $t = 0.5$ the accordance is very good. The lattice has a total of 200 sites. More details on the simulation scheme and on how errors and histograms were calculated will be given in Chapter IV.

that describes the time-dependent conditional probability distribution reads

$$\frac{\partial}{\partial T} p(N, T) = -\frac{\partial}{\partial N} \left[(\langle N(R) \rangle - N) p(N, T) \right] + \Sigma(R) \frac{\partial^2}{\partial N^2} \left[N p(N, T) \right] \quad (\text{III.8.1})$$

In the Itô prescription this equation is associated to the following Langevin equation

$$\dot{N}(R) = \bar{b}_0 V - \mu N(R) + \sigma \sqrt{\psi(R/\bar{\lambda}) N(R)} \xi(t) \quad (\text{III.8.2})$$

where $\xi(t)$ is a Gaussian white noise with covariance $\langle \xi(t) \xi(t') \rangle = 2 \delta(t - t')$.

Notice that eq (III.8.2) has the same exact form as eq (II.5.2) where the mean and the fluctuations have been rescaled to accommodate changes of size of the area (or volume, or length).

If the number of individuals in \mathcal{V} at time $t = 0$ is N_0 , solving eq (III.8.1) the probability to have N individuals at time t is given by the following equation [13]

$$p(N, t | N_0, 0) = \left(\frac{1}{\Sigma(R)} \right)^{\frac{\langle N \rangle}{\Sigma(R)}} N^{\frac{\langle N \rangle}{\Sigma(R)} - 1} e^{-\frac{N}{\Sigma(R)}} \frac{\left[\left(\frac{1}{\Sigma(R)} \right)^2 N_0 N e^{-\mu t} \right]^{\frac{1}{2} - \frac{\langle N \rangle}{2\Sigma(R)}}}{1 - e^{-\mu t}} \times \exp \left[-\frac{\frac{1}{\Sigma(R)} (N + N_0) e^{-\mu t}}{1 - e^{-\mu t}} \right] I_{\frac{\langle N \rangle}{\Sigma(R)} - 1} \left[\frac{\frac{2}{\Sigma(R)} \sqrt{N_0 N e^{-\mu t}}}{1 - e^{-\mu t}} \right] \quad (\text{III.8.3})$$

For $\bar{\lambda} \rightarrow 0$ it can be verified that indeed one retains the mean field solution of the model since $\Sigma(R) = \sigma^2/\mu$. In appendix E it is also shown that for $t \rightarrow \infty$ this equation converges to the stationary solution, i.e. eq (III.7.15).

In chapter II the species turnover distribution was introduced to account for the turnover in species abundance in the mean field model (see equation (II.6.2)). I recall here that the STD measures the probability that the ratio of abundances of a species separated by a time interval t , $N(t)/N(0)$, is equal to m . Under stationary conditions, in the SBD model it is possible to obtain its explicit form by just replacing $\langle n \rangle = b_0/\mu$ with $\langle N \rangle = \bar{b}_0 V/\mu$ and σ^2/μ with $\Sigma(R)$ in eq (II.6.3).

The result is the following

$$\begin{aligned}
 STD(m, t) = A \frac{m+1}{m} \frac{(e^{\mu t})^{\frac{\langle N \rangle}{2\Sigma(R)}}}{1 - e^{-\mu t}} \left(\frac{\sinh(\mu t/2)}{m} \right)^{\frac{\langle N \rangle}{\Sigma(R)} + 1} \times \\
 \times \left(\frac{4m^2}{(m+1)^2 e^{\mu t} - 4m} \right)^{\frac{\langle N \rangle}{\Sigma(R)} + \frac{1}{2}}
 \end{aligned} \tag{III.8.4}$$

with A being a normalisation constant, $\langle N \rangle = \frac{\bar{b}_0 V}{\mu}$ and $\Sigma(R)$ taking the form in eq (II.10.4).

These equations have been compared to simulations of the SBD model: figures III.7.1, III.7.2 and III.7.3 show comparison of eq (III.8.3) with the simulations of the system, which have been made using Doob-Gillespie algorithm (more details on the simulation scheme are given in chapter IV). It is possible to observe that as one moves away from stationarity the model performs worse, and in the cases of $T \ll 1$ the analytical and simulated distributions differ significantly. Nonetheless, the accord of the predicted distribution and the simulated one is very good even at relatively small times, i.e. for $T \approx 1$.

Equation (III.8.1) has the same structure as the mean field equation of the model, i.e. eq (II.5.1). This process, unlike the spatial one, satisfies the detailed balance condition at stationarity as the flux at $N = 0$ is set to zero. This result suggests that there are some families of spatially-explicit processes which, when conditioned on a volume, can be well approximated by spatially-implicit processes. Whilst the former breaks detailed balance, the latter turns out to be simpler and satisfies the detailed balance condition. In this model the region of this approximation is close to the critical point of the process, and in such regime it has been possible to calculate the conditional probability distribution of the process explicitly.

Chapter IV

Simulation Schemes and Data Analysis

IV.1 Simulations of the process

Simulations of spatial stochastic processes are often affected by severe drawbacks and limitations. From the theoretical side, adding spatial dispersal to a process is no more problematic than adding a new reaction channel to the system. But from the computational side, the memory requirements involved in the simulation of spatially extended systems can easily add up to the mega-Bytes for lattices of only thousands of sites. If one further wants to characterise the probability distribution of the process, then each realisation has to be run many times (tens or hundreds of thousands) and the memory needed easily scales up to the Gigabytes and beyond.

Issues arise also around the time needed for running the code. It is well known that there exist an exact way to simulate Markov jump processes, known as the Doob-Gillespie scheme [71]. It operates by evolving the system through time from an initial configuration to a desired time t , and the results are rigorous to computer accuracy (i.e. minimal errors are due to number storage, but this is easily negligible in most cases). However, this scheme is extremely slow and it may take several days to progress relatively small systems

to equilibrium. It goes without saying that the analysis of stationary distributions is often intractable in practice with the current computational power.

There exist many approximate ways to speed up the simulation of stochastic processes. Among the most well-known is the so called " τ -leap" algorithm [72, 35]. Instead of executing one reaction in every microscopic time interval and changing the participating species by stoichiometric populations, in the " τ -leap" algorithm one selects a coarse-time increment, which is usually larger than the microscopic one, "fires" each reaction multiple times and updates the populations after each time step accordingly. This approximate method is faster (depending on how large the coarse-time increment is taken), but it also presents many disadvantages. For example, it is often inconsistent with boundary conditions and it may generate negative abundances for rare species.

In the following, I will describe two algorithms for generating realisations of stochastic processes. The first will be the exact Doob-Gillespie algorithm.

IV.1.1 Doob-Gillespie Algorithm

In a one dimensional regular lattice (i.e. a segment) with M sites, I have imposed periodic boundary conditions: the site at position $M-1$ is neighbour with that at position 0 and vice versa. This framework is a good approximation of the infinite lattice when the correlation length of the system is much smaller than M .

I choose a homogeneous initial configuration with constant local abundance of individuals, i.e. every site has the same initial number of individuals.

The first step of the algorithm is to decide which reaction occurs. The probability of each reaction to take place is proportional to the rate of that reaction. For example, if in a generic process the rate of going from state i to state j is $R_{i,j}$, then the probability to jump

to state j in a time step δt when the system is in state i ($P_{i \rightarrow j}$) is going to be equal to

$$P_{i \rightarrow j} = \frac{R_{i,j}}{\sum_k R_{i,k}}$$

Therefore, one can decide which reaction occurs at a certain time t by generating a random number, uniformly distributed in the interval $[0, 1]$, and assigning to each of its values a reaction channel (proportionally to $P_{i \rightarrow j}$).

After updating the state of the system according to the selected reaction channel, one needs to update the time count. It can be demonstrated that the time interval between two reactions is exponentially distributed with mean dependent on the inverse of the total reactivity of the system. For example, if the system is in state i the time needed for another reaction to occur (indicated with T) will be exponentially distributed with mean $1/\sum_k R_{i,k}$. One can hence draw the value of T from this distribution and update the total time count. Then one proceeds at selecting the next reaction to 'fire' following the previous steps.

By repeating this procedure, it is possible to create a faithful simulation of the dynamical evolution of the system. For more details see [73]

In the one dimensional case and for relatively small lattices (≈ 200 sites), I have been able to simulate the full time development of the system for some parameter choices. Results are reported in figures III.7.1 and III.7.2. For larger values of $\bar{\lambda}$ (recall that it is the correlation length of the system, defined in chapter III), or in higher dimensions this algorithm is not a viable option, mostly due to restrictions in the maximum running time of the code.

Another simulation scheme can be implemented which is efficiently optimised for the stationary distributions of stochastic partial differential equations, and which allows to inspect a much larger set of parameters.

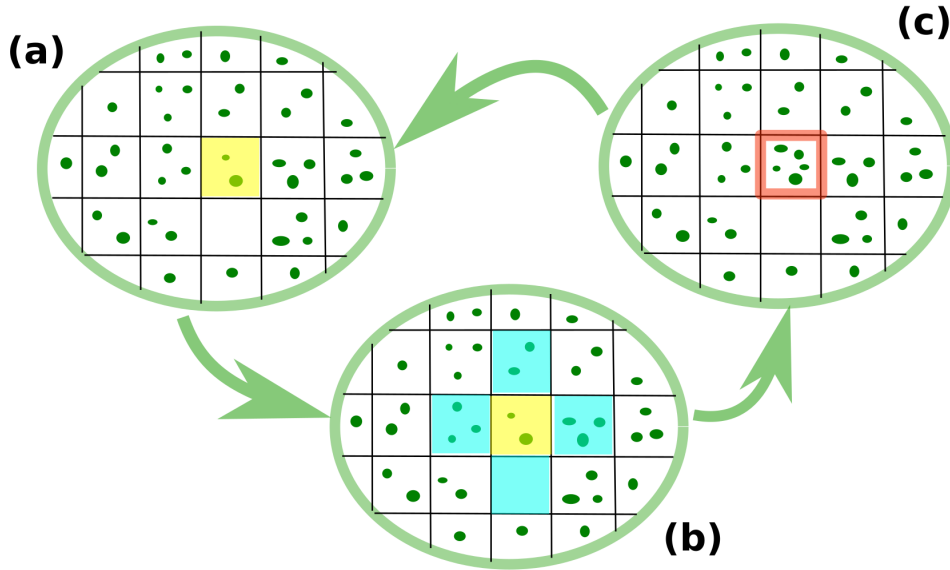


Figure IV.1.1: **Illustration of the phenomenological algorithm.** The figure illustrates the different steps of the phenomenological algorithm. In step (a) a site in the lattice is chosen (uniformly at random), then in step (b) the abundances in the nearest neighboring sites are considered and $Y(t)$ is calculated with eq (IV.1.4). In step (c), the value in the site is updated drawing from the distribution in eq (IV.1.6). Then the process is repeated until the simulated configuration reaches the desired level of accuracy.

IV.1.2 "Phenomenological" Algorithm

The critical limit, as defined in chapter III, has provided a novel 'diffusion approximation' for the analysis of the SBD model. The initial discrete random variables n_i , characterising the local number of individuals, were approximated by continuous random variables, and accordingly the master equation of the Markov jump process was transformed into a stochastic partial differential equation (SPDE), i.e. eq (III.4.4).

Simplistic numerical schemes for integrating SPDEs are affected by severe drawbacks. For instance, in a first-order explicit Euler method for the mean-field model the following update rule for $n(t + \Delta t)$ from $n(t)$ is used

$$n(t + \Delta t) = n(t) + \Delta t[b_0 - \mu n(t)] + \sigma \sqrt{\Delta t n(t)} N(0, 1) \quad (\text{IV.1.1})$$

where $N(0, 1)$ is a zero mean random Gaussian variable with variance one. For initial values $n(0)$ that are close to zero this method eventually produces negative $n(\cdot)$ values. In the spatial case these negative densities are even more harmful because they correlate with each other and drive entire clusters of sites to negative, non-physical values.

An efficient way of integrating some families of stochastic (partial) differential equations with multiplicative noise such as eq (II.7.1) can nonetheless be formulated. Building on a previous method introduced in the context of directed percolation [54], one can separate the integration of the spatial part of the equation (the discrete Laplacian) from the stochastic part.

I here recall the definition of the discrete Laplacian on a 2-dimensional regular lattice of mesh size a

$$\Delta_{\mathbf{x}} n_{\mathbf{x}}(t) = \sum_{i=1}^4 \left(n_{\mathbf{x}+a\mathbf{e}_i}(t) - n_{\mathbf{x}}(t) \right) \quad (\text{IV.1.2})$$

where $\mathbf{e}_1 = (1, 0)$, $\mathbf{e}_2 = (-1, 0)$, $\mathbf{e}_3 = (0, 1)$ and $\mathbf{e}_4 = (0, -1)$: these are the direction unitary vectors of the lattice. Obviously this notation can be generalised to any dimension d , with $\mathbf{e}_j = (0, \dots, 1, 0, \dots)$ and $\mathbf{e}_{j+1} = (0, \dots, -1, 0, \dots)$ having non zero elements at the $\lfloor j/2 \rfloor$ -th place.

I also recall that in the spatially explicit case within the critical limit the dynamics of the SBD model is described by the following stochastic partial differential equation (III.4.4)

$$\dot{n}_{\mathbf{x}}(t) = D \Delta_{\mathbf{x}} n_{\mathbf{x}}(t) + b_0 - \mu n_{\mathbf{x}}(t) + \sigma \sqrt{n_{\mathbf{x}}} \xi_i \quad (\text{IV.1.3})$$

with $\mathbf{x} \in \mathbb{L}$ (recall that \mathbb{L} is a regular, d -dimensional lattice of side a).

I therefore introduce the following notation

$$Y_{nn\{\mathbf{x}\}}(t) = D \sum_{i=1}^{2d} n_{\mathbf{x}+a\mathbf{e}_i}(t) + b_0 \quad \text{and} \quad \Omega = \frac{4D}{a^2} + \mu \quad (\text{IV.1.4})$$

where the notation $nn\{\mathbf{x}\}$ indicates the nearest neighboring sites of \mathbf{x} . I rewrite eq (IV.1.3)

as

$$\dot{n}_{\mathbf{x}}(t) = Y_{nn\{\mathbf{x}\}}(t) - \Omega n_{\mathbf{x}}(t) + \sigma \sqrt{n_{\mathbf{x}}} \xi_i \quad (\text{IV.1.5})$$

Notice that $Y_{nn\{\mathbf{x}\}}(t)$ is positive since both $n_{\mathbf{x}}$ and b_0 are strictly positive.

Conditional on $Y_{nn\{\mathbf{x}\}}(t)$, one can readily observe that eq (IV.1.5) has the same form as the Langevin equation of the mean field model, eq (II.5.2), where b_0 is substituted with $Y_{nn\{\mathbf{x}\}}(t)$ and μ with Ω . It appears, therefore, evident that $Y_{nn\{\mathbf{x}\}}(t)$ can be interpreted as an effective immigration parameter which accounts for the global as well as the local immigration in site \mathbf{x} from neighbouring sites.

Following the same steps outlined in chapter II for calculating eq (II.5.3), it is straightforward to prove that at stationarity the following holds

$$P(n_{\mathbf{x}} | Y_{nn\{\mathbf{x}\}}(t), t) = \left(\frac{\Omega}{\sigma^2} \right)^{\frac{Y_{nn\{\mathbf{x}\}}(t)}{\sigma^2}} \frac{N^{\frac{Y_{nn\{\mathbf{x}\}}(t)}{\sigma^2} - 1} e^{-\frac{N \Omega}{\sigma^2}}}{\Gamma\left(\frac{Y_{nn\{\mathbf{x}\}}(t)}{\sigma^2}\right)} \quad (\text{IV.1.6})$$

These observations set the ground for a novel numerical integration scheme for the field $n_{\mathbf{x}}(t)$ at stationarity in generic dimension d . As a first step (step (0)), one initializes the lattice with $n_{\mathbf{x}}^{(0)} > 0$. A typical choice is to set a constant value in each voxel. At the m -th step (labelled (m)) one randomly selects a site, labelled \mathbf{x} , and calculates

$$Y_{nn\{\mathbf{x}\}}^{(m)}(t) = D \sum_{j=1}^{2d} n_{\mathbf{x}+a\mathbf{e}_j}^{(m)} + b_0$$

Then the value of $n_{\mathbf{x}}^{(m)}$ is updated by sampling from eq (IV.1.6), the stationary distribution conditional on $Y_{nn\{\mathbf{x}\}}^{(m)}$, i.e.

$$n_{\mathbf{x}}^{(m+1)} = \text{Gamma}\left[\frac{Y_{nn\{\mathbf{x}\}}^{(m)}(t)}{\sigma^2}, \frac{\sigma^2}{\Omega}\right]$$

where $\text{Gamma}[\alpha, \beta]$ is the gamma distribution with shape parameter α and scale parameter β .

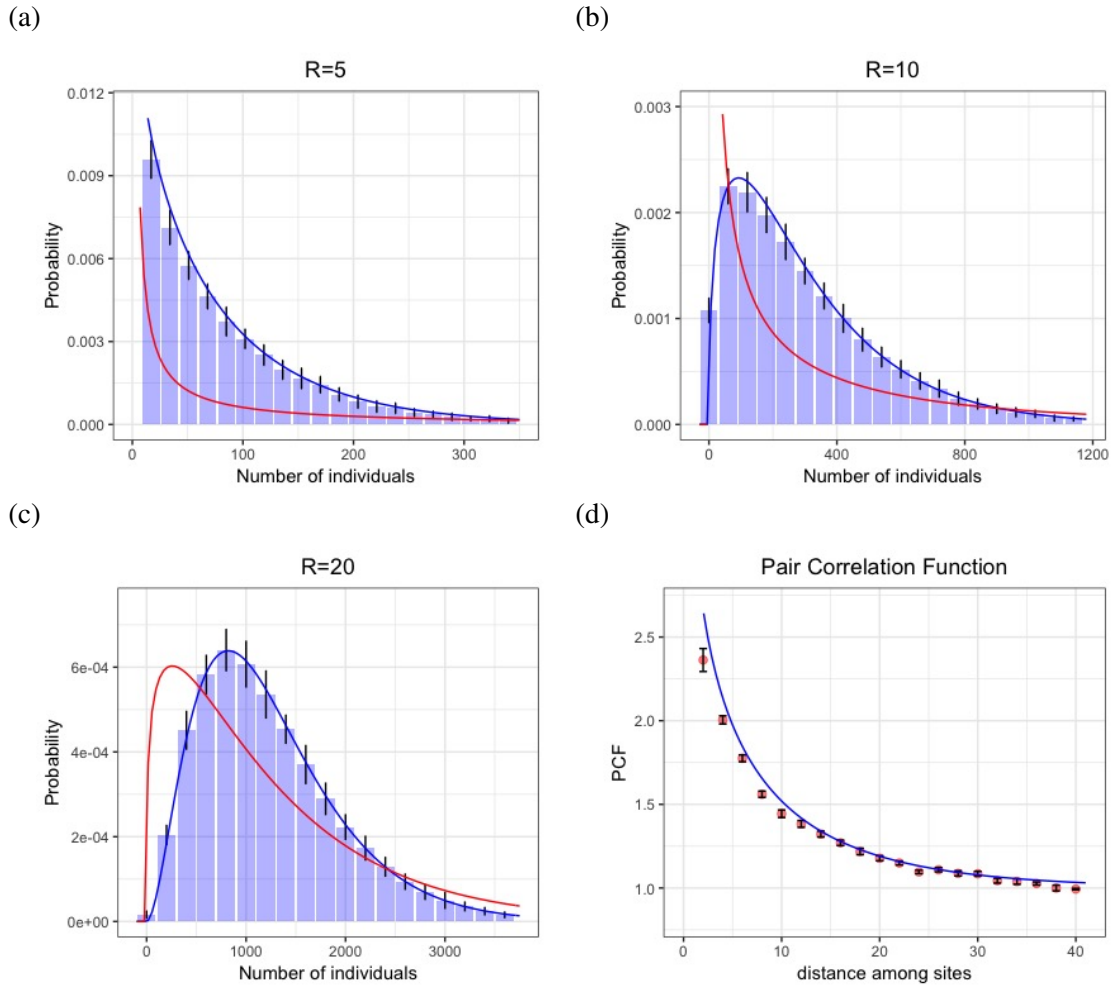


Figure IV.1.2: **Comparison of simulated data of the model with the theoretical prediction** of eq (III.7.15) at different times in dimension two. Histograms are simulated data, with the black segments indicating errors at two standard deviations. The blue line is the prediction made using eq (III.7.15), while the red line is the mean field solution, i.e. as the one reported in eq (II.5.3). The parameters of the model are $D = 20$, $b_0 = 0.1$, $\mu = 0.1$ and $\sigma = 10$. Panel (a) refers to an area of radius 5 sites, panel (b) to one of radius $R = 10$, and panel (c) to $R = 20$. Panel (d) instead compares the pair correlation function from simulated data at stationarity with the theoretical formula calculated in eq (II.8.4). The lattice has a total of 10,000 sites placed on a square lattice of 100×100 sites.

It is worth remarking that, since $n_{\mathbf{x}}^{(0)} \geq 0$, then also $Y_{nn\{\mathbf{x}\}}(t)$ and Ω are, and therefore by construction $n_{\mathbf{x}}^{(m)} > 0$ at any step m . The process whose steps have just been outlined is therefore guaranteed to avoid the inconsistencies caused by negative densities.

By repeating this process multiple times, the value in each and every site is updated. One continues this process until all the stationary summary statistics of interest do not change significantly between generations, or until they match a stationary summary statistics calculated analytically from the model (e.g. the two point correlation function) (fig IV.1.1). The data represented by the histograms in figures II.11.1 , II.10.2, III.6.1 and IV.1.2 have been calculated using this simulation scheme.

It is worth remarking that the algorithm does not simulate the temporal dynamics of the systems: the m -th iterative steps does not correspond to the m -th time-step of evolution of the system. The algorithm proceeds from a randomly generated initial configuration (which could be even uniform) towards a configuration (a field) which is sampled from the stationary probability distribution of eq (III.4.4).

Here, I will not give any mathematical proof that such approach converges to the actual stationary distribution of the process. To the best of our knowledge, such a proof has not yet been reported in the literature. Instead, I will compare its results with those of the correspondent birth-death Markov jump process simulated with the Doob Gillespie algorithm close to the critical point. Despite not being a proof, this gives a first term of comparison of the accuracy of the new, 'phenomenological' scheme. The results are shown in fig IV.1.3. The agreement is very good for every single point.

All the graphs presented in this thesis are the result of the following procedure. I have implemented the numerical scheme for several choices of parameters, and for each choice I have calculated 50000 independent realisations of the process. Error bars were calculated by grouping the results into 50 sets made of 1000 realizations each. The Doob-Gillespie algorithm was implemented only in the one dimensional case, while the so called 'Phenomenological' scheme was used also in the two dimensional case. I have compared the analytic pair correlation function and conditional probability distribution to the analytic one obtained through the mathematical analysis of previous sections. The results show excellent agreement in all expected regimes.

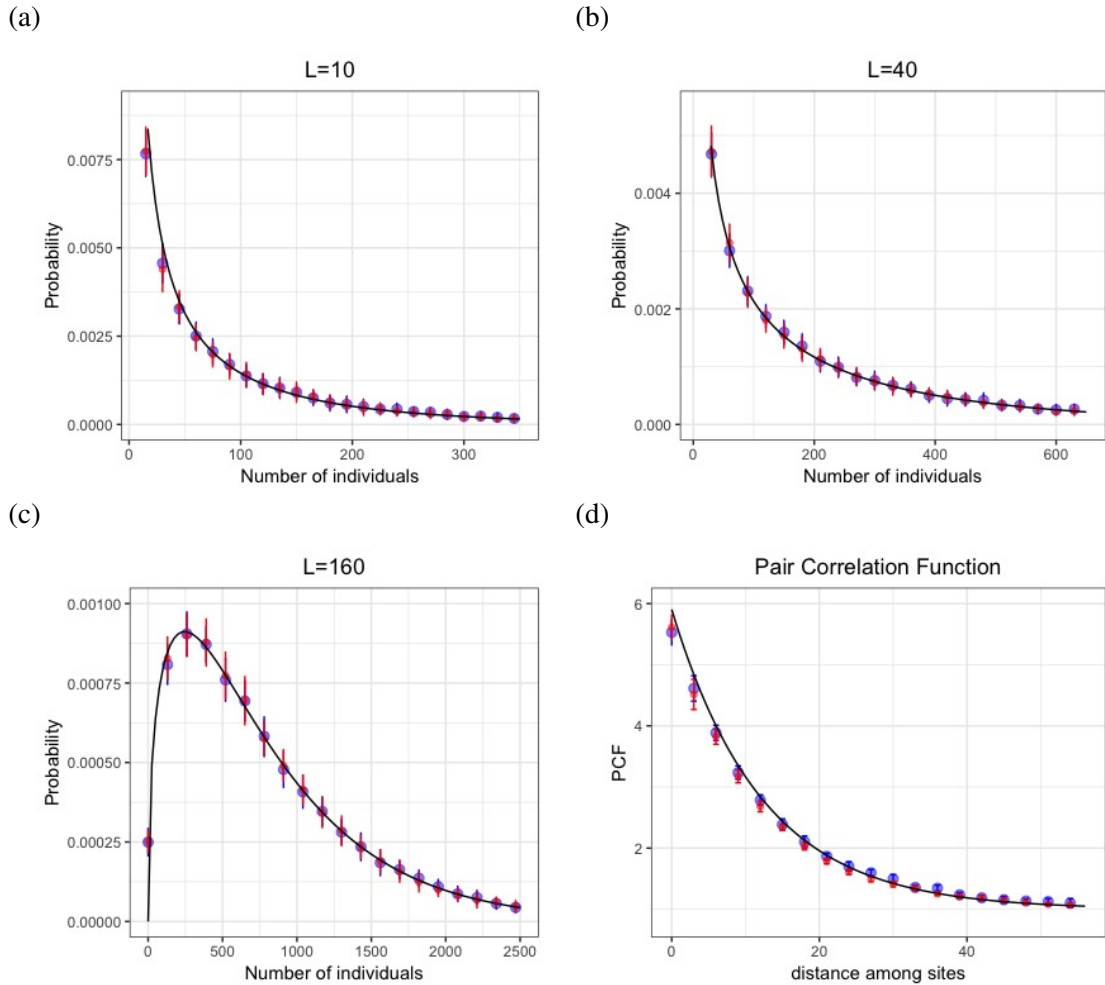


Figure IV.1.3: **Comparison of the conditional probability distribution** simulated on the same set of parameters and on lattices of the same size using different algorithms at stationarity and in one dimension. Blue dots represent data from the phenomenological scheme (and blue segments are the respective errorbars), while red dots are from the Doob-Gillespie algorithm (with respective errorbars). The black solid line is the analytic prediction from eq (III.7.15). The choice of parameters is $b = 600$, $d = 601$, $\gamma = 0.5$, $b_0 = 5$ ($D = 150$) and hence $\lambda \approx 12$. The lattices have 200 total sites, and periodic boundary conditions have been used.

IV.2 Ecological descriptors and data analysis

The rest of this chapter will focus on the analysis of real ecological data, and on the comparison between them and some theoretical predictions that are obtained through the

models that have been analysed in previous chapters.

Ecological patterns are deeply tied up in issues of scale. It is evident, even from the everyday personal experience, that environmental conditions vary in complex, multi-scaled ways in space and time. Different organisms move and respond to such external stimuli in different ways depending on their size, geographical position, attitude, age, ecc.

Nonetheless, important contributions to our understanding of community assembly have come from the study of ecological patterns across scales. Macro-ecology has been prolific at suggesting new tools and descriptors, each with the aim of shedding light on some specific trait [14]. For example, the Relative Species Abundance (RSA) describes the probability of finding a species with n individuals living on a specific area and it brings important information on the very own survival rates of individuals, on their chances of successfully giving birth, on their spatial dispersal, and ultimately also on the nature of interactions with other specimen. The RSA plays a pivotal role for conservation strategies and for assessing biodiversity. A plethora of models have tried to address the mechanisms underpinning its functional shape, and many have succeeded in matching empirical data fairly well. Most of them rely on mean-field models and assume well-mixed populations, even though the assumptions underpinning these models are usually not satisfied in real datasets [171, 172, 142].

The β -diversity examines the characteristic spatial turnover of species, and it is proportional to the probability that two individuals picked at random in the system at a certain distance r are con-specific. Since real populations are spatially clustered, aggregation decreases the similarity of communities that are farther apart, thus promoting a higher diversity. This implies that the β -diversity of empirical systems is typically a decreasing function of r . For understanding spatial turnover often the pair correlation function, defined as in equation (II.8.4), is preferred.

The Species-Area Relationship (SAR), instead, describes how the average number of species increases with the size of the sampled area. It has been observed to display three

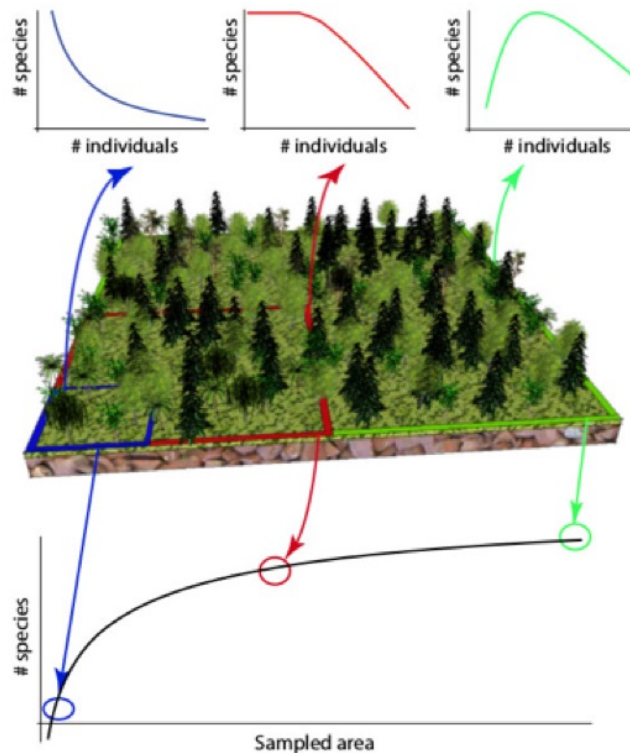


Figure IV.2.1: **Spatial Ecological descriptors.** Spatial ecological descriptors are deeply intertwined. The image illustrates the relationship between the relative species abundance and the species area relationship at the different scales. Figure from [10].

qualitatively different behaviors from local to continental spatial scales: in log-log scale it is approximately linear at very small and very large scales, while it is power-law-like at intermediate scales. This is often referred to as the 'triphase curve'. The SAR also retains the longest history of research and analysis, and it is of crucial importance for accounting rare and endangered species.

These three ecological patterns are not independent from one another, but are inter-related in a deep way [10, 142]. The following paragraph describes how to calculate the theoretical SAR from the RSA at the different scales under the assumption of neutral population dynamics.

IV.2.1 From $P(N|R)$ to the SAR

In the following analysis I always assume that, in a first approximation, ecosystems are two dimensional systems. The total number of individuals living in an area \mathcal{A} of radius R is indicated with $N(R) = \sum_{\mathbf{x} \in \mathcal{A}} n_{\mathbf{x}}$, consistently with the notation of previous chapters.

Neutral dynamics, i.e. the assumption that individuals are equal on a per capita basis regardless of their species, will also be considered. A given species is observable in \mathcal{A} if it has at least one individual. Therefore, being $P(N|R)$ the probability of it having an abundance of N individuals, $\int_1^\infty P(N|R)dN$ expresses the probability that the species is observable in \mathcal{A} . Indicating with S_0 the number of species registered in an area of radius R_0 , one can calculate the number of species in the area \mathcal{A} of radius R making use of the following equation

$$S(R) = S_0 \frac{\int_1^\infty P(N|R)dN}{\int_1^\infty P(N|R_0)dN} \quad (\text{IV.2.1})$$

IV.2.2 From the empirical two-points correlation to the RSA

In the general case, the two point correlation function is not sufficient to characterise the full conditional probability distribution of a system. The case of the SBD model is special because the $P(N|R)$ depends only three parameters: the spatial correlation length of the system $\bar{\lambda}$, the amplitude of the fluctuations $\frac{\sigma^2}{\mu}$, and the mean number of individuals in each site, $\langle n \rangle = \frac{\bar{b}_0}{\mu}$.¹

Here, I recall the definition of the pair correlation function

$$PCF(|\mathbf{x} - \mathbf{y}|) = \frac{\langle n(\mathbf{x})n(\mathbf{y}) \rangle}{\langle n \rangle^2}$$

¹Recall the definition of parameters: $\bar{\lambda} = \sqrt{D/\mu}$, $\mu = r - b$, $\sigma^2 = \frac{b+r}{2}$ with b and r the per-capita birth and death rates.

In the two dimensional case it takes the following explicit form (see eq (II.8.5)):

$$PCF(|\mathbf{x} - \mathbf{y}|) = 1 + \frac{1}{2\pi} \left(\frac{\bar{\rho}}{\bar{\lambda}} \right)^2 K_0 \left(\frac{|\mathbf{x} - \mathbf{y}|}{\bar{\lambda}} \right) \quad (\text{IV.2.2})$$

This expression depends on two parameters, namely $\bar{\lambda} = \sqrt{D/\mu}$ and $\bar{\rho} = \sqrt{\sigma^2/b_0}$.

This suggests a method for inferring spatial patterns from only measures of the PCF and of the local average abundance $\langle n \rangle$. From the fit of eq (IV.2.2) to empirical data, one can calculate the values of $\bar{\lambda}$ and of $\bar{\rho}$. At the same time, the local average abundance can be evaluated in a straightforward way by taking the average number of individuals for each species in the plot and dividing it by the total area. This yields the empirical value of $\langle n \rangle$. Once these empirical parameters are calculated, it is easy from the results of previous sections to upscale or downscale $P(N|R)$ from the size of the plot. The variance of $N(R)$ in the two dimensional case takes the following analytic form (from eq II.10.3)

$$\text{Var}(N(R)) = \langle n \rangle^2 \bar{\rho}^2 \pi R^2 \left(1 - \frac{2\bar{\lambda}}{R} \frac{K_1(R/\bar{\lambda}) I_1(R/\bar{\lambda})}{K_0(R/\bar{\lambda}) I_1(R/\bar{\lambda}) + K_1(R/\bar{\lambda}) I_0(R/\bar{\lambda})} \right) \quad (\text{IV.2.3})$$

where $I_\nu(x)$ and $K_\nu(x)$ are the usual modified Bessel functions of the first and second kind and of order ν [1]. Of course, these results are reliable only for systems where the spatial continuous framework is a good approximation, i.e. when $a \ll R, \bar{\lambda}$ (a is the empirical lattice side).

In order to calculate the spatially explicit Relative Species Abundance, one approach is to match the first two moments of the gamma distribution, similarly to what done in chapter II at eq (II.11.1) and in [138], i.e.

$$P(N|R) = \frac{1}{\beta(R)} \frac{(N/\beta(R))^{\alpha(R)-1}}{\Gamma(\alpha(R))} e^{-\frac{N}{\beta(R)}} \quad (\text{IV.2.4})$$

where $\Gamma(\cdot)$ is a gamma function, and, from the properties of the gamma distribution, it is

easy to calculate that $\alpha(R)$ and $\beta(R)$ must be

$$\alpha(R) = \frac{\langle N(R) \rangle^2}{\text{Var}(N(R))} \quad \beta(R) = \frac{\text{Var}(N(R))}{\langle N(R) \rangle}$$

with $\langle N(R) \rangle = \langle n \rangle \pi R^2$.

In the following paragraphs, I apply these techniques to infer ecological patterns from two ecological datasets, one coming from forest plots in the Republic of Panama and one from forest plots in peninsular Malaysia.

IV.2.3 Analysis of two lowland tropical forest inventories

Barro Colorado Island (BCI) is located in the man-made Gatun Lake in the middle of the Panama Canal. The island was set aside as a natural reserve on April 17, 1923, and over the last 40 years has been the subject of intense biological and ecological studies. Censa of the tree vegetation living on a 50ha forest stand have been carried out periodically, with the first in the period of 1981-1983, followed by 1985, 1990, 1995, 2000, 2005, 2010, and 2015. The data from 1980 to 2010 are available online (<https://repository.si.edu/handle/10088/20925>) and offer a unique insight into the spatial and temporal development of trees' community.

Despite part of BCI was cleared out around 100 years ago, most of the 50-ha plot itself is old-growth, undisturbed for over 600 years, and there is currently no cleared land within 6km from the plot. In each census, all free-standing woody stems with at least 10 mm diameter at breast height have been identified (but also many of smaller diameter), tagged and mapped. Over 350,000 individual trees have been censused over 35 years.

Since 1994 other smaller plots have been established around the Panama Canal watershed and, similarly, trees over 10 cm diameter have been censused. The large size of the plot has allowed the evaluation of individual species on a case-by-case basis, and it has been

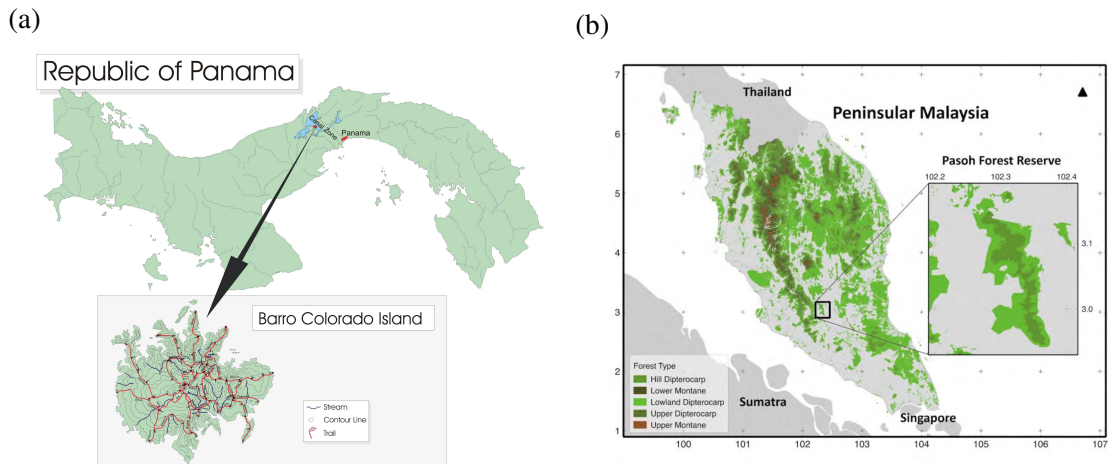


Figure IV.2.2: **Map of the two forest reserves** The figure shows the map of the two forest reserves. (a) refers to Barro Colorado Island, in the Republic of Panama (source https://biogeodb.stri.si.edu/bioinformatics/bci_soil_map/location_and_access.php), (b) to Pasoh Natural Reserve in Peninsular Malaysia [179].

possible to document the local extinction of very rare species. In 1983 a severe drought was reported that elevated the overall mortality rate of the forest. About 10% of the canopy is deciduous, with highly seasonal rainfall and a strong four-month dry season from December through April [46].

Pasoh Forest Reserve is situated 140km south-east of Kuala Lumpur in peninsular Malaysia, it is evergreen with an aseasonal climate characterised by regular rainfall. Similarly to BCI, several censa of a 50ha plot have been made over the years, providing detailed assessment of the dynamics of the forest. The first census dates back to 1987, with 815 species and 335000 individuals recorded. Other censa were taken in 1990 and 1995 [144, 46].

Compared to BCI, Pasoh is less dynamic, with substantially smaller average growth and mortality rates. It must be noted, however, that the high growth rate of BCI is entirely due to a minority of species with very high growth rates. Careful inspection undertaken in [46] shows that the largest group of species at BCI have growth rates in exactly the same range as species at Pasoh.

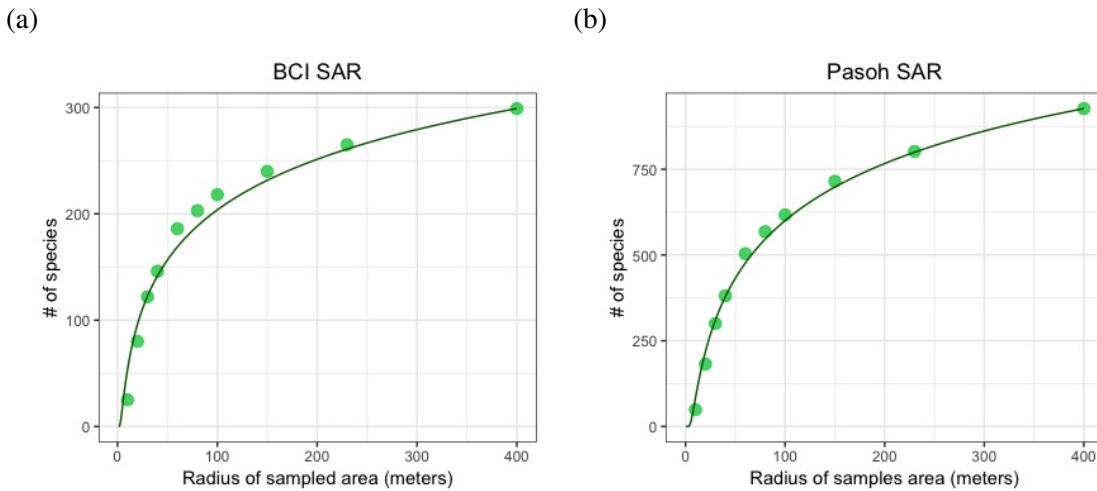


Figure IV.2.3: **Comparison of the predicted SAR** (green line), as calculated with the procedure in paragraph IV.2.2 and empirical data from the BCI dataset (left panel) and Pasoh (right panel). At the scale of the whole plot one registers ≈ 900 different species for Pasoh and 300 for BCI. It is worth remarking that the lines are not best fit to data, but rather predictions made from the larger scale of the plot and downscaled to smaller areas, following the procedure outlined in section IV.2.2

This section presents the analysis of the BCI censa from 1980 to 2010 and of one Pasoh census from 2005. Species identity, geographical location and diameter at breast height (DBH) were recorded for each major tree living within the plot. The datasets are used to test model predictions against empirical patterns, using the procedure outlined in the previous paragraph.

As a first step, one needs to take the position and species of each tree and build a matrix where single geographical locations are coarse-grained into a grid mesh of 10 meters of size. For each species the number of individuals within each sub-area is counted. Indicating with S the total number of species in the plot, data are organised into S separated matrices, each of 100×50 patches.

The next step is to look at each pair of sites located at \mathbf{x} and \mathbf{y} and calculate the empirical PCF. Recalling that in the neutral framework each species is considered to be an

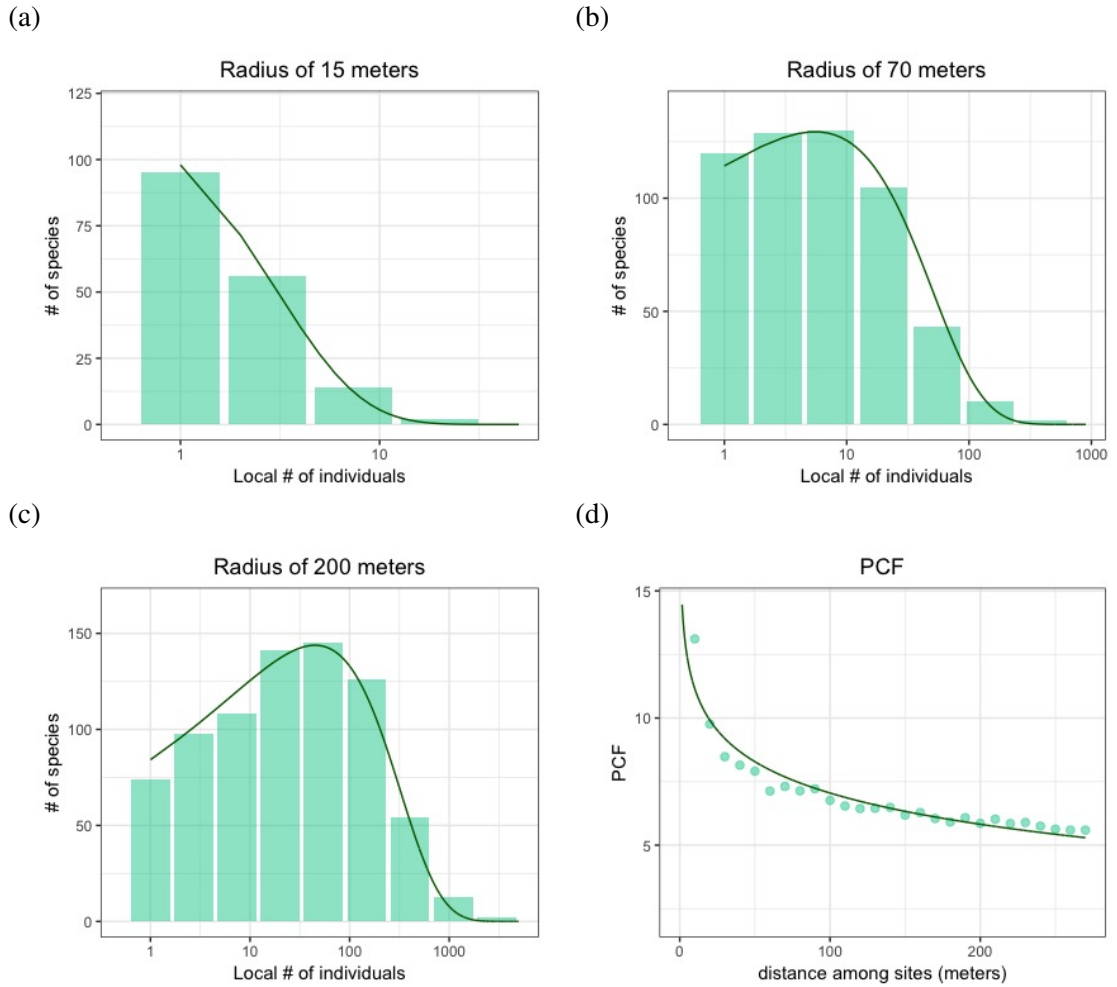


Figure IV.2.4: **Comparison of predicted and empirical RSA for Pasoh Panels** (a), (b) and (c) present the comparison between the empirical data of abundance of species as obtained from the lowland tropical forest inventory of Pasoh natural reserve (Malaysia) and the predictions from the model. Histograms represent the empirical data while the green lines are the predictions obtained from eq (IV.2.4). These are not best fit to the empirical data, but rather inferences that are formulated from the empirical measures of the Pair Correlation Function, as described in the main text. The size of the considered areas go from a radius of 15 meters to 200, and are reported in the title. The last panel on the right compares the empirical pair correlation function (green dots) and that obtained by fitting eq (IV.2.2). The correlation length that is obtained is $\bar{\lambda} \approx 2.5 \times 10^3$ meters, with $\bar{\rho} \approx 8.9 \times 10^3$ and $\langle n \rangle \approx 6.1 \times 10^{-4}$ trees per square meter for each species.

independent realisation of the process, the following formula holds

$$PCF(\mathbf{x}, \mathbf{y}) = \frac{\frac{1}{S} \sum_{\mu=1}^S n_{\mathbf{x}}^{(\mu)} n_{\mathbf{y}}^{(\mu)}}{\left(\frac{1}{S} \sum_{\mu=1}^S n_{\mathbf{x}}^{(\mu)} \right) \left(\frac{1}{S} \sum_{\mu=1}^S n_{\mathbf{y}}^{(\mu)} \right)} \quad (\text{IV.2.5})$$

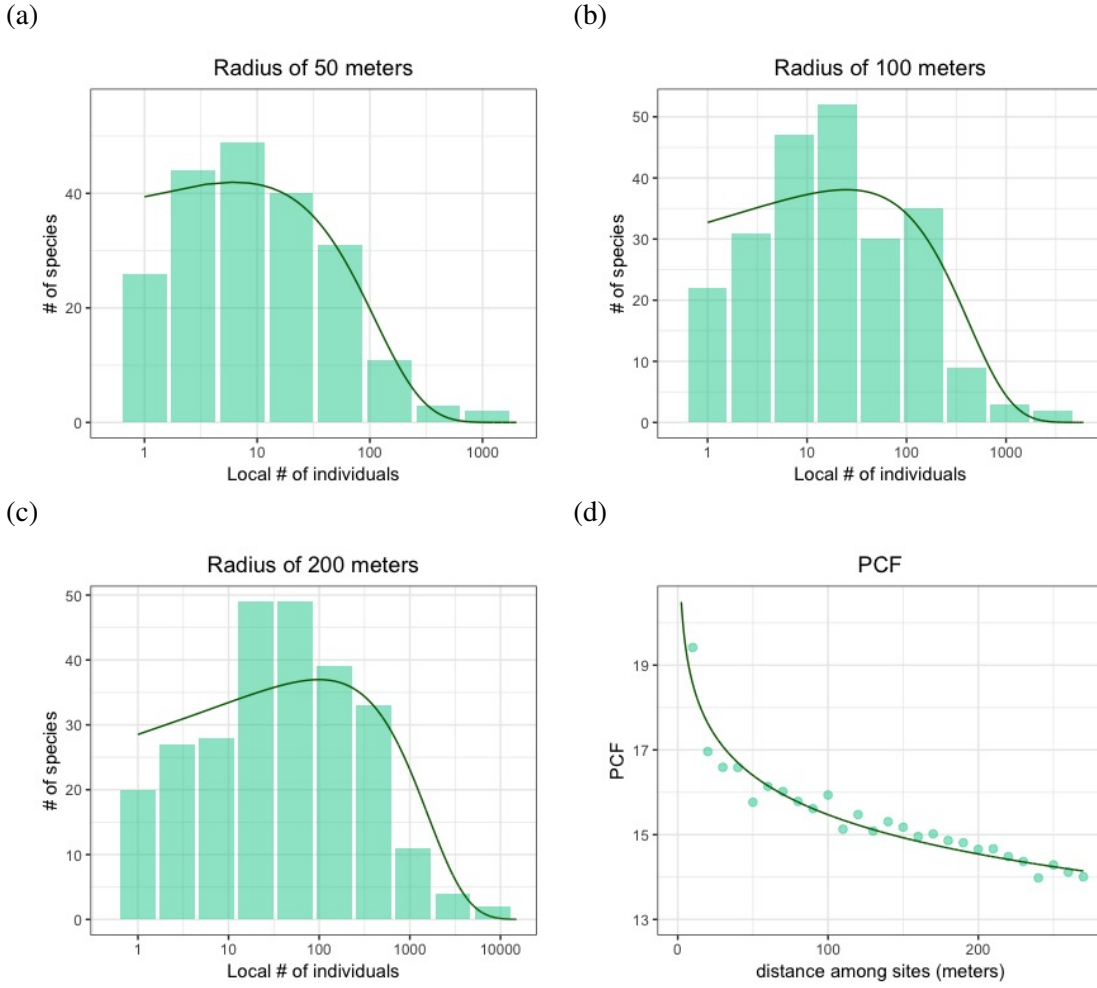


Figure IV.2.5: **Comparison of predicted and empirical RSA for BCI Panels** (a), (b) and (c) present the comparison between the empirical data of abundance of species as obtained from the lowland tropical forest inventory of Barro Colorado Island (Panama) and the prediction based on the model. Histograms represent the empirical data while the green lines are the predictions obtained from eq (IV.2.4). These are not best fit to the empirical data, but predictions that are formulated from the empirical measures of the Pair Correlation Function, as described in the main text. The size of the considered areas go from a radius of 50 meters to 200, and are reported in the title. The last plot on the right compares the empirical pair correlation function (green dots) and that obtained fitting eq (IV.2.2). The correlation length that is thus calculated is $\bar{\lambda} = 4 \times 10^6$ meters, with $\bar{\rho} = 1.2 \times 10^7$ and $\langle n \rangle = 1.3 \times 10^{-3}$ trees per square meter for each species.

where $n_{\mathbf{x}}^{(\mu)}$ is the number of individuals of species μ in site \mathbf{x} . By best-fitting the data to the analytic formula in eq (IV.2.2), one can hence calculate $\bar{\lambda}$ and $\bar{\rho}$. The empirical

average number of individuals in each patch is easily calculated to be $\langle n \rangle = N_0 / (A_0 * S)$, where N_0 is the total number of individual trees in the dataset, and A_0 the area of the whole forest plot.

Figures IV.2.4 and IV.2.5 show comparison of the empirical and predicted RSA for Pasoh and BCI. The accord between the predicted distribution and the data is very good for Pasoh, and presents minor deviations for BCI. Notice that both forest plots present very large fluctuation in the abundance of species, with a difference of three orders of magnitude between rare and dominant species. Notice also that spatial patterns are correlated over very large distances.

It is also possible to make predictions of the SAR with the approach described in the previous section. From the number of species at the full scale of the plot S one can downscale species presence to smaller areas and compare the predictions with those from the data of both databases. Results are shown in figure IV.2.3. The accord between predicted and empirical SAR is very good, especially for Pasoh.

Finally one can focus on analysing time-dependent patterns (see fig IV.2.6). The time-dependent species turnover distribution (STD), defined in chapter II, accounts for the probability that the ratio of the abundances of a species in a certain area separated by a time interval t , $N(t)/N(0)$, is equal to m , and under stationary conditions (and reflecting boundary conditions) it is calculated to have the expression reported in eq (III.8.4).

The spatial scaling of the turnover distribution in empirical data can be compared to theoretical predictions with a procedure similar to the one just outlined. I recall here one result from the chapter III, i.e. that the spatial STD (defined as the probability that the ratio of abundances of a species in a certain area at times separated by a time interval t , $N(t)/N(0)$, is equal to m) under stationary conditions in the SBD model takes the

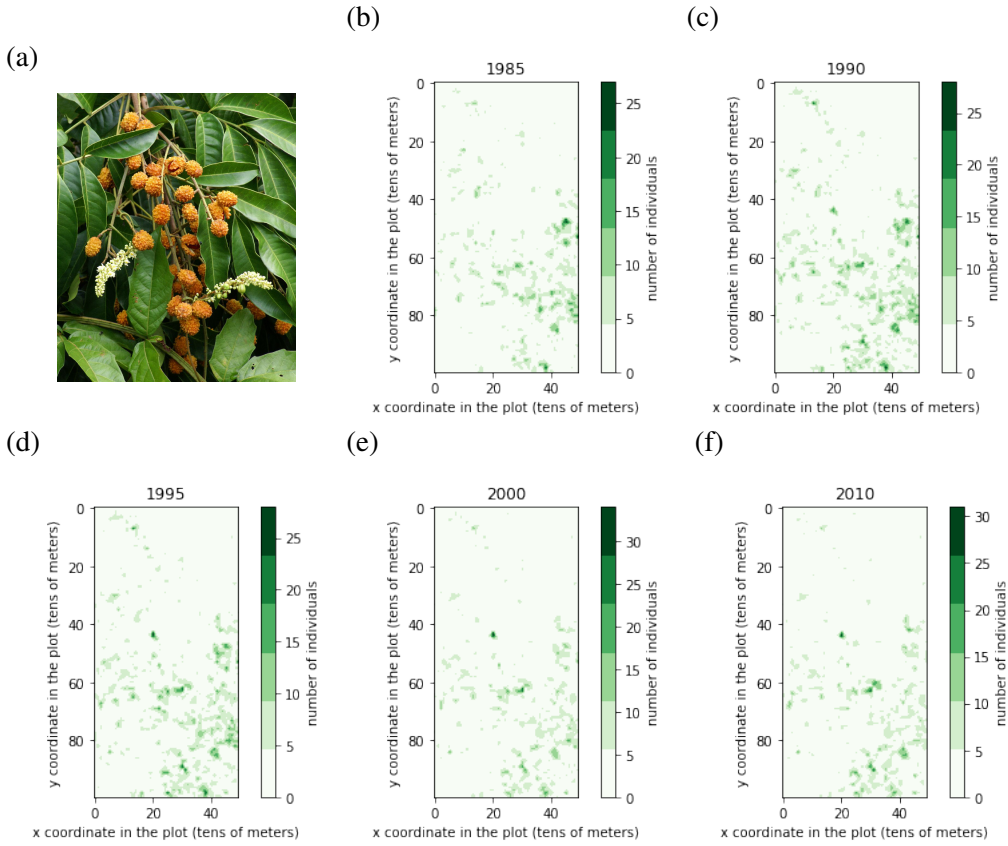


Figure IV.2.6: **Time variation of individuals' distribution** The figure reports the location of individual plants of the species *Trichilia tuberculata* within the BCI Plot in the period 1985-2010. Panel (a) is a picture of the flowers of the plant (image taken from <http://hasbrouck.asu.edu/neotrop/>). Panels (b)-(f) report the position of the plants over the years (as in the titles). Over the course of 25 years the configuration has changed considerably, with clusters constantly appearing and disappearing.

following form (see eq (III.8.4))

$$\begin{aligned}
 STD(m, t) = A \frac{m+1}{m} \frac{(e^{\mu t})^{\frac{\langle N \rangle}{2\Sigma(R)}}}{1 - e^{-\mu t}} \left(\frac{\sinh(\mu t/2)}{m} \right)^{\frac{\langle N \rangle}{\Sigma(R)} + 1} \times \\
 \times \left(\frac{4m^2}{(m+1)^2 e^{\mu t} - 4m} \right)^{\frac{\langle N \rangle}{\Sigma(R)} + \frac{1}{2}}
 \end{aligned} \tag{IV.2.6}$$

with A being a normalisation constant, $\langle N \rangle = \frac{\bar{b}_0 V}{\mu}$ and $\Sigma(R)$ taking the form in eq (II.10.4). The parameter μ hence describes the temporal scale of the model, while $\frac{\langle N \rangle}{\Sigma(R)}$

encapsulates the spatial scaling.

In chapter III it was calculated that for $\bar{\lambda} \rightarrow \infty$ and in dimension two the following holds: $\Sigma(R) \propto (R/\bar{\lambda})^2 \log(R/\bar{\lambda})$ (see eq (II.10.5) and eq (II.10.4)). As a consequence, the dependence over R in $\frac{\langle N \rangle}{\Sigma(R)}$ is proportional to the inverse of the logarithm of the radius (recall $\langle N \rangle = \bar{b}_0 \pi R^2 / \mu$), i.e. $\frac{\langle N \rangle}{\Sigma(R)} \propto \log^{-1}(R/\bar{\lambda})$. This spatial scaling is non-trivial and offers a new theoretical framework for understanding the effect of spatial dispersal into the temporal fluctuations of ecosystems. However, it is important to remark that a logarithmic scaling is very difficult to observe in empirical data and is often overlooked.

In figure IV.2.7 it is reported the comparison of the STD for different areas for the BCI dataset. The three curves are indeed very similar. One can also show the comparison between empirical data and the fit of μ using eq (III.8.4). The result is that the typical time-scale of the system $\tau = 1/\mu$ is ≈ 5000 years.

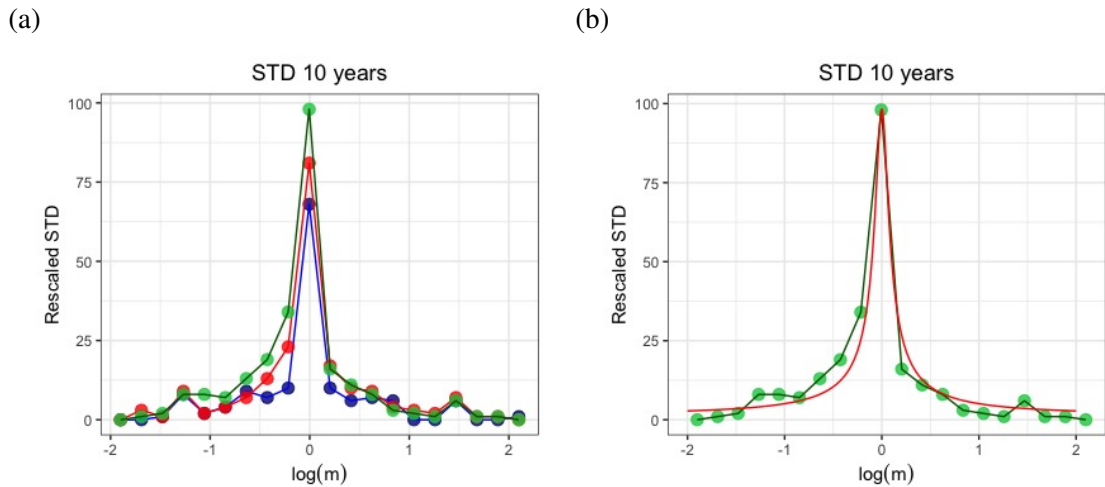


Figure IV.2.7: **Analysis of empirical Species Turnover Distribution** based on a time gap of ten years (i.e. $m = N(t = 10 \text{ years})/N(0)$). The y-axis values are rescaled by the total number of species (so the presented STD is not normalised). The chosen censa have been those of 1990 and 2000. Panel (a) reports the results for three different areas. The blue dots and lines are for an area of radius of 50 meters, red are for an area of radius 100 meters and green for 200 meters. Panel (b) reports the comparison of the STD from the area of radius 200 meters and the fit of equation (III.8.4). From the fit, one finds that the typical time-scale of the system $\tau \approx 5000$ years.

The assumption of a constant per capita death (and birth) rate is only a first order approximation, which in some cases, e.g. for the rare species in BCI, is not a faithful description [40]. Measuring fluctuations in natural populations and understanding the mechanisms that drive their dynamics is extremely difficult due to the amount of different phenomena involved and to the lack of long-term surveys. Environmental drivers, such as fire and droughts, are an important factor in directing the system in favour of one species over another. Climatic shifts alter species assemblages, but there is considerable disagreement over the relative importance of the different mechanisms, especially in light of the recent (in ecological times) fluctuations caused by anthropogenic disturbance (e.g. global warming) .

The next chapter proposes an extension of the SBD model that aims at studying the effects of environmental fluctuations over spatial patterns. Although a rigorous mathematical derivation will not be given, some analytic results will be presented using a procedure that mimics that of the phenomenological model of Chapter II. Compared to simulations, the analytic formulas show once again excellent agreement.

Chapter V

Environmental noise model

Tropical rainforests are not isolated systems. They are constantly affected by changes of environmental conditions which can arise from fluctuations in rainfall, temperature, fire, pests etc. The analysis of the SBD model has given important results over the spatial scaling when demographic fluctuations are dominant. However, environmental variability influences the success and ruin of one species over another, with examples documented in studies of birds, marine fish and plankton [24, 52].

Tropical rainforest are not exceptions and there is well-documented evidence that environmental fluctuations are consistently the largest factor in tree population dynamics on decadal timescales for certain species [40] (fig V.0.1).

In this section I examine an extension of the SBD model that gives a first analysis of the effects of spatial environmental fluctuations. The model is defined as before on a regular lattice, but now the birth and death rates are not linear and are uncorrelated across space.

Similarly to the procedure outlined in chapter II, an analytic formula for the conditional probability distribution of the spatially explicit model is calculated from the mean field distribution, and, although a rigorous mathematical derivation is not provided, comparison with simulated data reveals excellent agreement at all scales.

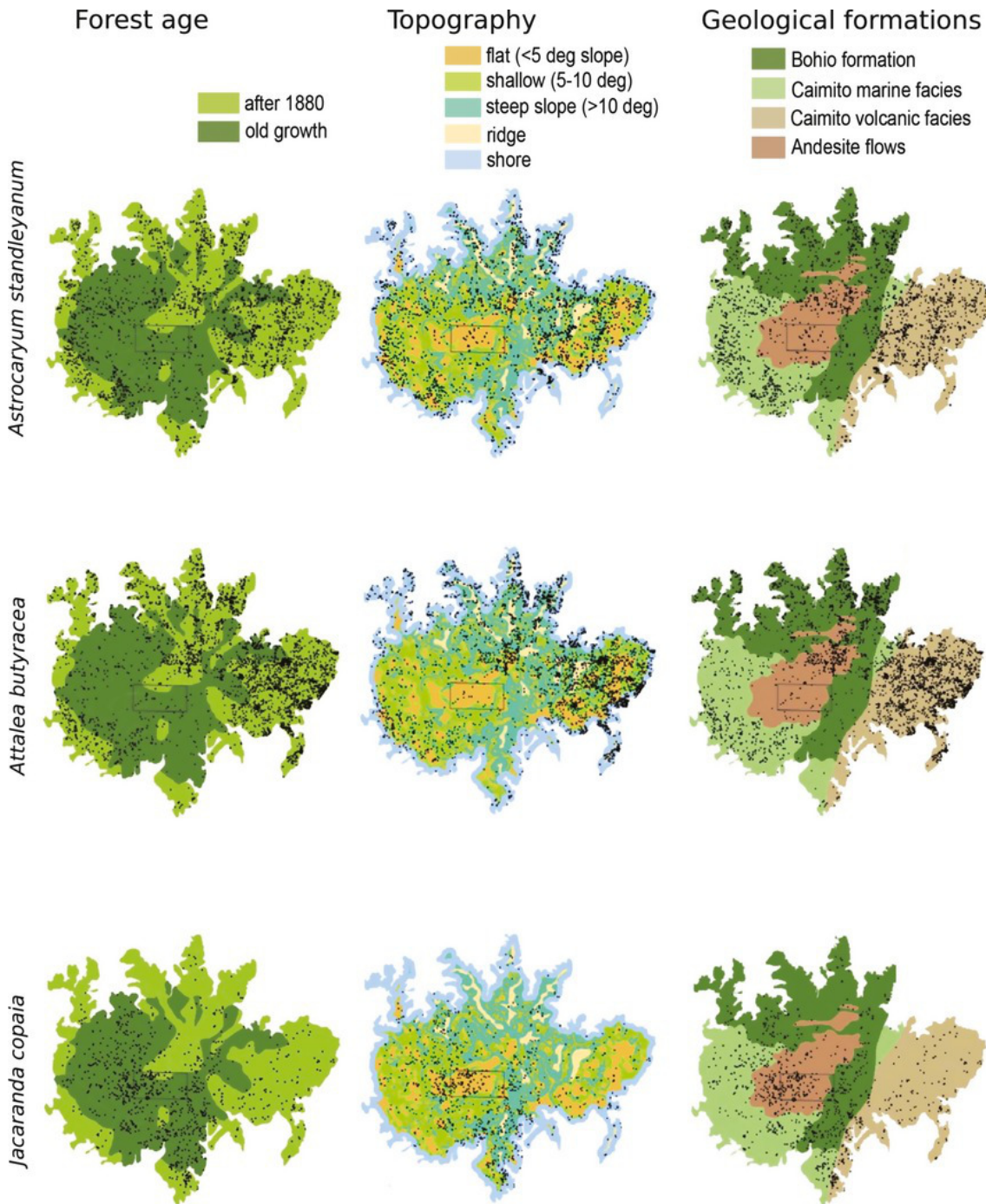


Figure V.0.1: **Geological and land variation in BCI.** Variation in age, topography and geological formations within the BCI island. The distribution of individuals of three tree species is also reported. Their geographical position may depend also on factors others than their intra-species demographic dynamics, such as land type, human influence and weather conditions. The rectangle reports the position of the forest stand whose data are used in this thesis. Figure from [69].

V.1 Phenomenological model with environmental noise

The birth-death model defined in chapter II was designed to retain constant per capita birth and death rates over space and time. Indeed, the mean field model considered linear rates, i.e. $b_n = b n + b_0$ and $d_n = r n$, with b, r, b_0 positive constants (recall eq (II.3.3)).

An obvious generalisation is to consider terms of higher order in the local occupation numbers, i.e. to consider the following

$$\begin{aligned} b_n &= b n + b_0 + b_e n^2 \\ d_n &= r n + r_e n^2 \end{aligned} \tag{V.1.1}$$

The terms b_e and r_e have to be considered as effective parameters which, together with environmental fluctuations, encode also the strength of the interactions with the other members of the species.

In this paragraph I analyse the mean field model that arises from these simple, yet instructive, non-linear rates. Then I expand the analysis to a phenomenological spatial model, following the method outlined in chapter II.

V.1.1 Mean field model with environmental noise

The dynamical evolution of the probability distribution of n in the mean field system with environmental noise is defined by the master equation (II.2.1) with rates as in eq (V.1.1), i.e.

$$\begin{aligned} \frac{\partial p_n(t)}{\partial t} &= p_{n+1}(t) [r (n+1) + r_e (n+1)^2] + \\ &+ p_{n-1}(t) [b (n-1) + b_0 + b_e (n-1)^2] + \\ &- p_n(t) (b n + b_0 + b_e n^2 + r n + r_e n^2) \end{aligned}$$

Instead of solving directly this equation, I here rely on the Kramers-Moyal expansion of the system as described in section II.4. This procedure is mathematically non-rigorous because it does not identify the parameter which determines the expansion. Nonetheless this is the typical approach in the literature and can give a first insight into the problem. A more rigorous expansion, similar to that described in chapter III, is likely possible to be implemented.

Following the notation of section II.4 the following equalities are found for the jump rates

$$\mathcal{W}^+(n) = b_n = b n + b_0 + b_e n^2$$

$$\mathcal{W}^-(n) = d_n = r n + r_e n^2$$

and therefore the Fokker-Planck equation that is obtained from eq (II.4.1) is

$$\frac{\partial p(n, t)}{\partial t} = - \frac{\partial}{\partial n} [A(n)p(n, t)] + \frac{1}{2} \frac{\partial^2}{\partial n^2} [B(n)p(n, t)] \quad (\text{V.1.2})$$

with

$$A(n) = d_n - b_n = -\mu n + b_0 + r_e n^2 - b_e n^2 \quad (\text{V.1.3})$$

$$B(n) = d_n + b_n = 2\sigma^2 n + b_0 + b_e n^2 + r_e n^2$$

Notice that the notation of previous chapters, i.e. $\mu = r - b$ and $\sigma^2 = \frac{b+r}{2}$, has been maintained.

The focus of this chapter will be on the new terms present at eq (V.1.1). In this sense, I consider that second order terms, i.e. those proportional to r_e and b_e , are much larger than all the other terms. This leads to the following scaling assumptions

$$\frac{\sigma^2}{r_e + b_e} \approx 0 \quad \text{and} \quad \frac{b_0}{r_e + b_e} \approx 0$$

Another assumption is that the temporal scale of the second order fluctuations is much smaller than the temporal scale of demographic fluctuations, i.e.

$$\frac{r_e - b_e}{\mu} \approx 0$$

In other words, the temporal scale of interactions among individuals is much smaller than their average life-span. Therefore the rates in (V.1.3) become

$$\begin{aligned} A(n) &= \mu \left(n - \frac{b_0}{\mu} + \frac{r_e - b_e}{\mu} n^2 \right) \approx \mu n - b_0 \\ B(n) &= d_n + b_n = (b_e + r_e) \left[2 \frac{\sigma^2}{b_e + r_e} n + \frac{b_0}{b_e + r_e} + n^2 \right] \approx (b_e + r_e) n^2 \end{aligned}$$

and accordingly the Fokker-Planck equation of the model becomes

$$\frac{\partial p(n, t)}{\partial t} = \frac{\partial}{\partial n} \left[(b_0 - \mu n) p(n, t) \right] + \frac{r_e + b_e}{2} \frac{\partial^2}{\partial n^2} \left[n^2 p(n, t) \right] \quad (\text{V.1.4})$$

In the Itô prescription, this equation is associated to the following Langevin equation

$$\dot{n} = -\mu n + b_0 + \sigma_e n \xi^{(e)} \quad (\text{V.1.5})$$

where $\xi^{(e)}$ is a zero mean Gaussian white noise which models the effect of environmental noise, and has covariance $\langle \xi^{(e)}(t) \xi^{(e)}(t') \rangle = 2\delta(t - t')$. I have also introduced the following constant

$$\sigma_e = \sqrt{\frac{r_e + b_e}{2}}$$

Imposing stationary conditions, it is easy to verify that the solution of eq (V.1.4) is the following

$$P(n) = \frac{(b_0/\sigma_e^2)^{1+\frac{\mu}{\sigma_e^2}}}{\Gamma(1+\frac{\mu}{\sigma_e^2})} n^{-2-\frac{\mu}{\sigma_e^2}} e^{-\frac{b_0}{\sigma_e^2 n}} \quad (\text{V.1.6})$$

which corresponds to an inverse gamma distribution of shape $1 + \mu/\sigma_e^2$ and scale b_0/σ_e^2 . An

inverse gamma distribution (probability density function) of shape α and scale β (defined for $x > 0$) takes in fact the following form

$$P(n) = \frac{\beta^\alpha}{\Gamma(\alpha)} x^{-\alpha-1} e^{-\beta/x}$$

One important remark is that the moments of such distribution are not always well defined. This can be immediately seen upon calculating the following integral, which would yield the second moment of n

$$\langle n^2 \rangle = \int_0^\infty dn n^2 P(n) = \int_0^\infty dn \frac{(b_0/\sigma_e^2)^{1+\frac{\mu}{\sigma_e^2}}}{\Gamma(1+\frac{\mu}{\sigma_e^2})} n^{-\frac{\mu}{\sigma_e^2}} e^{-\frac{b_0}{\sigma_e^2 n}}$$

The integral is finite only for $\mu/\sigma_e^2 > 1$. For $\mu/\sigma_e^2 \leq 1$ it diverges because the integrand is $\mathcal{O}(n^{-\mu/\sigma_e^2})$ as $n \rightarrow \infty$. In such parameters' regimes the second moment of n , and therefore its variance, are not defined. From a mathematical point of view this complicates the analysis of the spatial extension of such model that I am about to introduce. Nonetheless, with the appropriate precautions it is possible to bypass such hurdles and achieve well-defined results.

Further extensions of the 'environmental noise' model would integrate both the environmental noise and the demographic-type noise in a unified framework (i.e. a white noise proportional to the square root of n). One important consequence of such extension is that the conditional probability distribution displays an intermediate regime where the tail of the distribution is exponentially distributed. Preliminary work has showed that such systems can be studied with an approach similar to the one that we have used in previous chapters. However, further analysis is needed and as a consequence no result regarding this important generalisation has been reported in this thesis.

The following paragraphs focus on the phenomenological spatial extension of the model introduced at eq (V.1.5).

V.1.2 Spatial model with environmental noise

Following the steps of paragraph II.7, I now extend the model at eq (V.1.4) to a spatially explicit model. I therefore assume that space is partitioned into a mesh of voxels with each vertex having $2d$ nearest neighbours, with d being the space dimension. Within each voxel, individuals are considered well-mixed, diluted and treated as point-like particles. The lattice side a is taken to be much smaller than all the other macroscopic length scales of interest, including the characteristic spatial correlation length of the system.

Inspired by the form of eq (V.1.5), I consider the following set of coupled stochastic differential equations

$$\dot{n}_i = D\Delta_i n_i - \mu n_i + b_0 + \sigma_e n_i \xi_i^{(e)} \quad (\text{V.1.7})$$

where $n_i(t)$ is the density of individuals (or the continuous number of individuals in the diffusion approximation) in site $i \in \mathbb{L}$ at time t and $\xi_i^{(e)}(t)$ is a zero mean Gaussian white noise (depending on site i) with correlation $\langle \xi_i^{(e)}(t) \xi_j^{(e)}(t') \rangle = 2\delta(t-t')\delta_{i,j}$. D is the diffusion coefficient and Δ_i is the discrete Laplace operator defined as

$$\Delta_i n_i(t) = \sum_{j:|i-j|=1} [n_j(t) - n_i(t)]$$

Such spatial model with environmental noise could probably be introduced with more mathematical rigour, similarly to the procedure used in chapter III with the SBD model. However, in this chapter I am only giving an overview of some preliminary results, which nonetheless give a useful first insight into the properties of the system.

Indicating with $\{n\}$ a configuration of population sizes on the lattice, i.e. $\{n\} = \{n_1, n_2, \dots\}$ with n_i the number of individuals in site i , the probability distribution of

$\{n\}$ at time t , $p(\{n\}, t)$, satisfies the following Fokker-Planck equation

$$\begin{aligned} \frac{\partial}{\partial t} p(\{n\}, t) = \sum_{i \in \mathbb{L}} \left\{ \frac{\partial}{\partial n_i} \left[- \left(D \Delta_i n_i - \mu n_i + b_0 \right) p(\{n\}, t) \right] + \right. \\ \left. + \sigma_e^2 \frac{\partial^2}{\partial n_i^2} \left[n_i^2 p(\{n\}, t) \right] \right\} \end{aligned} \quad (\text{V.1.8})$$

which derives from eq (V.1.7) in the Itô prescription. In the following, the model defined by equations (V.1.7) and (V.1.8) will be referred to with the abbreviation EN (short for environmental noise model).

As a next step in the analysis, following the procedure of the previous chapters, the mean number of individuals per site and the two points spatial correlation is calculated. This is done by first deriving the equation of the spatial generating function.

V.2 Spatial generating function and two point correlation

Maintaining the notation of the previous chapters the spatial generating function is defined as

$$\zeta(\{H_i\}, t) = \langle e^{\sum_{i \in \mathbb{L}} H_i n_i} \rangle \quad \text{for } H_i \leq 0 \quad (\text{V.2.1})$$

Multiplying eq (V.1.8) on both sides for $e^{\sum_{i \in \mathbb{L}} H_i n_i}$ and integrating, it is easy to prove that the following equation holds

$$\frac{\partial}{\partial t} \zeta(\{H\}, t) = \sum_{i \in \mathbb{L}} \left\{ H_i \left[D \Delta_i \frac{\partial \zeta}{\partial H_i} - \mu \frac{\partial \zeta}{\partial H_i} + b_0 \zeta \right] + \sigma_e^2 H_i^2 \frac{\partial^2 \zeta}{\partial H_i^2} \right\} \quad (\text{V.2.2})$$

which describes the dynamics of $\zeta(\{H\}, t)$ over time. In order to calculate the mean number of individuals in site l at stationarity, i.e. $\langle n_l \rangle$, one needs to partial-differentiate over H_l on both sides of eq (V.2.2) and subsequently impose $\{H\} = 0$. The resulting

equation is the following

$$D\Delta_l \langle n_l \rangle - \mu \langle n_l \rangle + b_0 \langle n_l \rangle = 0$$

Since the system is homogeneous, at stationarity $\langle n_l \rangle$ must be independent of l . Therefore $\Delta_l \langle n_l \rangle = 0$ and one readily finds that $\langle n_l \rangle = \langle n \rangle = b_0/\mu$.

The case of the two-points correlation function, i.e. $\langle n_i n_j \rangle$, is more elaborate. As observed in the mean field case, for some choices of parameters the moments of the distribution are not well-defined. Notice that such pathology does not arise as a consequence of spatial diffusion since it is found also in the mean-field system.

Partial-differentiating over H_l and H_k at eq (V.2.2), and considering stationary conditions, the following equation is obtained

$$\begin{aligned} D \Delta_k \frac{\partial^2 \zeta}{\partial H_k \partial H_l} + D \Delta_l \frac{\partial^2 \zeta}{\partial H_k \partial H_l} - 2\mu \frac{\partial^2 \zeta}{\partial H_k \partial H_l} + \\ + b_0 \frac{\partial \zeta}{\partial H_l} + b_0 \frac{\partial \zeta}{\partial H_k} + 2\sigma_e^2 \frac{\partial^2 \zeta}{\partial H_k^2} \delta_{k,l} + \\ + \sum_{i \in \mathbb{L}} \left\{ H_i \left[D \Delta_i \frac{\partial^3 \zeta}{\partial H_i \partial H_k \partial H_l} - \mu \frac{\partial^3 \zeta}{\partial H_i \partial H_k \partial H_l} + b_0 \frac{\partial^2 \zeta}{\partial H_k \partial H_l} \right] + \right. \\ \left. + 2\sigma_e^2 H_i \delta_{i,k} \frac{\partial^3 \zeta}{\partial H_i^2 \partial H_l} + 2\sigma_e^2 H_i \delta_{i,l} \frac{\partial^2 \zeta}{\partial H_i^2 \partial H_k} + \sigma_e^2 H_i^2 \frac{\partial^4 \zeta}{\partial H_i^2 \partial H_l \partial H_k} \right\} = 0 \end{aligned} \quad (\text{V.2.3})$$

In order to avoid the divergences I introduce the following function

$$\gamma(k, l, \{H\}) = \left[\frac{\partial^2 \zeta}{\partial H_k \partial H_l} - \frac{b_0}{\mu} \frac{\partial \zeta}{\partial H_k} \right] \left(\frac{\partial^2 \zeta}{\partial H_k^2} \right)^{-1} \quad (\text{V.2.4})$$

Using the notation $\gamma^{(0)}(k, l) = g_e(k, l, \{H\}) \Big|_{\{H\}=0}$ one can observe that the following equality holds

$$\gamma^{(0)}(k, l) = \frac{\langle n_l n_k \rangle}{\langle n_k^2 \rangle} - \frac{b_0 \langle n_k \rangle}{\mu \langle n_k^2 \rangle} = \frac{\langle n_l n_k \rangle}{\langle n^2 \rangle} - \frac{b_0 \langle n \rangle}{\mu \langle n^2 \rangle} \quad (\text{V.2.5})$$

It is possible to prove that $\gamma^{(0)}(k, l)$ is indeed well defined. This will appear evident in the following, since it will be calculated explicitly.

From eq (V.2.3) the equation for $\gamma^{(0)}(k, l)$ at stationarity is readily obtained to be

$$D\Delta_k\gamma^{(0)}(k, l) + D\Delta_l\gamma^{(0)}(k, l) - 2\mu\gamma^{(0)}(k, l) + 2\sigma_e^2\delta_{k,l} = 0 \quad (\text{V.2.6})$$

One could hence consider the equation of the Fourier transform of $\gamma^{(0)}(k, l)$, solve it, and then invert it. However it is possible to skip these steps by observing that eq (V.2.6) is equal to eq (II.8.1) provided $G_{i,j}$ is substituted with $\gamma^{(0)}(k, l)$ and $\sigma^2\langle n \rangle$ with σ_e^2 .

Introducing a system of Cartesian coordinates and making the substitution $ik \rightarrow \mathbf{x}$ and $l \rightarrow \mathbf{y}$, the solution of eq (V.2.6) is therefore the following

$$\gamma^{(0)}(\mathbf{x}, \mathbf{y}) = \left(\frac{a}{2\pi}\right)^d \frac{\sigma_e^2}{\mu} \int_{\mathcal{C}} d\mathbf{p} \frac{e^{i\mathbf{p}\cdot(\mathbf{x}-\mathbf{y})}}{1 + \frac{2D}{\mu a^2} \sum_{i=1}^d (1 - \cos(p_i a))} \quad (\text{V.2.7})$$

where p_i is the i -th Cartesian component of \mathbf{p} and \mathcal{C} is the hypercubic (d -dim) primitive unit cell with size $2\pi/a$.

Similarly to the case of the SBD and Phenomenological model one can obtain a good deal of simplification by considering the continuous spatial limit. One first needs to rescale the parameters as $\bar{D} = D a^2$ and $\bar{\sigma}_e = \sigma_e/a^d$, with \bar{D} and $\bar{\sigma}_e$ finite as $a \rightarrow 0$. I also introduce the following notation (in accord with the notation of previous chapters)

$$\bar{\lambda} = a\sqrt{\frac{\bar{D}}{\mu}} = \sqrt{\frac{\bar{D}}{\mu}}$$

In the continuous spatial limit eq (V.2.7) is easily solved by following the same steps as in section II.8. The final result is

$$\gamma^{(0)}(|\mathbf{x} - \mathbf{y}|) = \frac{\bar{\sigma}_e^2}{\mu(2\pi\bar{\lambda}^2)^{d/2}} \left(\frac{|\mathbf{x} - \mathbf{y}|}{\bar{\lambda}}\right)^{\frac{2-d}{2}} K_{\frac{2-d}{2}}\left(\frac{|\mathbf{x} - \mathbf{y}|}{\bar{\lambda}}\right) \quad (\text{V.2.8})$$

where $K_\nu(\cdot)$ is the usual modified Bessel function of the second kind or McDonald's function [1] and \mathbf{x} and \mathbf{y} are the (continuous) coordinate vectors.

V.3 An ansatz for the EN model

In chapter III it was observed that the conditional distribution of the spatially explicit model can be obtained (approximately) as the solution of a stochastic differential equation where changes of scale are encoded in the appropriate scaling of parameters. In this paragraph I simplify the stochastic equation defining the EN model, eq (V.1.7), to obtain a differential equation for the conditional distribution in the EN model.

From equation (V.1.7) the following steps are taken

1. neglect the diffusive term, i.e. $D\Delta_i n_i$
2. Replace n_i with $N(R)/V$ and σ_e with $\sigma_e \sqrt{\psi(R/\bar{\lambda})}$
3. Replace $\xi_i^{(e)}$ with $\xi^{(e)}(t)/\sqrt{V}$, with $\xi^{(e)}(t)$ being a zero mean gaussian white noise of autocorrelation $\langle \xi^{(e)}(t)\xi^{(e)}(t') \rangle = \delta(t-t')$

The result is the following stochastic differential equation

$$\frac{\dot{N}(t)}{V} = -\mu \frac{N(t)}{V} + b_0 + \sigma_e \sqrt{\frac{\psi(R/\bar{\lambda})}{V}} \frac{N(t)}{V} \xi^{(e)}(t)$$

which, multiplying by V , yields an implicit SDE for the conditional probability distribution

$$\dot{N}(t) = -\mu N(t) + b_0 V + \sigma_e \sqrt{\frac{\psi(R/\bar{\lambda})}{V}} N(t) \xi^{(e)}(t) \quad (\text{V.3.1})$$

Such procedure might seem completely arbitrary and surely at this stage does not hold any mathematical rigour. The main idea is that changes of the scale of the area A influence the strength of the fluctuations of abundances without affecting the shape of the

equation. This procedure encodes some intuition on the mathematical properties of the system that come from the parallel with the SBD model analysed in chapters II and III. At this stage, these have to be considered as pure conjectures. Comparison to simulated data will highlight if this approach holds any resemblance with the EN model or not.

I here also introduce the following function:

$$\Sigma_e(R) = \frac{\sigma_e^2}{\mu V} \psi(R/\bar{\lambda}) \quad (\text{V.3.2})$$

In the Itô prescription eq (V.3.1) is readily seen to be associated to the following Fokker-Planck equation

$$\frac{\partial}{\partial T} p(N, T) = \frac{\partial}{\partial N} \left[(b_0 V - \mu N) p(N, T) \right] + \Sigma_e(R) \frac{\partial^2}{\partial N^2} \left[N^2 p(N, T) \right]$$

with $T := \mu t$.

The equation just calculated is equal to the mean field equation of the model, eq (V.1.5) where b_0 has been replaced by $\bar{b}_0 V$ and σ_e by $\sigma_e \sqrt{\psi(R/\bar{\lambda})/V}$. Tantamount, from eq (V.1.6) it is immediate to calculate the stationary solution of eq (V.3.1)

$$P(N|V) = \frac{1}{\Gamma(1 + \frac{1}{\Sigma_e(R)})} \left(\frac{\langle N(R) \rangle}{\Sigma_e(R)} \right)^{1 + \frac{1}{\Sigma_e(R)}} N^{-2 - \frac{1}{\Sigma_e(R)}} e^{-\frac{\langle N(R) \rangle}{\Sigma_e(R) N}} \quad (\text{V.3.3})$$

where $\langle N(R) \rangle = \bar{b}_0 V / \mu$, which leads to an inverse gamma distribution of shape $1 + 1/\Sigma_e(R)$ and scale $\langle N(R) \rangle / \Sigma_e(R)$.

In the following I compare eq (V.3.3) with data from the simulations of the model. As done in chapter IV, in order to do so a phenomenological simulation scheme has been implemented, similar to the one introduced in section IV.1.2.

V.4 Simulation scheme in the EN model

The first step is separating the integration of the spatial part at equation (V.1.7) from the rest of the equation (the discrete Laplacian) in eq (V.1.7), recalling that $\Delta_i n_i = \sum_{j:|i-j|=1} [n_j - n_i]$.

Going over similar steps to those outlined in chapter IV, I introduce the following notation

$$Y_{nn\{i\}}(t) = \frac{D}{a^2} \sum_{j \in nn\{i\}} n_j(t) + b_0 \quad \text{and} \quad \Omega = \frac{4D}{a^2} + \mu$$

where $nn\{i\}$ is the set of nearest neighboring sites of i . I thus rewrite eq (V.1.7) as

$$\dot{n}_i(t) = Y_{nn\{i\}}(t) - \Omega n_i(t) + \sigma_e n_i \xi_i \quad (\text{V.4.1})$$

Conditional on $Y_{nn\{i\}}(t)$, eq (IV.1.5) has the same form as the Langevin equation of the mean field model, eq (V.1.5), provided b_0 is substituted with $Y_{nn\{i\}}$ (and hence $Y_{nn\{i\}}$ can be interpreted as an effective immigration parameter) and μ with Ω . At stationarity the following holds

$$P(n_i | Y_{nn\{i\}}(t)) = \frac{1}{\Gamma(1 + \frac{\Omega}{\sigma_e^2})} \left(\frac{Y_{nn\{i\}}(t)}{\sigma^2} \right)^{1 + \frac{\Omega}{\sigma_e^2}} n_i^{-2 - \frac{\Omega}{\sigma_e^2}} e^{-\frac{Y_{nn\{i\}}}{\sigma_e^2 n_i}} \quad (\text{V.4.2})$$

and this can be used to simulate the field $n_i(t)$ at stationarity in generic dimension d .

More schematically, at the first step (step (0)) the lattice is initialised with $n_i^{(0)} > 0$. At the m -th step (labelled (m)) a random site (labelled i) is selected. Then the following is calculated

$$Y_{nn\{i\}}^{(m)}(t) = \frac{D}{a^2} \sum_{j \in nn\{i\}} n_j^{(m)} + b_0$$

and then the value of $n_i^{(m)}$ is updated. This is done sampling from eq (IV.1.6), i.e.

$$n_i^{(m+1)} = \text{InvGamma}\left[1 + \frac{\Omega}{\sigma_e^2}, \frac{Y_{nn\{i\}}^{(m)}}{\sigma_e^2}\right]$$

where $\text{InvGamma}[\alpha, \beta]$ is the inverse gamma distribution with shape parameter α and scale parameter β . By repeating this process multiple times the value in each and every site is updated, and after a significant number of steps (typically of the order of $\sim 10^2$ for each single site) the result is a field n_i with $i \in \mathbb{L}$ which is approximately sampled from the stationary distribution of eq (V.1.7).

V.5 Comparison of analytic solution and simulated data

I have implemented the numerical scheme presented in the previous paragraph for two choices of parameters in the one and two dimensional case, and for each I have calculated 50000 independent realisations of the process. Error bars are calculated by grouping the results into 50 sets made of 1000 realizations each. I have compared the analytic pair correlation function and conditional probability distribution with the analytic one obtained using eq (V.3.3). The results are presented in figures V.5.1 and V.5.2.

The agreement between the analytic function of eq (V.3.3) and simulated data is remarkable in both cases and at all scales. Comparison with the mean field distribution also shows that this is not just a consequence of a perturbation of equation (V.1.6). This result may have an explanation similar to that presented in chapter III for the SBD model. Due to time constraints I have not been able to analyse this further.

For large populations the conditional probability distribution at eq (V.3.3) assumes a power law behavior. Indeed for large N the following is found

$$P(N|V) \propto N^{-2 - \frac{1}{\Sigma_e(R)}}$$

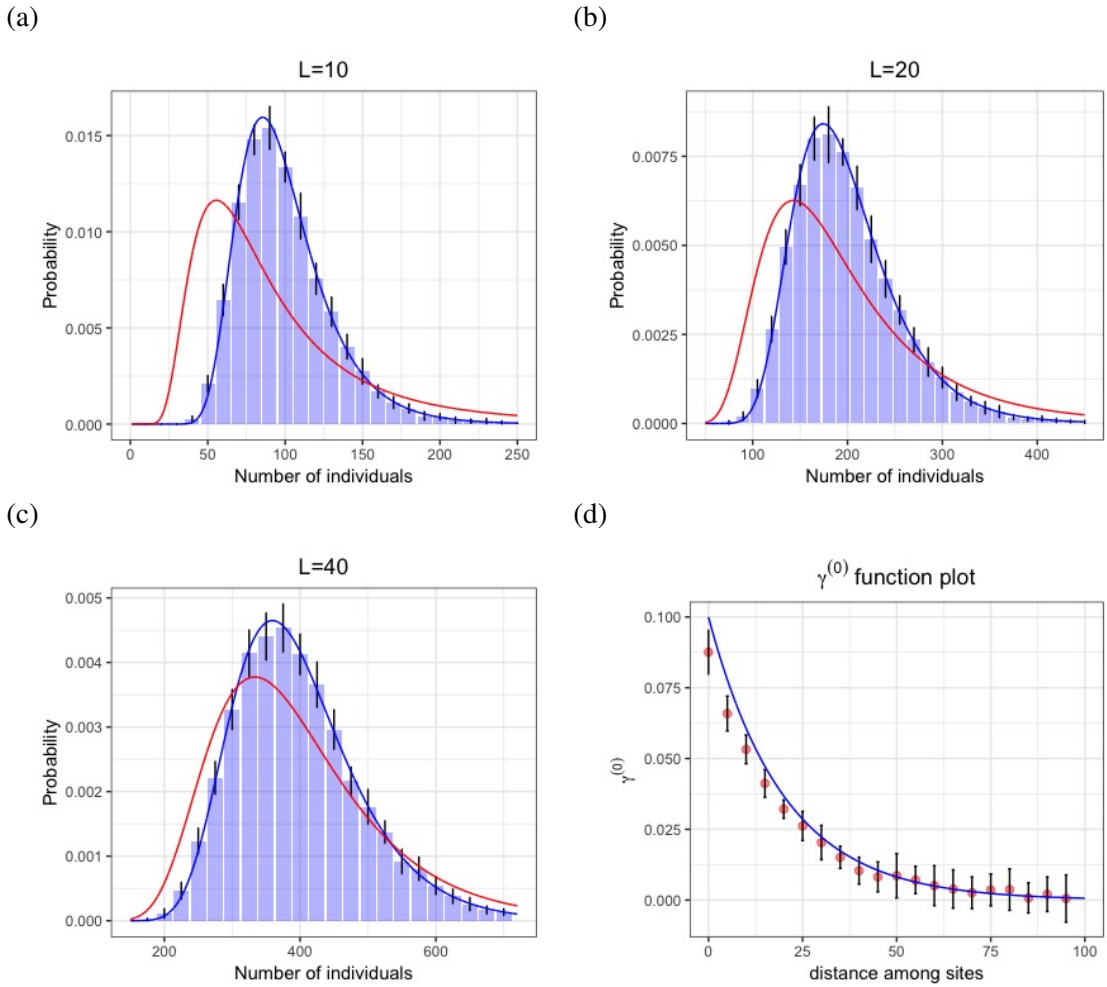


Figure V.5.1: **Comparison of simulated data of the model with the theoretical prediction** of eq (V.3.3) in dimension one. Histograms are simulated data, with the black segments indicating errors at two standard deviations. The blue line is the prediction while the red line is the mean field solution, i.e. as reported in eq (V.1.6). The parameters of the model are $D = 400$, $b_0 = 10$, $\mu = 1$ and $\sigma_e = 2$. Panel (a) refers to a segment of length 10 sites, panel (b) to one of length $R = 20$, and panel (c) to $L = 40$. Panel (d) instead compares the $\gamma^{(0)}$ function from simulated data with the theoretical formula calculated in eq (V.2.8). The lattice has a total of 400 sites with periodic boundary conditions.

Since $\Sigma_e(R) \propto \sigma_e^2/\mu$, when the environmental fluctuations are very large one observes that the distribution of abundances of individuals is distributed as a power law of exponent -2 , i.e. a Zipf law. This is in line with the results of self organised criticality, where power-law distribution of abundances are found very often in systems subject to large

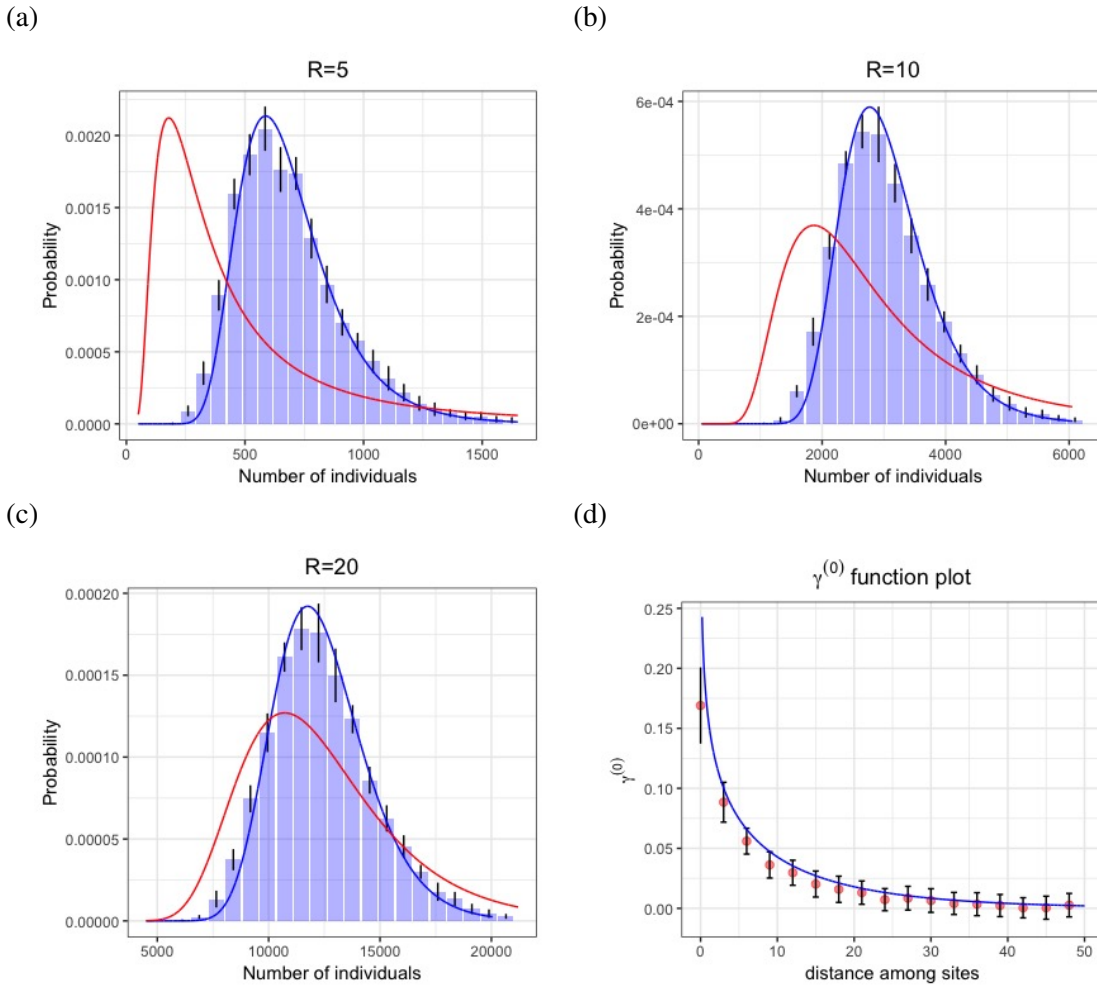


Figure V.5.2: **Comparison of simulated data of the model with the theoretical prediction** of eq (V.3.3) in dimension two. Histograms are simulated data, with the black segments indicating errors at two standard deviations. The blue line is the prediction while the red line is the mean field solution, i.e. as reported in eq (V.1.6). The parameters of the model are $D = 300$, $b_0 = 10$, $\mu = 1$ and $\sigma_e = 10$. Panel (a) refers to an area of radius 5 sites, panel (b) to one of radius $R = 10$, and panel (c) to $R = 20$. Panel (d) instead compares the $\gamma^{(0)}$ function from simulated data with the theoretical formula calculated in eq (V.2.8). The lattice has a total of 40000 organised in a 200×200 lattice with periodic boundary conditions

environmental fluctuations [156, 126].

Chapter VI

Conclusions

In the mathematical modelling of ecological systems, the explicit analysis of spatial effects has often been overlooked for its intrinsic complexity. Nonetheless, the introduction of space in stochastic models has the potential to further unveil the rules that determine the stability of communities of living organisms, and thus to provide important information on their evolution [162, 87, 25, 159, 165, 167, 168, 14].

The connection with the models of non-equilibrium phase transitions in physics has shown that non-trivial scaling relationships can arise, for example, in the individuals' abundance distributions [87, 188], in their group dynamics [126], and even in the distribution of body masses [74, 185]. The concepts of supercritical and subcritical regimes have helped to discern and categorize the different data into universal classes when the study of the processes were beyond the reach of analytical treatment.

The main result of this thesis, shown in Chapter II and Chapter III, is that there is a strict relationship between the shape of the probability distribution of a spatial birth-death stochastic process and that of its corresponding mean-field process, obtained switching off spatial dispersal. The conditional distributions that emerge retain the mean-field shape with appropriately rescaled parameters.

It has been often observed in ecology, physics, biology and even in studies of human population distribution in cities, that the variance of the abundance of individuals living in a certain area is proportional to a power-function of its mean [75, 97]. In this thesis, however, it is shown that deviations from the simple power function are to be expected even just as a consequence of the spatial dispersal of individuals (chapters II and III). This new, non-trivial dependence may disclose a much more general connection between simple microscopic stochastic processes and empirical datasets. In fact, deviations from the Taylor's law that now are considered as 'out of model' may be just the signature of spatial effects.

Power-law scaling and critical behaviours (i.e. large fluctuations of the probability distribution) have often been observed together in natural systems, to the point that in some contexts they are used as synonyms. Examples are self-organised criticality ([126] but also many models of classic ferromagnetism [106]). In this thesis, particular emphasis has been given to separating the concepts of large fluctuations of abundances (labeled as 'critical behavior'), scale invariance of the shape of the probability distribution, and power-law scaling. Indeed, one other important result is that critical behaviours are linked to the form invariance of the probability distribution without necessarily observing the emergence of a power-law.

The invariance of the shape of the probability distribution has been demonstrated in the case of a linear birth-death process close to its critical point, but similar results are likely to emerge in a much more general class of processes, as the analysis in chapter V suggests. In the case where environmental fluctuations are explicitly taken into account, the shape of the distribution (in the small immigration regime) reproduces the power-law behavior, which converges to a Zipf law in the case of large environmental fluctuations.

Another important result of this thesis is that there exist models where detailed balance is preserved at the community level despite being violated at the individual level. More precisely, although the local dynamics is not time reversible, when considering the probab-

ity of the number of individuals living in an area the equations that describe the dynamics satisfy time invariance.

Detailed balance is strongly violated in the reactions taking place in living systems: they consume metabolic energy to avoid equilibrium and death. Whether this lack of molecular-scale balance is violated and what this implies has been the subject of intense recent interest [77, 21].

The preservation of detailed balance at the community level is a consequence of the close-to-critical regime where the system seems to be poised. This suggests the tantalising hypothesis that communities of living organisms self-organise around regimes where the large scale community dynamics preserves detailed balance, and hence time invariance. This is reminiscent of recent results of self-organised criticality. In fact, in [90] it is shown that the evolutionary stable strategy of an assembly of living systems occurs when they organise, through adaptation or evolution, in the vicinity of a critical point. Therefore, if the priority of an ecosystem is stability, criticality could emerge spontaneously in the process of finding an evolutionary strategy that is both time-independent and robust against external threats.

As observed throughout this thesis, both theoretically and in the data of Pasoh and Barro Colorado Island, the key ecological patterns (such as SAR and RSA) are intimately intertwined and scale dependent in ecosystems [10, 12, 32]. Here, a general methodology to link these ecological patterns across scales has been achieved that is sufficiently robust for making insightful predictions of a range of natural or managed systems, as seen in Chapter IV. The same procedure could be applied also to other publicly available large-scale biodiversity data, such as those of oceanic plankton [30].

As a paradigm for ecosystems, the model that is analysed in this thesis is necessarily elementary and incomplete: it relies on some drastic simplifications, the most important of which are the neutrality of species, the absence of interactions and of a spatially correlated environmental noise [102, 28, 140]. Despite these models have showed to retain many key

features of real ecological datasets, there is evidence that the relative importance of the biological processes driving the dynamics changes across scales, and other sources of randomness become dominant [170, 70, 29, 83, 141, 160, 43, 41].

Another challenge is the reconciliation of classical concepts of niche theory with neutrality [65, 80, 132, 2, 19, 27, 55, 92, 83]. The competitive exclusion principle states that two species cannot occupy the same niche since the fighting for a common resource would not allow them to coexist. This strong statement comes in sharp contrast with neutral theory in that it implicitly assumes that the dynamics is governed by deterministic equations and by interactions among species. The mathematical models that analyse such hypothesis find their root in Lotka-Volterra equations [131]. Neutral theory, instead, implicitly assumes that random processes, such as dispersal, demographic stochasticity, speciation, and ecological drift have a stronger impact on the observed patterns than niche differences, at least within the same trophic level [94].

The introduction of the fitness of a species as an efficient parameter has yielded important mathematical insight. In [103] it has been shown that if the fitness values vary in a continuous landscape, the emerging distributions resemble those of classic neutral theory. The further inclusion of environmental noise has explained the short term population fluctuations and the decay of compositional similarity in real data [99]. Similar results were obtained in [91]. In [50] the presence of environmental noise is analysed with regards to a noise induced stabilisation mechanism, the so called 'storage effect', which gives an effective advantage to rarer species over more abundant ones. Such effect is not present if the temporal correlation of fluctuations are too large. In [123, 49] it is also explained how environmental fluctuations can permit to a deleterious mutation to persist over time in a community of competing species.

The study of biological interactions has found a powerful representation tool in the use of networks [136, 20, 164, 136]. In such framework, species are represented as nodes and edges represent inter-specific interactions (e.g., competition, predation, parasitism,

and mutualism). Connecting ecological networks and the stochastic dynamics of spatial models with such critical transitions within a unified theoretical framework would greatly enhance our understanding of community assembly.

An important research area, that recently has received considerable attention, aims at understanding the dynamical features that are early warnings of sudden transitions in ecological systems. In [181], for example, a cluster tracking technique is used to distinguish between smooth and catastrophic (i.e. sudden) transitions, and in [180] this technique is applied to vegetation data in the Sahel region in Africa. This type of analysis, in connection to the techniques described in chapter IV for downscaling and upscaling species occupancy, could lead to the design of natural communities that are less vulnerable to collapse [155, 48].

Interacting systems are often not amenable to analytical treatment. However, a computational approach may still hold important mathematical insight. In such context, the effect of space is still little explored, mostly due to restrictions of memory and running time of the code. The new simulation algorithms, outlined in Chapters IV and V, may prove useful for solving such issues. Particularly interesting would be the study of spatial dispersal and interactions in mutualistic networks and how they influence the robustness of the system.

The study of spatially extended communities of living organisms has traditionally focused on plants and animals [84, 86, 101], also in marine contexts [148, 157, 11, 33, 129], but numerous recent studies have showed that other systems display evident spatial biogeographical patterns. Examples are microorganisms [182, 98, 64, 134], including bacteria [76, 75, 93], archaea, viruses, fungi [85] and other microbial eukaryotes [7, 114], but also human population in urban settlements [97, 158] and epidemic spread [143].

With new technologies being developed at a very fast pace and at lower costs, the amount of spatial ecological data at our disposal will be greatly enhanced in the next years [119]. If on one side this could help design new and more effective conservation strategies, on

the other it may further unveil the intricacies of the natural laws acting around us.

Above all, in my research I have taken inspiration from the ecological world to extrapolate general properties of spatial stochastic processes which I think could be relevant and interesting for a broad spectrum of research questions. My concern has always been to provide clues for generating experimentally testable predictions and further inspections, which are, after all, the final purpose of any scientific quest.

Appendices

Appendix A

Calculation of the moments

In this first appendix I go into the details of the calculations whose results were presented in section II.10. The objective is calculating the solution of equation (II.9.2), which I here recall to be

$$\bar{\lambda}^2 \nabla_{\mathbf{x}}^2 \langle n(\mathbf{x}) N_{\nu} \rangle - \langle n(\mathbf{x}) N_{\nu} \rangle + \langle n \rangle \langle N(R) \rangle + \frac{\sigma^2}{\mu} \langle n \rangle \Theta(R - |\mathbf{x}|) = 0 \quad (\text{A.0.1})$$

This needs to be solved separately for $R < |x|$ and $R > |x|$.

From the properties of Bessel functions [1] for $|x| \leq R$ the implicit solution takes the following form

$$\langle n(\mathbf{x}) N_{\nu} \rangle = \langle n \rangle \langle N(R) \rangle + \frac{\sigma^2}{\mu} \langle n \rangle + A \left(\frac{|\mathbf{x}|}{\lambda} \right)^{1-\frac{d}{2}} I_{\frac{d}{2}-1} \left(\frac{|\mathbf{x}|}{\lambda} \right) \quad (\text{A.0.2})$$

while for $|x| > R$ the following is found

$$\langle n(\mathbf{x}) N_{\nu} \rangle = B \left(\frac{|\mathbf{x}|}{\lambda} \right)^{1-\frac{d}{2}} K_{\frac{d}{2}-1} \left(\frac{|\mathbf{x}|}{\lambda} \right) + \langle n \rangle \langle N(R) \rangle \quad (\text{A.0.3})$$

where I_{ν}, K_{ν} are modified Bessel functions of the first and second kind respectively and of order ν [1], and A and B are integration constants that will be fixed by continuity

conditions.

Considering that, by the properties of Bessel functions $I_\nu(z)$ and $K_\nu(z)$, the following equalities hold [1]

$$\frac{\partial}{\partial z}[z^{-\nu}I_\nu(z)] = z^{-\nu}I_{\nu+1}(z) \quad \frac{\partial}{\partial z}[z^{-\nu}K_\nu(z)] = -z^{-\nu}K_{\nu+1}(z)$$

one obtains

$$\begin{cases} \frac{\partial}{\partial |\mathbf{x}|} \langle n(\mathbf{x})N_\nu \rangle = A \left(\frac{|\mathbf{x}|}{\lambda}\right)^{1-\frac{d}{2}} I_{\frac{d}{2}}\left(\frac{|\mathbf{x}|}{\lambda}\right) & \text{for } |\mathbf{x}| \leq R \\ \frac{\partial}{\partial |\mathbf{x}|} \langle n(\mathbf{x})N_\nu \rangle = -B \left(\frac{|\mathbf{x}|}{\lambda}\right)^{1-\frac{d}{2}} K_{\frac{d}{2}}\left(\frac{|\mathbf{x}|}{\lambda}\right) & \text{for } |\mathbf{x}| \geq R \end{cases} \quad (\text{A.0.4})$$

By imposing that $\langle n(\mathbf{x})N_\nu \rangle$ and $\frac{\partial}{\partial |\mathbf{x}|} \langle n(\mathbf{x})N_\nu \rangle$ are continuous at $|\mathbf{x}| = R$ the following conditions for A and B are hence calculated

$$\begin{cases} A I_{\frac{d}{2}}\left(\frac{R}{\lambda}\right) = -B K_{\frac{d}{2}}\left(\frac{R}{\lambda}\right) \\ \left(\frac{\sigma^2}{\mu} \langle n \rangle + A \left(\frac{R}{\lambda}\right)^{1-\frac{d}{2}} I_{\frac{d}{2}-1}\left(\frac{R}{\lambda}\right) = B \left(\frac{R}{\lambda}\right)^{1-\frac{d}{2}} K_{\frac{d}{2}-1}\left(\frac{R}{\lambda}\right) \end{cases}$$

which lead to

$$\begin{cases} A = -\frac{\sigma^2}{\mu} \langle n \rangle \left(\frac{\bar{\lambda}}{R}\right)^{1-\frac{d}{2}} \frac{K_{\frac{d}{2}-1}\left(\frac{R}{\lambda}\right)}{I_{\frac{d}{2}-1}\left(\frac{R}{\lambda}\right)K_{\frac{d}{2}}\left(\frac{R}{\lambda}\right) + K_{\frac{d}{2}-1}\left(\frac{R}{\lambda}\right)I_{\frac{d}{2}}\left(\frac{R}{\lambda}\right)} \\ B = \frac{\sigma^2}{\mu} \langle n \rangle \left(\frac{\bar{\lambda}}{R}\right)^{1-\frac{d}{2}} \frac{I_{\frac{d}{2}-1}\left(\frac{R}{\lambda}\right)}{I_{\frac{d}{2}-1}\left(\frac{R}{\lambda}\right)K_{\frac{d}{2}}\left(\frac{R}{\lambda}\right) + K_{\frac{d}{2}-1}\left(\frac{R}{\lambda}\right)I_{\frac{d}{2}}\left(\frac{R}{\lambda}\right)} \end{cases}$$

Substituting the value of A into eq (A.0.2) the following expression for $\langle n(\mathbf{x})N(R) \rangle$ in the case $|\mathbf{x}| \leq R$ is indeed obtained

$$\langle n(\mathbf{x})N(R) \rangle = \langle n \rangle \langle N(R) \rangle + \frac{\sigma^2}{\mu} \langle n \rangle \Psi\left(\frac{|\mathbf{x}|}{\lambda}, \frac{R}{\lambda}\right) \quad (\text{A.0.5})$$

where

$$\Psi\left(\frac{|\mathbf{x}|}{\lambda}, \frac{R}{\lambda}\right) = 1 - \left(\frac{|\mathbf{x}|}{R}\right)^{1-\frac{d}{2}} \frac{K_{\frac{d}{2}}\left(\frac{R}{\lambda}\right) I_{\frac{d}{2}-1}\left(\frac{|\mathbf{x}|}{\lambda}\right)}{I_{\frac{d}{2}-1}\left(\frac{R}{\lambda}\right) K_{\frac{d}{2}}\left(\frac{R}{\lambda}\right) + K_{\frac{d}{2}-1}\left(\frac{R}{\lambda}\right) I_{\frac{d}{2}}\left(\frac{R}{\lambda}\right)} \quad (\text{A.0.6})$$

Substituting B in eq (A.0.3) instead the following is obtained for the case of $|\mathbf{x}| \geq R$

$$\begin{aligned} \langle n(\mathbf{x})N(R) \rangle &= \langle n \rangle \langle N(R) \rangle + \\ &+ \frac{\sigma^2}{\mu} \langle n \rangle \left(\frac{|\mathbf{x}|}{R}\right)^{1-\frac{d}{2}} \frac{I_{\frac{d}{2}}\left(\frac{R}{\lambda}\right) K_{\frac{d}{2}-1}\left(\frac{|\mathbf{x}|}{\lambda}\right)}{I_{\frac{d}{2}-1}\left(\frac{R}{\lambda}\right) K_{\frac{d}{2}}\left(\frac{R}{\lambda}\right) + K_{\frac{d}{2}-1}\left(\frac{R}{\lambda}\right) I_{\frac{d}{2}}\left(\frac{R}{\lambda}\right)} \end{aligned} \quad (\text{A.0.7})$$

These two function give the correlation between the number of individuals in a point \mathbf{x} and the sum of individuals in \mathcal{V} . Notice that in both cases the correlation decreases as $|\mathbf{x}|$ increases. Moreover, as $|\mathbf{x}| \rightarrow \infty$ one gets $\langle n(\mathbf{x})N(R) \rangle = \langle n(\mathbf{x}) \rangle \langle N(R) \rangle$, and hence the abundances in \mathbf{x} and those in \mathcal{V} become uncorrelated.

It is immediate to verify that the following equation holds

$$\langle N(R)^2 \rangle = \int_{\mathcal{V}} d\mathbf{x} \langle n(\mathbf{x})N(R) \rangle$$

Considering that the d dimensional surface S_d of the ball of radius z has measure

$$S_d(z) = \frac{d\pi^{\frac{d}{2}}}{\Gamma\left(\frac{d}{2} + 1\right)} z^{d-1}$$

using radial coordinate one finds the following equation for the second moment of $N(R)$

$$\langle N(R)^2 \rangle = \int_{\mathcal{V}} d\mathbf{x} \langle n(\mathbf{x})N(R) \rangle = \int_0^R dr \frac{d\pi^{\frac{d}{2}}}{\Gamma\left(\frac{d}{2} + 1\right)} r^{d-1} \langle n(\mathbf{x})N(R) \rangle \Big|_{|\mathbf{x}|=r}$$

Using the following property of the Bessel functions $I_\nu(z)$ [1]

$$\int z^\nu I_{\nu-1}(z) dz = z^\nu I_\nu(z)$$

and substituting into the previous equation one finds

$$\langle N_{\bar{\nu}}^2 \rangle = \langle N(R) \rangle^2 + \frac{\sigma^2}{\mu} \langle N(R) \rangle \psi\left(\frac{R}{\bar{\lambda}}\right) \quad (\text{A.0.8})$$

where the following has been defined

$$\psi\left(\frac{R}{\bar{\lambda}}\right) = 1 - \frac{d \bar{\lambda}}{R} \frac{K_{\frac{d}{2}}\left(\frac{R}{\bar{\lambda}}\right) I_{\frac{d}{2}}\left(\frac{R}{\bar{\lambda}}\right)}{I_{\frac{d}{2}-1}\left(\frac{R}{\bar{\lambda}}\right) K_{\frac{d}{2}}\left(\frac{R}{\bar{\lambda}}\right) + I_{\frac{d}{2}}\left(\frac{R}{\bar{\lambda}}\right) K_{\frac{d}{2}-1}\left(\frac{R}{\bar{\lambda}}\right)} \quad (\text{A.0.9})$$

This indeed is the expression of the second moment of $N(R)$ in the continuous spatial limit for the SBD model.

Appendix B

An equality for $g(\cdot)$

In this appendix I want to give a proof of equation (III.6.1), as mentioned in chapter III.

For simplicity of notation I only consider the one dimensional case, but the same reasoning can be applied in any dimension d . I take \mathcal{V} to be a segment of length $2R$ and indicate the set of points that constitute it with \mathcal{L} . I also take the origin of the coordinate system at its center. By changing slightly the notation I hence write $N_{\mathcal{L}} = N(-R, R)$, thus rendering explicit that \mathcal{L} extends from site $-R$ to R .

Since the system is homogeneous the following holds

$$\langle n_{i-a} n_j e^{hN(-R,R)} \rangle = \langle n_i n_{j+a} e^{hN(-R+a,R+a)} \rangle$$

In a non rigorous way one can directly observe that if $a \ll R$, the a term can be neglected at the argument of $N(-R+a, R+a)$, which yields

$$\begin{aligned} g(i-a, j, h, t) &= \langle n_{i-a} n_j e^{hN(-R,R)} \rangle = \langle n_i n_{j+a} e^{hN(-R,R)} \rangle = \\ &= g(i, j+a, h, t) \end{aligned}$$

With a bit more accuracy one can estimate the probability that $n_{R+a} > N_{\mathcal{V}}$ (equivalently

for $n_{-R-a} > N_{\mathcal{V}}$). Considering a generic point $k \in \mathbb{L}$ I indicate with $\mathbb{P}(n_{R+a} > n_k)$ the probability that the number of individuals in site $R+a$ is bigger than that in site k .

By the rules of total probability, therefore, the following holds

$$\mathbb{P}(n_{R+a} > n_k) = 1 - \mathbb{P}(n_k \geq n_{R+a}) = 1 - \mathbb{P}(n_k < n_{R+a}) - \mathbb{P}(n_k = n_{R+a})$$

Since the system is homogeneous it is obvious that $\mathbb{P}(n_{R+a} > n_k) = \mathbb{P}(n_k > n_{R+a})$, and so the following holds for any $k \in \mathbb{L}$

$$\mathbb{P}(n_{R+a} > n_k) \leq \frac{1}{2}$$

Since $N_{\mathcal{V}} = \sum_{k \in \mathcal{V}} n_k$, i.e. it is a sum of non-negative random variables, if $n_{R+a} > N_{\mathcal{V}}$ it necessarily has to be bigger than all the n_k for $k \in \mathcal{V}$. Indicating with $M = 2R/a$ the number of sites in \mathcal{L} , the following equation holds

$$\mathbb{P}(n_{R+a} > N_{\mathcal{V}}) \leq \prod_{k \in \mathcal{V}} \mathbb{P}(n_{R+a} > n_k) \leq \left(\frac{1}{2}\right)^M$$

Now, if $a \ll R$ necessarily $M \gg 1$ (since R is kept fixed) and therefore such probability becomes very small.

Equivalently one can demonstrate that $\langle n_{i+a} n_j e^{hN(-R,R)} \rangle \approx \langle n_i n_{j-a} e^{hN(-R,R)} \rangle$ when $a \ll R$.

Therefore, when $a \ll R$ the following equality approximately holds

$$\begin{aligned} \Delta_i g(i, j) &= \left(g(i+a, j) + g(i-a, j) - 2g(i, j) \right) = \\ &= \left(g(i, j-a) + g(i, j+a) - 2g(i, j) \right) = \\ &= \Delta_j g(i, j) \end{aligned}$$

and therefore

$$\sum_{i \in \mathcal{V}} \Delta_i g(i, j, h, V, T) = \frac{\partial}{\partial h} \Delta_j f(j, h, V, T) \quad (\text{B.0.1})$$

All these results are valid approximately for $a \ll R$, but their precision increases the smaller a is with respect to R and become rigorous in the limit of $a/R \rightarrow 0$.

Appendix C

Ansatz for $f(\mathbf{x})$ in the case of $|\mathbf{x}| > R$

In chapter III an approximate functional form of $f(\mathbf{x})$ in the case of $\mathbf{x} \in \mathcal{V}$ is analysed. The approach starts from considering an expansion for $f(\mathbf{x})$, which, retaining only the first two terms of the expansion for f in h , reads

$$f(\mathbf{x}) = \frac{1}{V} \frac{\partial Z}{\partial h} \left[1 + hA_1(\mathbf{x}, R) \right]$$

Recalling that in the mean field case $f(\mathbf{x}) = \langle n \rangle Z$ outside of \mathcal{V} , following the parallel with the previous formula in the case of $\mathbf{x} \notin \mathcal{V}$ I consider the following ansatz for $f(\mathbf{x})$

$$f(\mathbf{x}) = \langle n \rangle Z \left[1 + hB_1(\mathbf{x}, R) \right]$$

The value of $B_1(|\mathbf{x}| = R, R)$ is fixed by taking $h = 0$ and imposing that $f(\mathbf{x})$ and $\partial_{\mathbf{x}} f(\mathbf{x})$ are continuous at $|\mathbf{x}| = R$. Doing so the following equality is obtained

$$\frac{\langle N^2 \rangle}{V} + \langle n \rangle A_1(|\mathbf{x}| = R, R) = \langle n \rangle \langle N \rangle + \langle n \rangle B_1(|\mathbf{x}| = R, R)$$

which, upon multiplying everything by V becomes

$$\langle N^2 \rangle + \langle N \rangle A_1(|\mathbf{x}| = R, R) = \langle N \rangle^2 + \langle N \rangle B_1(|\mathbf{x}| = R, R)$$

This in turn yields

$$B_1(|\mathbf{x}| = R, R) = \frac{\text{Var}(N)}{\langle N \rangle} + A_1(|\mathbf{x}| = R, R) = \frac{1}{\langle n \rangle} \left(\langle n(\mathbf{x})N \rangle_{|\mathbf{x}|=R} - \langle n \rangle \langle N_V \rangle \right)$$

I now extend $B_1(|\mathbf{x}| = R, R)$ to the case of $|\mathbf{x}\rangle > R$ in the following way:

$$B_1(|\mathbf{x}|, R) = \frac{1}{\langle n \rangle} \left(\langle n(\mathbf{x})N \rangle - \langle n \rangle \langle N_V \rangle \right) + \bar{f}(\mathbf{x})$$

where $\langle n(\mathbf{x})N \rangle$ takes the form of eq (II.9.6) and the function $\bar{f}(\mathbf{x})$ must satisfy $\bar{f}(\mathbf{x}) = 0$ and $\partial_{|\mathbf{x}|} \bar{f}(\mathbf{x}) = 0$ for $|\mathbf{x}| = R$, so that the continuity at $|\mathbf{x}| = R$ is maintained.

The equation for $f(\mathbf{x})$ therefore becomes

$$f(\mathbf{x}, h) = \langle n \rangle Z \left[1 + h \frac{1}{\langle n \rangle} \left(\langle n(\mathbf{x})N \rangle - \langle n \rangle \langle N_V \rangle \right) + h \bar{f}(\mathbf{x}) \right] \quad (\text{C.0.1})$$

In order to calculate in which regimes this is an accurate approximation of the real value of $f(\mathbf{x})$ I will now substitute eq (C.0.1) into the equation for the dynamics of $f(\mathbf{x})$.

I recall here eq (III.6.4), i.e. the equation for the dynamics of $f(\mathbf{x})$ at stationarity in the case $x \notin \mathcal{V}$

$$\begin{aligned} \bar{\lambda}^2 \nabla_{\mathbf{x}}^2 f(\mathbf{x}, h) - f(\mathbf{x}, h) + \langle n \rangle Z + h \left[\bar{\lambda}^2 \frac{\partial}{\partial h} \nabla_{\mathbf{x}}^2 f(\mathbf{x}, h) - \frac{\partial}{\partial h} f(\mathbf{x}, h) + \langle n \rangle V f(\mathbf{x}, h) \right] + \\ + \frac{\sigma^2}{\mu} h^2 \frac{\partial}{\partial h} f(\mathbf{x}, h) = 0 \end{aligned}$$

By substitution into eq (C.0.1) the following holds

$$\begin{aligned} & Zh \bar{\lambda}^2 \nabla_{\mathbf{x}}^2 \langle n(\mathbf{x})N \rangle + Zh \bar{\lambda}^2 \langle n \rangle \nabla_{\mathbf{x}}^2 \bar{f}(\mathbf{x}) - \langle n \rangle Z \left(1 + hB_1(\mathbf{x}, R) \right) + \langle n \rangle Z + \\ & + h \left\{ \bar{\lambda}^2 \frac{\partial}{\partial h} \left[Zh \nabla_{\mathbf{x}}^2 \langle n(\mathbf{x})N \rangle + Zh \langle n \rangle \nabla_{\mathbf{x}}^2 \bar{f}(\mathbf{x}) \right] - \frac{\partial}{\partial h} \left[\langle n \rangle Z \left(1 + hB_1(\mathbf{x}, R) \right) \right] \right\} + \\ & + \langle n \rangle V \langle n \rangle Z \left(1 + hB_1(\mathbf{x}, R) \right) \left. \right\} + \frac{\sigma^2}{\mu} h^2 \frac{\partial}{\partial h} \left[\langle n \rangle Z \left(1 + hB_1(\mathbf{x}, R) \right) \right] = 0 \end{aligned}$$

Recalling also eq (II.9.2) one can observe that

$$\bar{\lambda}^2 \nabla_{\mathbf{x}}^2 \langle n(\mathbf{x})N \rangle = \langle n(\mathbf{x})N \rangle - \langle n \rangle \langle N \rangle = \langle n \rangle B_1(\mathbf{x}, R)$$

Substituting into the previous equation and simplifying one finally finds the following equation for $\bar{f}(\mathbf{x})$

$$\begin{aligned} & + Zh \bar{\lambda}^2 \langle n \rangle \nabla_{\mathbf{x}}^2 \bar{f}(\mathbf{x}) + h \left\{ \frac{\partial}{\partial h} \left[Zh \bar{\lambda}^2 \langle n \rangle \nabla_{\mathbf{x}}^2 \bar{f}(\mathbf{x}) - Z \right] + \langle n \rangle V Z \left(1 + hB_1(\mathbf{x}, R) \right) \right\} + \\ & + \frac{\sigma^2}{\mu} h^2 \frac{\partial}{\partial h} \left[Z \left(1 + hB_1(\mathbf{x}, R) \right) \right] = 0 \end{aligned}$$

I now also recall eq (III.7.14), the equation for the generating function $Z(h)$, i.e.

$$-\frac{\partial Z}{\partial h} + \langle n \rangle V Z + \Sigma(R) h \frac{\partial Z}{\partial h} = 0$$

By substituting into the previous equation one finds that the equation for $\bar{f}(\mathbf{x})$ reduces to

$$\begin{aligned} & + Zh \bar{\lambda}^2 \langle n \rangle \nabla_{\mathbf{x}}^2 \bar{f}(\mathbf{x}) + h \frac{\partial}{\partial h} \left[Zh \bar{\lambda}^2 \langle n \rangle \nabla_{\mathbf{x}}^2 \bar{f}(\mathbf{x}) \right] + h^2 \langle n \rangle V Z B_1(\mathbf{x}, R) + \\ & + \left(\frac{\sigma^2}{\mu} - \Sigma(R) \right) h^2 \frac{\partial Z}{\partial h} + \frac{\sigma^2}{\mu} h^2 \frac{\partial}{\partial h} \left[Zh B_1(\mathbf{x}, R) \right] = 0 \end{aligned}$$

which needs to be solved with boundary conditions $\bar{f}(\mathbf{x}) = 0$ and $\partial_{|\mathbf{x}|} \bar{f}(\mathbf{x}) = 0$ for $|\mathbf{x}| = R$. Observe that in the case $\bar{\lambda} = 0$ both $B_1(\mathbf{x}, R) = 0$ and $\Sigma(R) = \sigma^2/\mu$, and therefore the solution is simply $\bar{f}(\mathbf{x}) \equiv 0$ (and $f(\mathbf{x}) = \langle n \rangle Z$). For $\bar{\lambda} > 0$ however the expression of $\bar{f}(\mathbf{x})$

is not trivial and the equation is not easily solved.

Appendix D

Model with independent dispersal

In the main text of the thesis I analyse the analytic properties of a model where individuals can diffuse in space only in the moment they are born. This is intended to mimic the dynamics of seed dispersal in plants and trees. In this part I show that the analysis undertaken in chapter III can be extended to other models, and similar results can be obtained even when spatial dispersal is independent of birth.

Here, I consider a spatial meta-community model where local communities are located on a d -dimensional regular graph (or lattice). Within each community individuals are treated as diluted, well-mixed and point-like particles.

The model is defined by the following birth-death dynamics: each individual dies at a constant death rate r and gives birth at a constant rate b . The newborn always remains in the same local community of the parent, but at any time it can also hop from a site to one of its $2d$ nearest neighbours with probability D . Communities are colonized from the external at a constant immigration rate b_0 , which also prevents the system from reaching the banal absorbing state without individuals and acts as a mild advantage for rare species.

I indicate with \mathbb{L} the lattice, whose linear side is a . If X_i , $i \in \mathbb{L}$, indicates an individual living in site i , the reactions defining the model's dynamics can be cast into the following

form



where j indicates a nearest neighbor of site i . Notice the change between the reaction (III.1.1) and (D.0.1) and between reaction (III.1.2) and (D.0.2). In this model spatial movement is decoupled from birth, so that individuals can hop onto nearest neighboring sites at any time.

Indicating with $P(\{n\}, t)$ the probability to find the system in the configuration $\{n\}$ at time t the following master equation describes the dynamics of the system

$$\begin{aligned} \frac{\partial}{\partial t} P(\{n\}, t) = \sum_{i \in \mathbb{L}} \left\{ D \sum_{j:|j-i|=1} [(n_j + 1) P(\{\dots n_i - 1, n_j + 1, \dots\}, t)] + \right. & (\text{D.0.5}) \\ & + [b(n_i - 1) + b_0] P(\{\dots n_i - 1, \dots\}, t) + \\ & - D \sum_{j:|j-i|=1} n_i P(\{n\}, t) - [bn_i + b_0] P(\{n\}, t) + \\ & + r(n_i + 1) P(\{\dots n_i + 1, \dots\}, t) + \\ & \left. - rn_i P(\{n\}, t) \right\} \end{aligned}$$

where the dots represent that all other occupation numbers remain as in $\{n\}$ and it is intended that $P(\cdot) = 0$ whenever any of the entrances is negative.

Similarly to what done in section III.2, the first step is to introduce the spatial generating function of the model, which is defined as

$$\zeta(\{H\}, t) = \langle e^{\sum_{k \in \mathbb{L}} n_k H_k} \rangle = \sum_{\{n\}} e^{\sum_{k \in \mathbb{L}} n_k H_k} p(\{n\}, t) \quad (\text{D.0.6})$$

Multiplying through eq (D.0.5) by $e^{\sum_{k \in \mathbb{L}} n_k H_k}$ and averaging one obtains the following equations for $\zeta(\{H\}, t)$

$$\begin{aligned} \frac{\partial}{\partial t} \zeta(\{H\}, t) = & \sum_{i \in \mathbb{L}} \left\{ D \sum_{j:|j-i|=1} [e^{H_i-H_j} \frac{\partial \zeta}{\partial H_j}] + \right. & (D.0.7) \\ & + b e^{H_i} \frac{\partial \zeta}{\partial H_i} + b_0 e^{H_i} \zeta(\{H\}, t) + \\ & - D 2d \frac{\partial \zeta}{\partial H_i} - b \frac{\partial \zeta}{\partial H_i} - b_0 \zeta(\{H\}, t) + \\ & \left. + r e^{-H_i} \frac{\partial \zeta}{\partial H_i} - r \frac{\partial \zeta}{\partial H_i} \right\} \end{aligned}$$

which can be rearranged as

$$\begin{aligned} \frac{\partial}{\partial t} \zeta(\{H\}, t) = & \sum_{i \in \mathbb{L}} \left\{ D \sum_{j:|j-i|=1} [(e^{H_i-H_j} - 1) \frac{\partial \zeta}{\partial H_j}] + \right. & (D.0.8) \\ & + b (e^{H_i} - 1) \frac{\partial \zeta}{\partial H_i} + b_0 (e^{H_i} - 1) \zeta(\{H\}, t) + \\ & \left. + r (e^{-H_i} - 1) \frac{\partial \zeta}{\partial H_i} \right\} \end{aligned}$$

Introducing the parameter $\varepsilon = \frac{2(r-b)}{r+b}$ I assume the following parameter scaling: $\frac{b_0}{\mu} \varepsilon = \mathcal{O}(1)$ as $\varepsilon \rightarrow 0^+$. In order to fix the spatial scaling I consider the independent parameter $\eta = \frac{D}{\sigma^2}$ and make the assumption $\eta = \mathcal{O}(\varepsilon)$ as $\varepsilon \rightarrow 0^+$. I hence assume that the generating function $\zeta(\{H\}, t)$ is analytic at $H_i = 0$ for any i and that the most important contribution to the equation of $\zeta(\{H\}, t)$ comes from a negative real neighborhood of the origin with thickness $\mathcal{O}(\varepsilon)$.

I take the change of variables $H_i = \varepsilon S_i$ and expand eq (D.0.8) in powers of ε , assuming $S_i = \mathcal{O}(1)$ and $S_i \leq 0$. I also define the following constants

$$\lambda = \sqrt{\frac{D}{\mu}} \quad \rho = \sqrt{\frac{\sigma^2}{b_0}} \quad ,$$

This rescaling procedure is exactly equivalent to the one undertaken in section III.4 to

calculate the critical limit of eq (III.2.2). Retaining only the leading order in ε (with the scaling assumptions for the parameters considered above) the following equation is obtained

$$\frac{\partial}{\partial t} \zeta(\{S\}, t) = \sum_{i \in \mathbb{L}} \sigma^2 S_i \left\{ \eta \Delta_i \frac{\partial \zeta}{\partial S_i} - \varepsilon \frac{\partial \zeta}{\partial S_i} + \frac{\varepsilon}{\rho^2} \zeta + \varepsilon S_i \frac{\partial \zeta}{\partial S_i} \right\} . \quad (\text{D.0.9})$$

Rescaling time as $T := \mu t$ and going back to the original notation $S_i \rightarrow H_i \varepsilon$ one obtains

$$\frac{\partial \zeta}{\partial T} = \sum_{i \in \mathbb{L}} H_i \left\{ \lambda^2 \Delta_i \frac{\partial \zeta}{\partial H_i} - \frac{\partial \zeta}{\partial H_i} + \langle n \rangle \zeta + \frac{\sigma^2}{\mu} H_i \frac{\partial \zeta}{\partial H_i} \right\} , \quad (\text{D.0.10})$$

which is exactly equivalent to eq (III.4.2) and which is associated to the following Fokker-Planck equation

$$\begin{aligned} \frac{\partial}{\partial T} P(\{n\}, T) = \sum_{i \in \mathbb{L}} \left\{ \frac{\partial}{\partial n_i} \left[- \left(\lambda^2 \Delta_i n_i - n_i + \langle n \rangle \right) P(\{n\}, T) \right] + \right. \\ \left. + \frac{\sigma^2}{\mu} \frac{\partial^2}{\partial n_i^2} \left[n_i P(\{n\}, T) \right] \right\} \end{aligned}$$

Since all the results of chapters III and IV stem from this equation, the same results that are obtained for the model of seed dispersal hold also for the diffusion model presented in this section, provided that on both cases the system is close to the critical point (defined by the $\varepsilon \rightarrow 0$ limit). Comparison to simulated data calculated with the Doob-Gillespie algorithm show excellent agreement in all the expected regimes (see fig D.0.1).

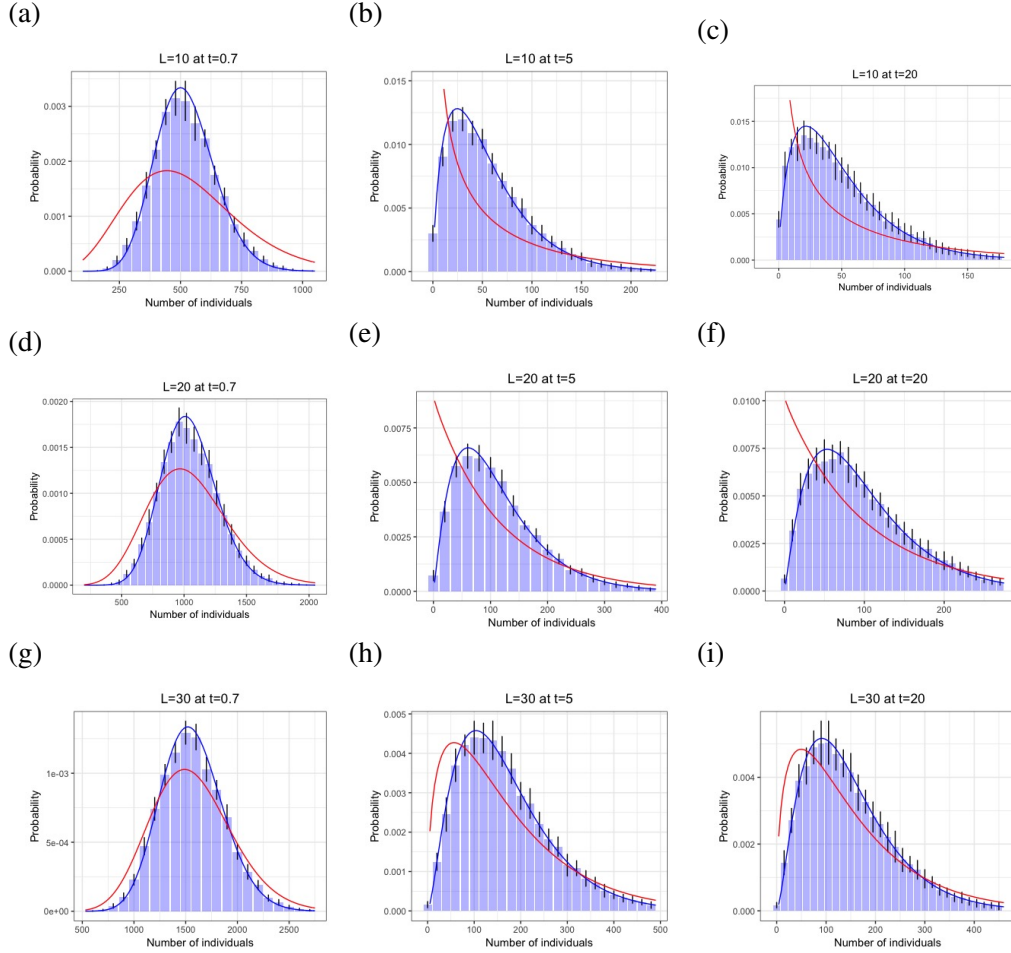


Figure D.0.1: **Comparison of simulated data with the theoretical prediction of eq (III.8.3) at different times in dimension one for the model with independent dispersal.** Histograms are simulated data, with the black segments indicating errors at two standard deviations. The blue line is the prediction made using eq (III.8.3), while the red line is the mean field solution, i.e. eq (III.8.3) with $\Sigma(R) = \sigma^2/\mu$. The parameters of the model are $D = 200$, $b_0 = 5$, $b = 100$ and $d = 101$. Length of the segment and times are reported in the titles of the plots. The lattice has a total of 200 sites and periodic boundary conditions have been used. The simulations have been calculated using the Doob-Gillespie scheme.

Appendix E

Time dependent analysis: calculations

In this appendix I expand the analysis of time dependent patterns. To do so I start by making an ansatz for the form of $f(\mathbf{x}, V, h, T)$ and then I give explicit account of the errors that are introduced with this procedure.

E.0.1 Time-dependent ansatz for $f(\mathbf{x}, h, V, T)$

Taking inspiration from eq (III.7.9) I here consider the following time-dependent ansatz for $f(\cdot)$:

$$f(\mathbf{x}, h, V, T) = \frac{1}{V} \frac{\partial Z}{\partial h}(h, T) \left[1 + h A_1(\mathbf{x}) \right] . \quad (\text{E.0.1})$$

Notice that the dependence over time has been included only at the very first factor, while the parenthesis is kept time-invariant.

I now substitute $f(\mathbf{x}, h, V, T)$ from eq (E.0.1) into eq (III.6.2), and as before I make use of eq (III.7.12) to substitute $\bar{\lambda} \nabla_{\mathbf{x}}^2 \langle n(\mathbf{x}) N(R) \rangle$. The equation that is obtained is the following

$$\frac{\partial}{\partial T} Z(h|V, T) = h \left[- \left(1 - h \Sigma(R) \right) \frac{\partial Z}{\partial h} + \langle N(R) \rangle Z \right] \quad (\text{E.0.2})$$

Inverting this equation (i.e. performing an inverse Laplace transform at both sides) the

following Fokker-Planck equation for the conditional probability distribution is obtained

$$\frac{\partial}{\partial T} p(N, T) = -\frac{\partial}{\partial N} \left[(\langle N(R) \rangle - N) p(N, T) \right] + \Sigma(R) \frac{\partial}{\partial N^2} \left[N p(N, T) \right] \quad (\text{E.0.3})$$

which in the Itô prescription is associated to

$$\dot{N}(R) = \bar{b}_0 V - \mu N(R) + \sigma \sqrt{\psi(R/\bar{\lambda}) N(R)} \xi(t) \quad (\text{E.0.4})$$

where $\xi(t)$ is a Gaussian white noise with covariance $\langle \xi(t) \xi(t') \rangle = 2 \delta(t - t')$. It has therefore been obtained equations (III.8.1) and (III.8.2) reported in the main text.

For $\bar{\lambda} \rightarrow 0$ one retains the mean field solution of the model since $\Sigma(R) = \sigma^2/\mu$. One can also verify that for $t \rightarrow \infty$ this distribution always converges to the stationary solution, i.e. eq (III.7.15). Indeed, since the Bessel function $I_\nu(z) \sim (\frac{1}{2}z)^\nu/\Gamma(\nu + 1)$ as $z \rightarrow 0$, as $t \rightarrow \infty$ one finds

$$\frac{\left[\left(\frac{1}{\Sigma(R)} \right)^2 N_0 N e^{-\mu t} \right]^{\frac{1}{2} - \frac{\langle N \rangle}{2\Sigma(R)}}}{1 - e^{-\mu t}} I_{\frac{\langle N \rangle}{\Sigma(R)} - 1} \left[\frac{\frac{2}{\Sigma(R)} \sqrt{N_0 N e^{-\mu t}}}{1 - e^{-\mu t}} \right] \rightarrow 1$$

and therefore the result is the following

$$p(N, t \rightarrow \infty | N_0, 0) = P(N) = \left(\frac{1}{\Sigma(R)} \right)^{\frac{\langle N \rangle}{\Sigma(R)}} N^{\frac{\langle N \rangle}{\Sigma(R)} - 1} e^{-\frac{N}{\Sigma(R)}}$$

As with the stationary case I now want to evaluate the accuracy of this approach .

E.0.2 Accuracy of the method in the time-dependent case

As was done in section III.7.3, the first step is to substitute $f(\mathbf{x}, V, h, T)$ from the ansatz at eq (E.0.1) into equation (III.6.3). Following analogous steps, i.e. taking eq (III.7.10) and

substituting the LHS of eq (III.7.13) into eq (III.7.16), the following equation is obtained

$$\begin{aligned} \frac{\partial}{\partial T} \frac{\partial}{\partial h} Z(h) [1 + hA_1(\mathbf{x}, R)] = & \frac{\partial}{\partial h} \left\{ h \left[- \left(1 - h\Sigma(R) \right) \frac{\partial Z}{\partial h} + \langle n \rangle L Z \right] \right\} + \\ & + A_1(\mathbf{x}, R) \left\{ \frac{\partial}{\partial h} \left[\frac{\sigma^2}{\mu} h^3 \frac{\partial Z}{\partial h} \right] + h^2 \langle n \rangle V \frac{\partial Z}{\partial h} \right\} \end{aligned} \quad (\text{E.0.5})$$

Bringing all the terms depending on A_1 at right hand side one finds

$$\frac{\partial}{\partial T} \frac{\partial}{\partial h} Z(h, T) = \frac{\partial}{\partial h} \left\{ h \left[- \left(1 - h\Sigma(R) \right) \frac{\partial Z}{\partial h} + \langle n \rangle L Z \right] \right\} + \quad (\text{E.0.6})$$

$$+ A_1(\mathbf{x}, R) \left\{ \frac{\partial}{\partial h} \left[\frac{\sigma^2}{\mu} h^3 \frac{\partial Z}{\partial h} \right] + h^2 \langle n \rangle V \frac{\partial Z}{\partial h} + h \frac{\partial}{\partial T} \frac{\partial Z}{\partial h} \right\} \quad (\text{E.0.7})$$

In the regimes where the terms at the second line are negligible over the terms at the first line, one can observe that the equation that is left is exactly equivalent to the derivative of eq (E.0.2) and is therefore solved. Tantamount to the stationary case, one can also observe that this is verified when $A_1 = 0$, examples of which are the regimes of small and large $\bar{\lambda}$.

Contrarily to before, however, the last term inside the parenthesis at eq (E.0.7) is $\mathcal{O}(h)$, and it is not negligible for large populations with respect to the terms in the first line. As a result, in the intermediate regimes between $\bar{\lambda} = 0$ and $\bar{\lambda} \rightarrow \infty$ there are cases where the analytic approximation for $p(N, t)$ does not give accurate results.

Therefore as the system stirs away from the mean field case of $\bar{\lambda} = 0$, one still obtains an accurate approximation of the true conditional distribution of the system with eq (III.8.3) relatively close to stationarity. It is important to remark that this is *not* equivalent to considering a perturbation around stationarity. This can be directly observed, for example, from the comparison with simulated data in fig III.7.3.

Appendix F

Codes for simulations

F.1 Phenomenological algorithm in one dimension

```
import random as ran
import numpy as np
import time
import math
import os
import sys
from scipy.stats import gamma

def init_latt(N,param):
    shape=param[1]/param[3]**2
    scale=param[3]**2/param[2]
    lattice=[np.random.gamma(shape, scale) for index in range(N)]
    #lattice=[param[1]/param[2] for index in range(N)]
    return lattice
```

```

def step(N, latt , param ): #param=[D, b, mu, sigma]
    i=ran . randrange (0 ,N)
    destra=i+1
    sinistra=i-1
    if destra==N: destra=0
    if sinistra== -1: sinistra=N-1
    #per mettere periodic BC
    Y=param [0]*( latt [ destra ]+ latt [ sinistra ])+param [1]
    Omega=param [2]+2* param [0]
    scale=param [3]**2/Omega
    shape=Y/ param [3]**2
    latt [ i]=np . random . gamma( shape , scale )

```

N=500

```

t0 = time . time ()
param =[30 ,0.5 ,0.01 ,10]
iterazioni =50000000
latt=init_latt (N, param )

```

```

for itera in range(1, iterazioni+1):
    step(N, latt , param )

```

F.2 Gillespie algorithm in one dimension

N=200

```
lattice =[100]*N
```

D=500

b=200

```

b0=10
d=203+2*D
tot_ind=100*N
tempo=0

iterazioni=60000000

tempi_registra=[0.01,0.02,0.05,0.07,0.1,0.2,0.5,0.7,1,2,5,10,20,50]
t_r=0
nome_reticolo=sys.argv[1]
name='latt'+str(nome_reticolo)
myfile = open('./results'++'/'+name+'.txt', 'w')

for itera in range(0,iterazioni):
    choice=ran.randrange(0,(2*D+b+d)*tot_ind+b0*N)
    delta_tempo=np.random.exponential(scale=1/((2*D+b+d)*tot_ind+b0*N))
    if tempo<tempi_registra[t_r] and tempi_registra[t_r]<(tempo+delta_tempo):
        for value in lattice:
            myfile.write(str(value)+'_')
        myfile.write('\n')
        t_r+=1
        print(tempo)
    tempo+=delta_tempo
    if choice<2*D*tot_ind:
        choice2=ran.randrange(0,tot_ind)
        count=0
        for i in range(0,N):
            count+=lattice[i]
            if count>choice2:
                site=i
                break
        choice3=ran.randrange(0,2)
        if choice3==0:

```

```

    if site !=0:
        #lattice[site]-=1
        lattice[site-1]+=1
    elif site ==0:
        lattice[N-1]+=1
        #lattice[0]-=1
elif choice3 ==1:
    if site !=N-1:
        #lattice[site]-=1
        lattice[site+1]+=1
    elif site ==N-1:
        #lattice[N-1]-=1
        lattice[0]+=1
    tot_ind+=1
elif 2*D*tot_ind-1 < choice < (2*D+b)*tot_ind :

    choice2=ran.randrange(0,tot_ind)
    count=0
    for i in range(0,N):
        count+=lattice[i]
        if count > choice2:
            site=i
            break
    lattice[site]+=1
    tot_ind+=1
elif (2*D+b)*tot_ind-1 < choice < (2*D+b+d)*tot_ind :

    choice2=ran.randrange(0,tot_ind)
    count=0
    for i in range(0,N):
        count+=lattice[i]
        if count > choice2:
            site=i

```

```

                break
        lattice [ site ] -= 1
        tot_ind -= 1
    elif (2*D+b+d)*tot_ind - 1 < choice < (2*D+b+d)*tot_ind + b0*N:
        site = ran.randrange(0,N)
        lattice [ site ] += 1
        tot_ind += 1

myfile.close()

```

F.3 Environmental noise simulations

```

def init_latt(N, param):
    shape = param[2] / param[3] ** 2 + 1
    scale = param[3] ** 2 / param[1]
    lattice = [np.random.gamma(shape, scale) for index in range(N)]
    #lattice = [param[1] / param[2] for index in range(N)]
    return lattice

def step(N, latt, param): #param=[D, b, mu, sigma]
    i = ran.randrange(0, N)
    destra = i + 1
    sinistra = i - 1
    if destra == N: destra = 0
    if sinistra == -1: sinistra = N - 1
    #per mettere periodic BC
    Y = param[0] * (latt[destra] + latt[sinistra]) + param[1]
    Omega = param[2] + 2 * param[0]

```

```
scale=param[3]**2/Y
shape=Omega/param[3]**2+1
latt[i]=1/np.random.gamma(shape, scale)
```

```
N=400
```

```
t0 = time.time()
```

```
param=[400,10,1,2]
```

```
scarica_ret=1
```

```
iterazioni=200000000
```

```
latt=init_latt(N,param)
```

```
nome_reticolo=sys.argv[1]
```

```
for itera in range(1,iterazioni+1):
```

```
    step(N,latt,param)
```

Bibliography

- [1] M. Abramowitz and I. A. Stegun. *Handbook of Mathematical Functions with Formulas, Graphs, and Mathematical Tables*. Dover, New York, ninth dover printing, tenth gpo printing edition, 1964.
- [2] P. B. Adler, J. HilleRisLambers, and J. M. Levine. *A niche for neutrality*. *Ecology Letters*, **10**(2):95–104, 2007.
- [3] A. P. Allen and V. M. Savage. *Setting the absolute tempo of biodiversity dynamics*. *Ecology Letters*, **10**(7):637–646, 2007.
- [4] D. Alonso, R. S. Etienne, and A. J. McKane. *The merits of neutral theory*. *Trends in Ecology and Evolution*, **21**(8):451 – 457, 2006.
- [5] D. Alonso and A. J. McKane. *Sampling hubbell’s neutral theory of biodiversity*. *Ecology Letters*, **7**(10):901–910, 2004.
- [6] D. Alonso, A. Ostling, and R. S. Etienne. *The implicit assumption of symmetry and the species abundance distribution*. *Ecology Letters*, **11**(2):93–105, 2008.
- [7] F. Altermatt, E. A. Fronhofer, A. Garnier, A. Giometto, F. Hammes, J. Klecka, D. Legend, E. Mächler, T. M. Massie, F. Pennekamp, et al. *Big answers from small worlds: a user’s guide for protist microcosms as a model system in ecology and evolution*. *Methods in Ecology and Evolution*, **6**(2):218–231, 2015.
- [8] O. Arrhenius. *Species and area*. *Journal of Ecology*, **9**(1):95–99, 1921.
- [9] F. Auerbach. *Das gesetz der bevölkerungskonzentration*. *Petermanns Geographische Mitteilungen*, **59**:74–76, 1913.
- [10] S. Azaele, A. Maritan, S. J. Cornell, S. Suweis, J. R. Banavar, D. Gabriel, and W. E. Kunin. *Towards a unified descriptive theory for spatial ecology: predicting biodiversity patterns across spatial scales*. *Methods in Ecology and Evolution*, **6**(3):324–332, 2015.

- [11] S. Azaele, R. Muneeppeerakul, A. Maritan, A. Rinaldo, and I. Rodriguez-Iturbe. *Predicting spatial similarity of freshwater fish biodiversity. Proceedings of the National Academy of Sciences*, **106**(17):7058–7062, 2009.
- [12] S. Azaele, R. Muneeppeerakul, A. Rinaldo, and I. Rodriguez-Iturbe. *Inferring plant ecosystem organization from species occurrences. Journal of Theoretical Biology*, **262**(2):323 – 329, 2010.
- [13] S. Azaele, S. Pigolotti, J. R. Banavar, and A. Maritan. *Dynamical evolution of ecosystems. Nature*, **444**(7121):926, 2006.
- [14] S. Azaele, S. Suweis, J. Grilli, I. Volkov, J. R. Banavar, and A. Maritan. *Statistical mechanics of ecological systems: Neutral theory and beyond. Reviews of Modern Physics*, **88**(3):035003, 2016.
- [15] P. Babak. *Continuous probabilistic approach to species dynamics in hubbell’s zero-sum local community. Phys. Rev. E*, **74**:021902, Aug 2006.
- [16] P. Babak and F. He. *A neutral model of edge effects. Theoretical Population Biology*, **75**(1):76 – 83, 2009.
- [17] J. R. Banavar, A. Maritan, and A. Rinaldo. *Size and form in efficient transportation networks. Nature*, **399**(6732):130, 1999.
- [18] J. R. Banavar, A. Maritan, and I. Volkov. *Applications of the principle of maximum entropy: from physics to ecology. Journal of Physics: Condensed Matter*, **22**(6):063101, jan 2010.
- [19] G. Barabás, R. D’Andrea, R. Rael, G. Meszéna, and A. Ostling. *Emergent neutrality or hidden niches? Oikos*, **122**(11):1565–1572, 2013.
- [20] U. Bastolla, M. A. Fortuna, A. Pascual-García, A. Ferrera, B. Luque, and J. Bascompte. *The architecture of mutualistic networks minimizes competition and increases biodiversity. Nature*, **458**:1018–1020, 2009.
- [21] C. Battle, C. P. Broedersz, N. Fakhri, V. F. Geyer, J. Howard, C. F. Schmidt, and F. C. MacKintosh. *Broken detailed balance at mesoscopic scales in active biological systems. Science*, **352**(6285):604–607, 2016.
- [22] G. Bell. *The distribution of abundance in neutral communities. The American Naturalist*, **155**(5):606–617, 2000. PMID: 10777433.
- [23] E. Bertuzzo, S. Suweis, L. Mari, A. Maritan, I. Rodríguez-Iturbe, and A. Rinaldo. *Spatial effects on species persistence and implications for biodiversity. Proceedings of the National Academy of Sciences*, **108**(11):4346–4351, 2011.

- [24] O. N. Bjørnstad and B. T. Grenfell. *Noisy clockwork: time series analysis of population fluctuations in animals*. *Science*, **293**(5530):638–643, 2001.
- [25] A. J. Black and A. J. McKane. *Stochastic formulation of ecological models and their applications*. *Trends in Ecology and Evolution*, **27**(6):337 – 345, 2012.
- [26] R. A. Blythe and A. J. McKane. *Stochastic models of evolution in genetics, ecology and linguistics*. *Journal of Statistical Mechanics: Theory and Experiment*, **2007**(07):P07018–P07018, jul 2007.
- [27] M. B. Bonsall, V. A. A. Jansen, and M. P. Hassell. *Life history trade-offs assemble ecological guilds*. *Science*, **306**(5693):111–114, 2004.
- [28] C. Borile, D. Molina-Garcia, A. Maritan, and M. A. Muñoz. *Coexistence in neutral theories: interplay of criticality and mild local preferences*. *Journal of Statistical Mechanics: Theory and Experiment*, **2015**(1):P01030, jan 2015.
- [29] C. Borile, M. A. Muñoz, S. Azaele, J. R. Banavar, and A. Maritan. *Spontaneously broken neutral symmetry in an ecological system*. *Phys. Rev. Lett.*, **109**:038102, Jul 2012.
- [30] P. Bork, C. Bowler, C. De Vargas, G. Gorsky, E. Karsenti, and P. Wincker. *Tara oceans studies plankton at planetary scale*, 2015.
- [31] M. Bramson, J. T. Cox, and R. Durrett. *Spatial models for species area curves*. *Ann. Probab.*, **24**(4):1727–1751, 10 1996.
- [32] T. Butler and N. Goldenfeld. *Robust ecological pattern formation induced by demographic noise*. *Phys. Rev. E*, **80**:030902, Sep 2009.
- [33] F. Carrara, F. Altermatt, I. Rodriguez-Iturbe, and A. Rinaldo. *Dendritic connectivity controls biodiversity patterns in experimental metacommunities*. *Proceedings of the National Academy of Sciences*, **109**(15):5761–5766, 2012.
- [34] C. Castellano, S. Fortunato, and V. Loreto. *Statistical physics of social dynamics*. *Reviews of modern physics*, **81**(2):591, 2009.
- [35] A. Chatterjee, D. G. Vlachos, and M. A. Katsoulakis. *Binomial distribution based τ -leap accelerated stochastic simulation*. *The Journal of chemical physics*, **122**(2):024112, 2005.
- [36] J. Chave. *Neutral theory and community ecology*. *Ecology Letters*, **7**(3):241–253, 2004.
- [37] J. Chave and E. G. Leigh Jr. *A spatially explicit neutral model of β -diversity in tropical forests*. *Theoretical population biology*, **62**(2):153–168, 2002.

- [38] J. Chave, H. C. Muller-Landau, and S. A. Levin. *Comparing classical community models: Theoretical consequences for patterns of diversity*. *The American Naturalist*, **159**(1):1–23, 2002. PMID: 18707398.
- [39] R. A. Chisholm. *Time-dependent solutions of the spatially implicit neutral model of biodiversity*. *Theoretical Population Biology*, **80**(2):71 – 79, 2011.
- [40] R. A. Chisholm, R. Condit, K. A. Rahman, P. J. Baker, S. Bunyavejchewin, Y.-Y. Chen, G. Chuyong, H. Dattaraja, S. Davies, C. E. Ewango, et al. *Temporal variability of forest communities: empirical estimates of population change in 4000 tree species*. *Ecology letters*, **17**(7):855–865, 2014.
- [41] R. A. Chisholm, H. C. Muller-Landau, K. Abdul Rahman, D. P. Bebbler, Y. Bin, S. A. Bohlman, N. A. Bourg, J. Brinks, S. Bunyavejchewin, N. Butt, H. Cao, M. Cao, D. Cárdenas, L.-W. Chang, J.-M. Chiang, G. Chuyong, R. Condit, H. S. Dattaraja, S. Davies, A. Duque, C. Fletcher, N. Gunatilleke, S. Gunatilleke, Z. Hao, R. D. Harrison, R. Howe, C.-F. Hsieh, S. P. Hubbell, A. Itoh, D. Kenfack, S. Kiratiprayoon, A. J. Larson, J. Lian, D. Lin, H. Liu, J. A. Lutz, K. Ma, Y. Malhi, S. McMahan, W. McShea, M. Meegaskumbura, S. Mohd. Razman, M. D. Morecroft, C. J. Nytch, A. Oliveira, G. G. Parker, S. Pulla, R. Punchi-Manage, H. Romero-Saltos, W. Sang, J. Schurman, S.-H. Su, R. Sukumar, I.-F. Sun, H. S. Suresh, S. Tan, D. Thomas, S. Thomas, J. Thompson, R. Valencia, A. Wolf, S. Yap, W. Ye, Z. Yuan, and J. K. Zimmerman. *Scale-dependent relationships between tree species richness and ecosystem function in forests*. *Journal of Ecology*, **101**(5):1214–1224, 2013.
- [42] R. A. Chisholm and J. P. O’Dwyer. *Species ages in neutral biodiversity models*. *Theoretical Population Biology*, **93**:85 – 94, 2014.
- [43] J. S. Clark. *Beyond neutral science*. *Trends in Ecology and Evolution*, **24**(1):8 – 15, 2009.
- [44] B. D. Coleman. *On random placement and species-area relations*. *Mathematical Biosciences*, **54**(3):191 – 215, 1981.
- [45] B. D. Coleman, M. A. Mares, M. R. Willig, and Y.-H. Hsieh. *Randomness, area, and species richness*. *Ecology*, **63**(4):1121–1133, 1982.
- [46] R. Condit, P. S. Ashton, N. Manokaran, J. V. LaFrankie, S. P. Hubbell, and R. B. Foster. *Dynamics of the forest communities at pasoh and barro colorado: comparing two 50-ha plots*. In *Changes And Disturbance In Tropical Rainforest In South-East Asia*, pages 15–24. World Scientific, 1999.

- [47] R. Condit, N. Pitman, E. G. Leigh, J. Chave, J. Terborgh, R. B. Foster, P. Núñez, S. Aguilar, R. Valencia, G. Villa, H. C. Muller-Landau, E. Losos, and S. P. Hubbell. *Beta-diversity in tropical forest trees*. *Science*, **295**(5555):666–669, 2002.
- [48] L. Dai, D. Vorselen, K. S. Korolev, and J. Gore. *Generic indicators for loss of resilience before a tipping point leading to population collapse*. *Science*, **336** **6085**:1175–7, 2012.
- [49] M. Danino and N. M. Shnerb. *Theory of time-averaged neutral dynamics with environmental stochasticity*. *Phys. Rev. E*, **97**:042406, Apr 2018.
- [50] M. Danino, N. M. Shnerb, S. Azaele, W. E. Kunin, and D. A. Kessler. *The effect of environmental stochasticity on species richness in neutral communities*. *Journal of Theoretical Biology*, **409**:155 – 164, 2016.
- [51] C. Darwin. *On the origin of species, 1859*. Routledge, 2004.
- [52] T. J. Davies, A. P. Allen, L. Borda-de Água, J. Regetz, and C. J. Melián. *Neutral biodiversity theory can explain the imbalance of phylogenetic trees but not the tempo of their diversification*. *Evolution*, **65**(7):1841–1850, 2011.
- [53] T. Dobzhansky. *Genetics and the Origin of Species*. Classics of Modern Evolution Series. Columbia University Press, 1982.
- [54] I. Dornic, H. Chaté, and M. A. Munoz. *Integration of langevin equations with multiplicative noise and the viability of field theories for absorbing phase transitions*. *Physical review letters*, **94**(10):100601, 2005.
- [55] X. Du, S. Zhou, and R. S. Etienne. *Negative density dependence can offset the effect of species competitive asymmetry: A niche-based mechanism for neutral-like patterns*. *Journal of Theoretical Biology*, **278**(1):127 – 134, 2011.
- [56] R. Durrett and S. Levin. *Spatial models for species-area curves*. *Journal of Theoretical Biology*, **179**(2):119 – 127, 1996.
- [57] R. D’Andrea, M. Riolo, and A. M. Ostling. *Generalizing clusters of similar species as a signature of coexistence under competition*. *PLoS computational biology*, **15**(1):e1006688, 2019.
- [58] R. S. Etienne and D. Alonso. *A dispersal-limited sampling theory for species and alleles*. *Ecology Letters*, **8**(11):1147–1156, 2005.
- [59] R. S. Etienne and D. Alonso. *Neutral community theory : How stochasticity and dispersal-limitation can explain species coexistence*. 2007.

- [60] R. S. Etienne and H. Olf. *How dispersal limitation shapes species–body size distributions in local communities. The American Naturalist*, **163**(1):69–83, 2004. PMID: 14767837.
- [61] R. S. Etienne and J. Rosindell. *The spatial limitations of current neutral models of biodiversity. PloS one*, **6**(3):e14717, 2011.
- [62] W. Ewens. *The sampling theory of selectively neutral alleles. Theoretical Population Biology*, **3**(1):87 – 112, 1972.
- [63] R. N. Felice and A. Goswami. *Developmental origins of mosaic evolution in the avian cranium. Proceedings of the National Academy of Sciences*, **115**(3):555–560, 2018.
- [64] B. J. Finlay and T. Fenchel. *The Ubiquity of Small Species: Patterns of Local and Global Diversity. BioScience*, **54**(8):777–784, 08 2004.
- [65] C. K. Fisher and P. Mehta. *The transition between the niche and neutral regimes in ecology. Proceedings of the National Academy of Sciences*, **111**(36):13111–13116, 2014.
- [66] R. A. Fisher and J. H. Bennett. *The genetical theory of natural selection: a complete variorum edition*. Oxford University Press, 1999.
- [67] H. García Martín and N. Goldenfeld. *On the origin and robustness of power-law species–area relationships in ecology. Proceedings of the National Academy of Sciences*, **103**(27):10310–10315, 2006.
- [68] C. Gardiner. *Handbook of stochastic methods for physics, chemistry, and the natural sciences*. Springer series in synergetics. Springer-Verlag, 1985.
- [69] C. X. Garzon-Lopez, P. A. Jansen, S. A. Bohlman, A. Ordonez, and H. Olf. *Effects of sampling scale on patterns of habitat association in tropical trees. Journal of Vegetation Science*, **25**(2):349–362, 2014.
- [70] B. Gilbert and M. J. Lechowicz. *Neutrality, niches, and dispersal in a temperate forest understory. Proceedings of the National Academy of Sciences*, **101**(20):7651–7656, 2004.
- [71] D. T. Gillespie. *Exact stochastic simulation of coupled chemical reactions. The journal of physical chemistry*, **81**(25):2340–2361, 1977.
- [72] D. T. Gillespie. *Approximate accelerated stochastic simulation of chemically reacting systems. The Journal of Chemical Physics*, **115**(4):1716–1733, 2001.

- [73] D. T. Gillespie. *Stochastic simulation of chemical kinetics*. *Annu. Rev. Phys. Chem.*, **58**:35–55, 2007.
- [74] A. Giometto, F. Altermatt, F. Carrara, A. Maritan, and A. Rinaldo. *Scaling body size fluctuations*. *Proceedings of the National Academy of Sciences*, **110**(12):4646–4650, 2013.
- [75] A. Giometto, M. Formentin, A. Rinaldo, J. E. Cohen, and A. Maritan. *Sample and population exponents of generalized taylor’s law*. *Proceedings of the National Academy of Sciences*, **112**(25):7755–7760, 2015.
- [76] A. Giometto, A. Rinaldo, F. Carrara, and F. Altermatt. *Emerging predictable features of replicated biological invasion fronts*. *Proceedings of the National Academy of Sciences*, **111**(1):297–301, 2014.
- [77] F. Gnesotto, F. Mura, J. Gladrow, and C. Broedersz. *Broken detailed balance and non-equilibrium dynamics in living systems: a review*. *Reports on Progress in Physics*, **81**(6):066601, 2018.
- [78] N. Goldenfeld and C. Woese. *Life is physics: evolution as a collective phenomenon far from equilibrium*. *Annu. Rev. Condens. Matter Phys.*, **2**(1):375–399, 2011.
- [79] J. L. Gooch and T. J. Schopf. *Genetic variability in the deep sea: relation to environmental variability*. *Evolution*, pages 545–552, 1972.
- [80] D. Gravel, C. D. Canham, M. Beaudet, and C. Messier. *Reconciling niche and neutrality: the continuum hypothesis*. *Ecology Letters*, **9**(4):399–409, 2006.
- [81] J. Grilli, S. Azaele, J. R. Banavar, and A. Maritan. *Absence of detailed balance in ecology*. *EPL (Europhysics Letters)*, **100**(3):38002, 2012.
- [82] J. Grilli, S. Azaele, J. R. Banavar, and A. Maritan. *Spatial aggregation and the species-area relationship across scales*. *Journal of theoretical biology*, **313**:87–97, 2012.
- [83] B. Haegeman and M. Loreau. *A mathematical synthesis of niche and neutral theories in community ecology*. *Journal of Theoretical Biology*, **269**(1):150 – 165, 2011.
- [84] J. M. Halley and Y. Iwasa. *Neutral theory as a predictor of avifaunal extinctions after habitat loss*. *Proceedings of the National Academy of Sciences*, **108**(6):2316–2321, 2011.
- [85] C. A. Hanson, J. A. Fuhrman, M. C. Horner-Devine, and J. B. Martiny. *Beyond biogeographic patterns: processes shaping the microbial landscape*. *Nature Reviews Microbiology*, **10**(7):497, 2012.

- [86] J. Harte. *Ecology: Tail of death and resurrection*. *Nature*, **424**:1006–1007, 2003.
- [87] J. Harte, A. B. Smith, and D. Storch. *Biodiversity scales from plots to biomes with a universal species–area curve*. *Ecology letters*, **12**(8):789–797, 2009.
- [88] F. He and S. P. Hubbell. *Species–area relationships always overestimate extinction rates from habitat loss*. *Nature*, **473**:368–371, 2011.
- [89] J. Hidalgo, J. Grilli, S. Suweis, A. Maritan, and M. A. Muñoz. *Cooperation, competition and the emergence of criticality in communities of adaptive systems*. *Journal of Statistical Mechanics: Theory and Experiment*, **2016**(3):033203, mar 2016.
- [90] J. Hidalgo, J. Grilli, S. Suweis, M. A. Muñoz, J. R. Banavar, and A. Maritan. *Information-based fitness and the emergence of criticality in living systems*. *Proceedings of the National Academy of Sciences*, **111**(28):10095–10100, 2014.
- [91] J. Hidalgo, S. Suweis, and A. Maritan. *Species coexistence in a neutral dynamics with environmental noise*. *Journal of Theoretical Biology*, **413**:1 – 10, 2017.
- [92] R. D. Holt. *Emergent neutrality*. *Trends in Ecology & Evolution*, **21**(10):531 – 533, 2006.
- [93] M. C. Horner-Devine, M. D. Lage, J. B. Hughes, and B. J. M. Bohannan. *A taxa–area relationship for bacteria*. *Nature*, **432**:750–753, 2004.
- [94] S. P. Hubbell. *The unified neutral theory of biodiversity and biogeography (MPB-32)*. Princeton University Press, 2001.
- [95] P. Huxley, Thomas Henry. *Evidence as to man’s place in nature*. New York, D. Appleton and company., 1863. <https://www.biodiversitylibrary.org/bibliography/4806> — I. On the natural history of man-like apes.—II. On the relations of man to the lower animals.—III. On some fossil remains of man.
- [96] R. F. i Cancho and R. V. Solé. *Least effort and the origins of scaling in human language*. *Proceedings of the National Academy of Sciences*, **100**(3):788–791, 2003.
- [97] C. James, S. Azaele, A. Maritan, and F. Simini. *Zipf’s and taylor’s laws*. *Physical Review E*, **98**(3):032408, 2018.
- [98] P. Jeraldo, M. Sipos, N. Chia, J. M. Brulc, A. S. Dhillon, M. E. Konkel, C. L. Larson, K. E. Nelson, A. Qu, L. B. Schook, F. Yang, B. A. White, and N. Goldenfeld. *Quantification of the relative roles of niche and neutral processes in structuring gastrointestinal microbiomes*. *Proceedings of the National Academy of Sciences*, **109**(25):9692–9698, 2012.

- [99] M. Kalyuzhny, R. Kadmon, and N. M. Shnerb. *A neutral theory with environmental stochasticity explains static and dynamic properties of ecological communities*. *Ecology letters*, **18**(6):572–580, 2015.
- [100] N. V. Kampen. *Stochastic processes in physics and chemistry*. North Holland, 2007.
- [101] T. H. Keitt and H. E. Stanley. *Dynamics of north american breeding bird populations*. *Nature*, **393**:257–260, 1998.
- [102] D. Kessler, S. Suweis, M. Formentin, and N. M. Shnerb. *Neutral dynamics with environmental noise: Age-size statistics and species lifetimes*. *Phys. Rev. E*, **92**:022722, Aug 2015.
- [103] D. A. Kessler and N. M. Shnerb. *Neutral-like abundance distributions in the presence of selection in a continuous fitness landscape*. *Journal of Theoretical Biology*, **345**:1 – 11, 2014.
- [104] D. A. Kessler and N. M. Shnerb. *Generalized model of island biodiversity*. *Phys. Rev. E*, **91**:042705, Apr 2015.
- [105] M. Kimura. *The Neutral Theory of Molecular Evolution*. Cambridge University Press, 1983.
- [106] P. L. Krapivsky, S. Redner, and E. Ben-Naim. *A kinetic view of statistical physics*. Cambridge University Press, 2010.
- [107] R. Lande. *Statistics and partitioning of species diversity, and similarity among multiple communities*. *Oikos*, pages 5–13, 1996.
- [108] R. Lande, S. Engen, and B.-E. Saether. *Stochastic population dynamics in ecology and conservation*. Oxford University Press on Demand, 2003.
- [109] N. Lebedev and R. Silverman. *Special Functions & Their Applications*. Dover Books on Mathematics. Dover Publications, 2012.
- [110] E. G. LEIGH JR. *Neutral theory: a historical perspective*. *Journal of Evolutionary Biology*, **20**(6):2075–2091.
- [111] S. A. Levin and R. Durrett. *From individuals to epidemics*. *Philosophical Transactions of the Royal Society of London. Series B: Biological Sciences*, **351**(1347):1615–1621, 1996.
- [112] T. M. Liggett. *Interacting particle systems*, volume 276. Springer Science & Business Media, 2012.

- [113] M. Loreau. *Are communities saturated?* *Ecology Letters*, **3**(2):73–76, 2000.
- [114] M. D. Lynch and J. D. Neufeld. *Ecology and exploration of the rare biosphere.* *Nature Reviews Microbiology*, **13**(4):217, 2015.
- [115] R. H. MacArthur. *On the relative abundance of bird species.* *Proceedings of the National Academy of Sciences of the United States of America*, **43**(3):293, 1957.
- [116] R. H. MacArthur and E. O. Wilson. *The theory of island biogeography*, volume 1. Princeton university press, 2001.
- [117] Y. E. Maruvka, D. A. Kessler, and N. M. Shnerb. *The birth-death-mutation process: A new paradigm for fat tailed distributions.* *PLOS ONE*, **6**(11):1–7, 11 2011.
- [118] Y. E. Maruvka, N. M. Shnerb, D. A. Kessler, and R. E. Ricklefs. *Model for macroevolutionary dynamics.* *Proceedings of the National Academy of Sciences*, **110**(27):E2460–E2469, 2013.
- [119] D. C. Marvin, L. P. Koh, A. J. Lynam, S. Wich, A. B. Davies, R. Krishnamurthy, E. Stokes, R. Starkey, and G. P. Asner. *Integrating technologies for scalable ecology and conservation.* *Global Ecology and Conservation*, **7**:262 – 275, 2016.
- [120] N. Masuda, N. Gibert, and S. Redner. *Heterogeneous voter models.* *Phys. Rev. E*, **82**:010103, Jul 2010.
- [121] B. McGill. *Strong and weak tests of macroecological theory.* *Oikos*, **102**(3):679–685, 2003.
- [122] A. McKane, D. Alonso, and R. V. Solé. *Mean-field stochastic theory for species-rich assembled communities.* *Phys. Rev. E*, **62**:8466–8484, Dec 2000.
- [123] I. Meyer and N. M. Shnerb. *Noise-induced stabilization and fixation in fluctuating environment.* In *Scientific Reports*, 2018.
- [124] M. Mobilia. *Does a single zealot affect an infinite group of voters?* *Phys. Rev. Lett.*, **91**:028701, Jul 2003.
- [125] M. Mobilia, A. Petersen, and S. Redner. *On the role of zealotry in the voter model.* *Journal of Statistical Mechanics: Theory and Experiment*, **2007**(08):P08029–P08029, aug 2007.
- [126] T. Mora and W. Bialek. *Are biological systems poised at criticality?* *Journal of Statistical Physics*, **144**(2):268–302, 2011.
- [127] P. A. P. A. P. Moran. *The statistical processes of evolutionary theory /Patrick A.P. Moran.* Oxford : Clarendon Press, 1962. Includes bibliography.

- [128] R. Muneeppeerakul, S. Azaele, S. A. Levin, A. Rinaldo, and I. Rodriguez-Iturbe. *Evolution of dispersal in explicitly spatial metacommunities*. *Journal of Theoretical Biology*, **269**(1):256 – 265, 2011.
- [129] R. Muneeppeerakul, E. Bertuzzo, H. J. Lynch, W. F. Fagan, A. Rinaldo, and I. Rodriguez-Iturbe. *Neutral metacommunity models predict fish diversity patterns in mississippi–missouri basin*. *Nature*, **453**:220–222, 2008.
- [130] M. E. Newman. *Power laws, pareto distributions and zipf’s law*. *Contemporary physics*, **46**(5):323–351, 2005.
- [131] A. E. Noble, A. Hastings, and W. F. Fagan. *Multivariate moran process with lotka-volterra phenomenology*. *Phys. Rev. Lett.*, **107**:228101, Nov 2011.
- [132] J. P. O’Dwyer and R. Chisholm. *A mean field model for competition: from neutral ecology to the red queen*. *Ecology Letters*, **17**(8):961–969, 2014.
- [133] J. P. O’Dwyer and J. L. Green. *Field theory for biogeography: a spatially explicit model for predicting patterns of biodiversity*. *Ecology letters*, **13**(1):87–95, 2010.
- [134] J. P. O’Dwyer, S. W. Kembel, and T. J. Sharpton. *Backbones of evolutionary history test biodiversity theory for microbes*. *Proceedings of the National Academy of Sciences*, **112**(27):8356–8361, 2015.
- [135] J. P. O’Dwyer and S. J. Cornell. *Cross-scale neutral ecology and the maintenance of biodiversity*. In *Scientific Reports*, 2018.
- [136] R. T. Paine. *Food web complexity and species diversity*. *The American Naturalist*, **100**(910):65–75, 1966.
- [137] M. Pascual and F. Guichard. *Criticality and disturbance in spatial ecological systems*. *Trends in ecology and evolution*, **20**(2):88–95, 2005.
- [138] F. Peruzzo and S. Azaele. *A phenomenological spatial model for macro-ecological patterns in species-rich ecosystems*. In *Stochastic Processes, Multiscale Modeling, and Numerical Methods for Computational Cellular Biology*, pages 349–368. Springer, 2017.
- [139] S. Pigolotti and M. Cencini. *Speciation-rate dependence in species–area relationships*. *Journal of theoretical biology*, **260**(1):83–89, 2009.
- [140] S. Pigolotti and M. Cencini. *Journal of theoretical biology*, **256**(4):609–617, Aug 2010.
- [141] S. Pigolotti and M. Cencini. *Species abundances and lifetimes: From neutral to niche-stabilized communities*. *Journal of Theoretical Biology*, **338**:1 – 8, 2013.

- [142] S. Pigolotti, M. Cencini, D. Molina, and M. A. Muñoz. *Stochastic spatial models in ecology: a statistical physics approach*. *Journal of Statistical Physics*, **172**(1):44–73, 2018.
- [143] O. A. Pinto and M. A. Munoz. *Quasi-neutral theory of epidemic outbreaks*. *PloS one*, **6**(7):e21946, 2011.
- [144] J. B. Plotkin, J. Chave, and P. S. Ashton. *Cluster analysis of spatial patterns in malaysian tree species*. *The American Naturalist*, **160**(5):629–644, 2002. PMID: 18707513.
- [145] J. B. Plotkin, M. D. Potts, D. W. Yu, S. Bunyavejchewin, R. Condit, R. Foster, S. Hubbell, J. LaFrankie, N. Manokaran, L. H. Seng, R. Sukumar, M. A. Nowak, and P. S. Ashton. *Predicting species diversity in tropical forests*. *Proceedings of the National Academy of Sciences*, **97**(20):10850–10854, 2000.
- [146] F. W. Preston. *Time and space and the variation of species*. *Ecology*, **41**(4):612–627, 1960.
- [147] R. E. Ricklefs. *A comment on hubbell’s zero-sum ecological drift model*. *Oikos*, **100**(1):185–192, 2003.
- [148] A. Rinaldo, A. Maritan, K. K. Cavender-Bares, and S. W. Chisholm. *Cross-scale ecological dynamics and microbial size spectra in marine ecosystems*. *Proceedings of the Royal Society of London. Series B: Biological Sciences*, **269**(1504):2051–2059, 2002.
- [149] M. L. Rosenzweig et al. *Species diversity in space and time*. Cambridge University Press, 1995.
- [150] J. Rosindell and S. J. Cornell. *Species–area relationships from a spatially explicit neutral model in an infinite landscape*. *Ecology letters*, **10**(7):586–595, 2007.
- [151] J. Rosindell and S. J. Cornell. *Universal scaling of species-abundance distributions across multiple scales*. *Oikos*, **122**(7):1101–1111, 2013.
- [152] J. Rosindell, S. P. Hubbell, and R. S. Etienne. *The unified neutral theory of biodiversity and biogeography at age ten*. *Trends in Ecology and Evolution*, **26**(7):340–348, 2011.
- [153] J. Rosindell, S. P. Hubbell, F. He, L. J. Harmon, and R. S. Etienne. *The case for ecological neutral theory*. *Trends in Ecology and Evolution*, **27**(4):203–208, 2012.
- [154] J. L. Rosindell and S. J. Cornell. *Species-area curves, neutral models, and long-distance dispersal*. *Ecology*, **90** 7:1743–50, 2009.

- [155] M. Scheffer, S. R. Carpenter, T. M. Lenton, J. Bascompte, W. E. Brock, V. Dakos, J. van de Koppel, I. A. van de Leemput, S. A. Levin, E. H. van Nes, M. Pascual, and A. J. Vandermeer. *Anticipating critical transitions*. *Science*, **338** 6105:344–8, 2012.
- [156] D. J. Schwab, I. Nemenman, and P. Mehta. *Zipf’s law and criticality in multivariate data without fine-tuning*. *Physical review letters*, **113**(6):068102, 2014.
- [157] E. Ser-Giacomi, L. Zinger, S. Malviya, C. De Vargas, E. Karsenti, C. Bowler, and S. De Monte. *Ubiquitous abundance distribution of non-dominant plankton across the global ocean*. *Nature ecology & evolution*, **2**(8):1243, 2018.
- [158] F. Simini, M. C. González, A. Maritan, and A.-L. Barabási. *A universal model for mobility and migration patterns*. *Nature*, **484**(7392):96, 2012.
- [159] J. W. F. Slik, V. Arroyo-Rodríguez, S.-I. Aiba, P. Alvarez-Loayza, L. F. Alves, P. Ashton, P. Balvanera, M. L. Bastian, P. J. Bellingham, E. van den Berg, L. Bernacci, P. da Conceição Bispo, L. Blanc, K. Böhning-Gaese, P. Boeckx, F. Bongers, B. Boyle, M. Bradford, F. Q. Brearley, M. Breuer-Ndoundou Hockemba, S. Bunyavejchewin, D. Calderado Leal Matos, M. Castillo-Santiago, E. L. M. Catharino, S.-L. Chai, Y. Chen, R. K. Colwell, R. L. Chazdon, C. Clark, D. B. Clark, D. A. Clark, H. Culmsee, K. Damas, H. S. Dattaraja, G. Dauby, P. Davidar, S. J. DeWalt, J.-L. Doucet, A. Duque, G. Durigan, K. A. O. Eichhorn, P. V. Eisenlohr, E. Eler, C. Ewango, N. Farwig, K. J. Feeley, L. Ferreira, R. Field, A. T. de Oliveira Filho, C. Fletcher, O. Forshed, G. Franco, G. Fredriksson, T. Gillespie, J.-F. Gillet, G. Amarnath, D. M. Griffith, J. Grogan, N. Gunatilleke, D. Harris, R. Harrison, A. Hector, J. Homeier, N. Imai, A. Itoh, P. A. Jansen, C. A. Joly, B. H. J. de Jong, K. Kartawinata, E. Kearsley, D. L. Kelly, D. Kenfack, M. Kessler, K. Kitayama, R. Kooyman, E. Larney, Y. Laumonier, S. Laurance, W. F. Laurance, M. J. Lawes, I. L. d. Amaral, S. G. Letcher, J. Lindsell, X. Lu, A. Mansor, A. Marjokorpi, E. H. Martin, H. Meilby, F. P. L. Melo, D. J. Metcalfe, V. P. Medjibe, J. P. Metzger, J. Millet, D. Mohandass, J. C. Montero, M. de Morisson Valeriano, B. Mugerwa, H. Nagamasu, R. Nilus, S. Ochoa-Gaona, Onrizal, N. Page, P. Parolin, M. Parren, N. Parthasarathy, E. Paudel, A. Permana, M. T. F. Piedade, N. C. A. Pitman, L. Poorter, A. D. Poulsen, J. Poulsen, J. Powers, R. C. Prasad, J.-P. Puyravaud, J.-C. Razafimahaimodison, J. Reitsma, J. R. dos Santos, W. Roberto Spironello, H. Romero-Saltos, F. Rovero, A. H. Rozak, K. Ruokolainen, E. Rutishauser, F. Saiter, P. Saner, B. A. Santos, F. Santos, S. K. Sarker, M. Satdichanh, C. B. Schmitt, J. Schöngart, M. Schulze, M. S. Suganuma, D. Sheil, E. da Silva Pinheiro, P. Sist, T. Stevart, R. Sukumar, I.-F. Sun, T. Sunderland, H. S. Suresh, E. Suzuki, M. Tabarelli, J. Tang, N. Targhetta, I. Theilade, D. W. Thomas, P. Tchouto, J. Hurtado, R. Valencia, J. L. C. H. van Valkenburg, T. Van Do, R. Vasquez, H. Verbeeck, V. Adekunle, S. A. Vieira, C. O.

- Webb, T. Whitfeld, S. A. Wich, J. Williams, F. Wittmann, H. Wöll, X. Yang, C. Y. Adou Yao, S. L. Yap, T. Yoneda, R. A. Zahawi, R. Zakaria, R. Zang, R. L. de Assis, B. Garcia Luize, and E. M. Venticinque. *An estimate of the number of tropical tree species. Proceedings of the National Academy of Sciences*, **112**(24):7472–7477, 2015.
- [160] R. V. Solé, D. Alonso, and J. Saldaña. *Habitat fragmentation and biodiversity collapse in neutral communities. Ecological Complexity*, **1**(1):65 – 75, 2004.
- [161] T. Spanio, J. Hidalgo, and M. A. Muñoz. *Impact of environmental colored noise in single-species population dynamics. Phys. Rev. E*, **96**:042301, Oct 2017.
- [162] D. Storch, P. Keil, and W. Jetz. *Universal species–area and endemics–area relationships at continental scales. Nature*, **488**(7409):78, 2012.
- [163] S. Suweis, E. Bertuzzo, L. Mari, I. Rodriguez-Iturbe, A. Maritan, and A. Rinaldo. *On species persistence-time distributions. Journal of theoretical biology*, **303**:15–24, 2012.
- [164] S. Suweis, F. Simini, J. R. Banavar, and A. Maritan. *Emergence of structural and dynamical properties of ecological mutualistic networks. Nature*, **500**:449–452, 2013.
- [165] J.-C. Svenning and R. Condit. *Biodiversity in a warmer world. Science*, **322**(5899):206–207, 2008.
- [166] L. Taylor and R. Taylor. *Aggregation, migration and population mechanics. Nature*, **265**(5593):415, 1977.
- [167] H. ter Steege, N. C. A. Pitman, D. Sabatier, C. Baraloto, R. P. Salomão, J. E. Guevara, O. L. Phillips, C. V. Castilho, W. E. Magnusson, J.-F. Molino, A. Monteagudo, P. Núñez Vargas, J. C. Montero, T. R. Feldpausch, E. N. H. Coronado, T. J. Killeen, B. Mostacedo, R. Vasquez, R. L. Assis, J. Terborgh, F. Wittmann, A. Andrade, W. F. Laurance, S. G. W. Laurance, B. S. Marimon, B.-H. Marimon, I. C. Guimarães Vieira, I. L. Amaral, R. Brienens, H. Castellanos, D. Cárdenas López, J. F. Duivenvoorden, H. F. Mogollón, F. D. d. A. Matos, N. Dávila, R. García-Villacorta, P. R. Stevenson Diaz, F. Costa, T. Emilio, C. Levis, J. Schiatti, P. Souza, A. Alonso, F. Dallmeier, A. J. D. Montoya, M. T. Fernandez Piedade, A. Araujo-Murakami, L. Arroyo, R. Gribel, P. V. A. Fine, C. A. Peres, M. Toledo, G. A. Aymard C., T. R. Baker, C. Cerón, J. Engel, T. W. Henkel, P. Maas, P. Petronelli, J. Stropp, C. E. Zartman, D. Daly, D. Neill, M. Silveira, M. R. Paredes, J. Chave, D. d. A. Lima Filho, P. M. Jørgensen, A. Fuentes, J. Schöngart, F. Cornejo Valverde, A. Di Fiore, E. M. Jimenez, M. C. Peñuela Mora, J. F. Phillips, G. Rivas, T. R. van Andel, P. von Hildebrand, B. Hoffman, E. L. Zent, Y. Malhi, A. Prieto, A. Rudas, A. R. Ruschell, N. Silva, V. Vos, S. Zent, A. A. Oliveira, A. C.

- Schutz, T. Gonzales, M. Trindade Nascimento, H. Ramirez-Angulo, R. Sierra, M. Tirado, M. N. Umaña Medina, G. van der Heijden, C. I. A. Vela, E. Vilanova Torre, C. Vriesendorp, O. Wang, K. R. Young, C. Baider, H. Balslev, C. Ferreira, I. Mesones, A. Torres-Lezama, L. E. Urrego Giraldo, R. Zagt, M. N. Alexiades, L. Hernandez, I. Huamantupa-Chuquimaco, W. Milliken, W. Palacios Cuenca, D. Pauletto, E. Valderrama Sandoval, L. Valenzuela Gamarra, K. G. Dexter, K. Feeley, G. Lopez-Gonzalez, and M. R. Silman. *Hyperdominance in the amazonian tree flora*. *Science*, **342**(6156), 2013.
- [168] C. D. Thomas, A. Cameron, R. E. Green, M. Bakkenes, L. J. Beaumont, Y. C. Collingham, B. Erasmus, M. F. de Siqueira, A. Grainger, L. E. Hannah, L. Hughes, B. Huntley, A. S. van Jaarsveld, G. F. Midgley, L. J. Miles, M. Ortega-Huerta, A. T. Peterson, O. L. Phillips, and S. E. Williams. *Extinction risk from climate change*. *Nature*, **427**:145–148, 2004.
- [169] D. Tilman. *Competition and biodiversity in spatially structured habitats*. *Ecology*, **75**(1):2–16, 1994.
- [170] D. Tilman. *Niche tradeoffs, neutrality, and community structure: A stochastic theory of resource competition, invasion, and community assembly*. *Proceedings of the National Academy of Sciences*, **101**(30):10854–10861, 2004.
- [171] A. Tovo, M. Formentin, S. Suweis, S. Stivanello, S. Azaele, and A. Maritan. *Inferring macro-ecological patterns from local species' occurrences*. *bioRxiv*, 2019.
- [172] A. Tovo, S. Suweis, M. Formentin, M. Favretti, I. Volkov, J. R. Banavar, S. Azaele, and A. Maritan. *Upscaling species richness and abundances in tropical forests*. *Science Advances*, **3**(10), 2017.
- [173] W. Ulrich, M. Ollik, and K. I. Ugland. *A meta-analysis of species–abundance distributions*. *Oikos*, **119**(7):1149–1155, 2010.
- [174] M. Vallade and B. Houchmandzadeh. *Analytical solution of a neutral model of biodiversity*. *Phys. Rev. E*, **68**:061902, Dec 2003.
- [175] M. Vallade and B. Houchmandzadeh. *Species abundance distribution and population dynamics in a two-community model of neutral ecology*. *Phys. Rev. E*, **74**:051914, Nov 2006.
- [176] I. Volkov, J. Banavar, F. He, S. Hubbell, and A. Maritan. *Density dependence explains tree species abundance and diversity in tropical forests*. *Nature*, **438**(7068):658–61, Dec. 2005.
- [177] I. Volkov, J. R. Banavar, S. P. Hubbell, and A. Maritan. *Neutral theory and relative species abundance in ecology*. *Nature*, **424**(6952):1035, 2003.

- [178] I. Volkov, J. R. Banavar, S. P. Hubbell, and A. Maritan. *Patterns of relative species abundance in rainforests and coral reefs*. *Nature*, **450**(7166):45–49, 2007.
- [179] J. Wadey, C. Fletcher, and A. Campos-Arceiz. *First photographic evidence of flat-headed cats (*prionailurus planiceps*) in pasoh forest reserve, peninsular malaysia*. *Tropical Conservation Science*, **7**(2):171–177, 2014.
- [180] H. Weissmann, R. Kent, Y. Michael, and N. M. Shnerb. *Empirical analysis of vegetation dynamics and the possibility of a catastrophic desertification transition*. *PLOS ONE*, **12**(12):1–13, 12 2017.
- [181] H. Weissmann and N. M. Shnerb. *Predicting catastrophic shifts*. *Journal of Theoretical Biology*, **397**:128 – 134, 2016.
- [182] S. Woodcock, C. J. Van Der Gast, T. Bell, M. Lunn, T. P. Curtis, I. M. Head, and W. T. Sloan. *Neutral assembly of bacterial communities*. *FEMS microbiology ecology*, **62**(2):171–180, 2007.
- [183] G. Yaari, Y. Ben-Zion, N. M. Shnerb, and D. A. Vasseur. *Consistent scaling of persistence time in metapopulations*. *Ecology*, **93**(5):1214–1227, 2012.
- [184] S. Zaoli, A. Giometto, J. Giezendanner, A. Maritan, and A. Rinaldo. *On the probabilistic nature of the species-area relation*. *Journal of Theoretical Biology*, **462**:391 – 407, 2019.
- [185] S. Zaoli, A. Giometto, A. Maritan, and A. Rinaldo. *Covariations in ecological scaling laws fostered by community dynamics*. *Proceedings of the National Academy of Sciences*, **114**(40):10672–10677, 2017.
- [186] R. K. P. Zia and B. Schmittmann. *Probability currents as principal characteristics in the statistical mechanics of non-equilibrium steady states*. *Journal of Statistical Mechanics: Theory and Experiment*, **2007**(07):P07012–P07012, jul 2007.
- [187] T. Zillio, J. R. Banavar, J. L. Green, J. Harte, and A. Maritan. *Incipient criticality in ecological communities*. *Proceedings of the National Academy of Sciences*, **105**(48):18714–18717, 2008.
- [188] T. Zillio, I. Volkov, J. R. Banavar, S. P. Hubbell, and A. Maritan. *Spatial scaling in model plant communities*. *Physical review letters*, **95**(9):098101, 2005.
- [189] G. K. Zipf. *Human behavior and the principle of least effort: An introduction to human ecology*. 1949.